Coded Systems and Techniques

for

Wireless Communications

with/without Relays

Swansea University
Prifysgol Abertawe

Duc To

College of Engineering

Swansea University

Submitted to Swansea University in fulfillment of the requirements

for the degree of

Doctor of Philosophy (Ph.D.)

March, 2011

ProQuest Number: 10821496

ProQuest 10821496

Abstract

Coding plays an essential role in wireless communications systems. In this thesis, we study the following techniques for coded systems, which are with or without relays.

First, in a bit-interleaved coded modulation with iterative decoding system, the extrinsic information transfer (EXIT) chart is used as a tool for symbol mapping design purposes. In order to achieve two desired properties: i) a fast convergence rate for fast fading channels and ii) a low outage probability for slow fading channels, we propose a design criterion for a constant gap between the two EXIT functions (the flatness criterion). The design problem is formulated by parameterizing EXIT function of the demapper. In conjunction with a given channel code, a searching algorithm is used to find a sufficiently good mapping. The simulation results confirm that the mapping rule obtained by the proposed criterion can provide the desirable properties with a 64-state convolutional code.

Second, in a multiband coded orthogonal frequency division multiplexing (OFDM) system with limited feedback, we propose an effective power allocation method across OFDM bands to maximize the throughput and achieve a quality of service target. To facilitate the proposed method, two optimization algorithms based on greedy and dynamic programming principles are discussed and a trade-off between the performance and complexity is provided. Simulation results show that the proposed power allocation method allows a signal to noise ratio gain of 2 dB at a goodput of 2.5 bits per second per Hz over the multiband OFDM systems with equal power allocation.

Next, we study an application of convolutional codes to two-way relay networks with physical-layer network coding. In this setup, for a given memory length constraint, the two source nodes can choose the same convolutional code with largest free distance to maximize the performance. Motivated by the fact that the relay node only needs to decode XORed messages, a low complexity decoding scheme is proposed using a reduced-state trellis, which is proved to achieve the same diversity gain as the full-state decoding for fading channels. The reduced-state decoding can be employed when two identical turbo codes (parallel concatenated convolutional codes) are used at two source nodes.

Finally, we consider a two-way relay system in which Alamouti's space-time block coding is used at the two source nodes. For the case of Binary Phase Shift Keying modulation, upper and lower bounds on symbol error probability of the system are derived. The derived
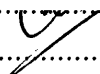
bounds show that a diversity order of two can be achieved even though the relay node has only a single antenna.

Declarations and statements

DECLARATION

This work has not previously been accepted in substance for any degree and is not being concurrently submitted in candidature for any degree.

Signed..(candidate)

Date.......................8/4/2011.....

STATEMENT 1

This thesis is the result of my own investigations, except where otherwise stated. Where correction services have been used, the extent and nature of the correction is clearly marked in a footnote(s).

Other sources are acknowledged by footnotes giving explicit references. A bibliography is appended.

Signed..(candidate)

Date.......................8/4/2011.....

STATEMENT 2

I hereby give consent for my thesis, if accepted, to be available for photocopying and for inter-library loan, and for the title and summary to be made available to outside organizations.

Signed..(candidate)

Date.......................8/4/2011.....

Contents

Acknowledgement

List of figures

List of tables

List of abbreviations

AWGN	additive white Gaussian noise
BCJR algorithm	Bahl-Cocke-Jelinek-Raviv algorithm
BER	bit error rate
BICM	bit-interleaved coded modulation
BICM-ID	bit-interleaved coded modulation with iterative decoding
BPSK	binary phase shift keying
cdf	cumulative density function
CIR	channel impulse response
CP	cyclic prefix
CSCG	circularly symmetric complex Gaussian
CSI	channel state information
EXIT	extrinsic information transfer
ID	iterative decoding
iid	independent identically distributed
ISI	intersymbol interference
LLR	log likelihood ratio
MAP	maximum a posteriori probability
MIMO	multiple-input multiple-output
MISO	multiple-input single-output
ML	maximum likelihood
MLSD	maximum likelihood sequence detection
MRC	maximal ratio combining
OFDM	orthogonal frequency division multiplexing
pdf	probability density function
PEP	pairwise error probability
PSK	phase shift keying
QAM	quadrature amplitude modulation
QPSK	quadrature phase shift keying
SEP	symbol error probability
SIMO	single-input multiple-output
SNR	signal-to-noise ratio
TCM	trellis coded modulation
V-BLAST	vertical Bell labs layered space time

List of notations

$\mathbf{A}/\mathbf{a}$	(boldface upper/lower letters) matrix/vector
$\mathbf{A}^{\mathrm{T}}, \mathbf{A}^{\mathrm{H}}$	transpose, Hermitian transpose, respectively
$[\mathbf{A}]_{p,q}$	the (p, q)th element of $\mathbf{A}$
$\mathbb{E}[\cdot]$	statistical expectation
$\Re(\cdot), \Im(\cdot)$	real and imaginary parts
$\mathcal{CN}(\mathbf{m}, \mathbf{C})$	complex Gaussian vector distribution with mean $\mathbf{m}$ and covariance $\mathbf{C}$
$\log(\cdot)$	natural logarithm
$\mathbf{0}_{m,n}$	matrix of size $m \times n$ with all entries of 0
$\mathbf{I}_n$	an $n \times n$ identity matrix
$|\beta|$	absolute value of scalar β
$\|\mathbf{a}\|$	2-norm of vector $\mathbf{a}$
$\mathbb{C}$	set of complex numbers
$\mathbb{Z}$	set of integer numbers.

1

Introduction

1.1 Overview

Communication services are becoming essential in our everyday life. Because of its convenience for mobile users, wireless communication services are widely spread [1]. Wireless communication systems provide services for mobile users and are built according to standards. Among them, the Global System for Mobile Communications (GSM), Universal Mobile Telecommunication Systems (UMTS), and IEEE 802.11, also known as Wi-Fi standard for wireless local area networks (WLANs), are a few examples.

Due to advanced multimedia technologies, high data rate transmission services, e.g., video streaming, teleconferencing, and network gaming, are becoming more in demand. Furthermore, supporting services in various environments becomes more challenging for system designers and engineers. For example, one may want to extend a wireless support area of an existing system to a particular direction without increasing the transmission power of the current transmitter. In this case, using relays can be a promising solution. However, fully exploiting the advantages of relays is still under investigation by the communication research community. Reflecting these trends of wireless communication development, the next generation wireless communication systems, including long term evolution (LTE)-Advanced [2, 3] (one of candidates for the global 4G mobile

wireless broadband technology known as IMT-Advance), have been developed in order to support requirements of spectral efficiency and power efficiency in various environments.

The most distinct feature of wireless communications is that the channel state may rapidly vary with time [4]. This phenomenon is known as fading. The performance of a wireless system is mainly limited due to a certain probability of deep fade. To cope with fading, the most common strategy is using diversity techniques, by which multiple replicas of a signal are transmitted or received over independent fading paths. Since the probability that at least one of the signal replicas is not in deep fade increases with the number of paths, the transmission reliability therefore can be increased.

In a wireless communication system, coding plays an essential role. When a channel code is employed, a redundancy is introduced to protect information from being corrupted by noise and fading over a wireless communication channel. The maximum time diversity gain a channel code can provide is equal to the minimum Hamming distance between two codewords. To exploit the full diversity provided by a channel code in a system working in the band-limited regime, a bitwise interleaver should be placed between the channel encoder and a high order (multiple levels/phases) modulator to conform a bit-interleaved coded modulation (BICM) structure [5]. At the BICM receiver, the decoding is divided into two separated steps, demodulation and channel decoding, to avoid an over complication of a joint optimal decoding [6]. Furthermore, the demodulator and channel decoder can exchange their detected/decoded information iteratively based on the *turbo principle* [7] to improve the performance. Such complete system is known as BICM with iterative decoding (BICM-ID) [8]. In BICM-ID, the interplay between channel codes and mapping rules can provide coding gains [9]. Finding a reasonably good mapping rule in conjunction with a particular channel code in BICM-ID is therefore highly desirable.

For a high data rate transmission, a wide bandwidth is required. In a wideband system, channel gains usually fluctuate over the frequency band. This, on one hand, can potentially provide a frequency diversity, while on the other hand, causes an intersymbol interference (ISI). The ISI phenomenon due to that the

2

received signal being a weighted sum of multiple symbols transmitted in different time instants may significantly degrade the performance. Orthogonal frequency division multiplexing (OFDM) [10] is an efficient technique to combat the ISI. Embedding BICM in an OFDM system, which is known as coded OFDM, can exploit a frequency diversity gain. In a coded OFDM system, since the performance for each OFDM symbol depends on the channel state within this OFDM, if a feedback link is available, a power control method can be employed for a better spectral/power efficiency.

In communicating between a base station and a mobile user with limited transmission powers, a relay can be useful. Furthermore, since both the base station and mobile user want to transmit information, the transmission is bidirectional and the system that consists of the base station, the mobile terminal, and the relay forms a two-way relay network (TWRN). Due to a possibly high interference from a transmit antenna to a receive antenna in each terminal, all terminals/nodes in the TWRN work in the half-duplex mode. Under this constraint, physical-layer network coding (PNC) [11] can be considered as an effective protocol for information exchange. With PNC, the relay only decodes the network coded signals from the signals sent by the two end terminals (source nodes) simultaneously and then broadcasts the decoded network coded signals to both end terminals in the next phase. When PNC is performed at the message level in conjunction with a channel code, a low complexity decoding for network coded messages needs to be investigated.

As mentioned earlier, diversity techniques are often required in a wireless communication systems. It is well-known that multiple antennas can provide antenna diversities [12]. The benefit of using multiple antennas at the two end terminals in a TWRN with PNC needs to be confirmed.

1.2 Contributions

The contributions of the thesis are as follows:

3

Symbol mapping design based on parameterized EXIT function Without iterative decoding, Gray mapping is considered to be the optimal choice in BICM systems [5]. However, in BICM-ID, Gray mapping is no longer optimal as the performance is not improved even though the number of iterations increases [9, 13, 14]. We consider the problem of symbol mapping design in conjunction with a specific channel code in a BICM-ID system. We use the extrinsic information transfer (EXIT) [15] chart as a design tool. In the EXIT chart, the characteristics of the tunnel between the two EXIT functions of the demapper/demodulator and channel decoder decide the convergence behavior, and then the system performance. When considering two scenarios: i) a fast fading channel with a limited number of decoding iterations and ii) a slow fading channel with an unlimited number of decoding iterations, we deem that there should be a certain gap between the two EXIT functions rather than that the tunnel is just open. For this problem, we propose a design criterion, called the flatness criterion, for symbol mapping design. Our criterion, as its name suggests, requires a flat tunnel between two EXIT curves. In addition, we propose to present the EXIT function of the demapper by a number of parameters. Based on this parametric approach, a least square problem is formulated for the flatness criterion. A sufficiently good mapping rule can be found by using a searching algorithm.

Power allocation for multiband coded OFDM systems with limited feedback For a multiband coded OFDM system with limited feedback, we propose an effective power allocation method across OFDM bands to maximize the throughput and achieve a quality of service (QoS) target. To facilitate the proposed method, two optimization algorithms based on greedy and dynamic programming principles are discussed and a trade-off between the performance and complexity is provided.

Low-complexity decoding based on reduced-trellis structure in two-way relay networks For a TWRN in which channel codes are used at all nodes, we employ PNC at the message level. If channel codes at two source nodes

are convolutional codes, we show that the Viterbi [16] or Bahl-Cocke-Jelinek-Raviv (BCJR) [17] algorithms can be used for the decoding at the relay nodes. Based on a full-trellis, in which the number of states is equal to the sum of two memory lengths of channel encoders at two source nodes, a Viterbi decoder can provide an approximate maximum likelihood (ML) performance. As the diversity order is shown to be equal to the minimum free distance of two channel codes, for a given memory length constraint, the optimal choice is using two identical convolutional codes of maximum free distance. Since the relay node only needs to decode XORed message rather than two individual messages in PNC, we show that the decoding can be performed using a reduced-state trellis with a lower complexity. It is proved that if the two source nodes use identical encoders, based on the reduced-state trellis, the diversity order remains unchanged while the performance is not significantly decreased. As the BCJR algorithm can be performed based on a reduced-state trellis, it is applicable for using turbo codes at the two source nodes.

Antenna diversity in two-way relay networks We consider a two-way relay system in which each source node is equipped with two antennas while there is only one antenna at the relay node. The reason of equipping the relay node with a single antenna is that one would like to keep a low implementation cost at the relay node. The Alamouti scheme [18] are employed at both the source nodes. We derive upper and lower bounds on symbol error probability (SEP) for Binary Phase Shift Keying (BPSK) modulation scheme. From the derived bounds, it is shown that a diversity order of two can be achieved even though the relay node has only a single antenna.

1.3   Thesis organization

This thesis is organized as follows. Chapter 2 introduces wireless channel models and reviews the contemporary coded systems available in the literature. The problem of symbol mapping design based on parameterized EXIT function is addressed in Chapter 3. Chapter 4 proposes a power control method and algorithms

for multiband coded OFDM systems with limited feedback. A low-complexity decoding technique in PNC of two-way relay networks is discussed in Chapter 5. Chapter 6 provides upper and lower bounds on SEP for two-way relay systems in which the two source nodes are equiped with two antennas while there is a single antenna at the relay. Finally, the thesis is concluded in Chapter 7.

Parts of this work have been presented in the following journal papers and conference proceedings:

- D. To and J. Choi, "Convolutional codes in two-way relay networks with physical-layer network coding," *IEEE Trans. Wireless Commun.*, vol. 9, no. 9, pp. 2724–2729, Sept. 2010.

- D. To, J. Choi, and I.-M. Kim, "Error probability analysis of bidirectional relay systems using Alamouti scheme," *IEEE Commun. Lett.*, vol. 14, no. 8, pp. 758–760, Aug. 2010.

- D. To and J. Choi, "Maximum flatness criterion based on EXIT charts for symbol mapping design," *IET Commun.*, 2010, accepted with minor revisions.

- D. To and J. Choi, "Reduced-state decoding in two-way relay networks with physical-layer network coding", in Proc. *IEEE Information Theory Workshop 2010 (ITW2010 Dublin)*, Dublin, Ireland, Sept. 2010.

- D. To and J. Choi, "Parameterized EXIT function for demapper and symbol mapping design", in Proc. *5th IEEE Int. Symp. Wireless Pervasive Comput. 2010 (ISWPC2010)*, Modena, Italy, May 2010, pp. 57–62.

2

Fundamentals of coded systems

2.1 Introduction

This chapter introduces some fundamentals of coded systems in wireless communications. The chapter starts with an introduction to wireless channel models in Section 2.2. Section 2.3 reviews channel codes. Section 2.4 is devoted to describe coded modulation systems including trellis coded modulation (TCM) and bit-interleaved coded modulation (BICM). Orthogonal frequency division multiplexing (OFDM) and multiple-input multiple-output (MIMO) systems are presented in Sections 2.5 and 2.6, respectively. In Section 2.7, two-way relay networks (TWRNs) and physical-layer network coding (PNC) are briefly introduced.

2.2 Wireless channel models

Through a wireless channel, a signal is physically represented by an electromagnetic wave. That means, the signal is transmitted from a transmit antenna to a receive antenna by a means of the electromagnetic propagation. The signal strength is dissipated while traveling in the propagating environment. In addition, due to the effects of a number of mechanisms of the radio transmission including *reflection*, *diffraction*, and *scattering*, the signal is transmitted from

the transmit to receive antenna via multiple paths [1]. The multipath signals at the receive antenna can be combined either constructively or destructively. Therefore, any change of the distance between transmitter and receiver causes a change of received signal strength. Such the change of signal strength is hard to be predicted due to the complication of a propagating environment of many involved objects. Nevertheless, certain knowledges on channel characteristics could be helpful in designing an effective communication system. For this reason, it could be wise to develop statistical models for wireless channels [1, 19].

In general, statistical channel models are classified into two types, which are: *large-scale propagation models* and *small-scale propagation models*. A large-scale propagation model, in characterizing effects known as *pathloss* and *shadowing*, describes the variation of the signal strength over a relatively large distance change. From the system design point of view, large-scale propagation models are necessary in determining some system parameters such as the coverage range of a transmitter. On the other hand, a small-scale propagation model emphasizes on describing the variation of the signal strength caused by a relatively small change of the distance, which is known as the *multipath* effect. Small-scale propagation models are important in developing signal processing techniques including modulation and coding methods for wireless communication systems. In this section, we focus on small-scale propagation models.

2.2.1 Time-varying channel impulse response

A model for a wireless channel from a transmit antenna to a receive antenna is presented as follows. Let $x_b(t)$, a complex function of time t, be an analog baseband signal. The baseband signal is then converted to become a bandpass signal which is carried by a *carrier frequency*, denoted by f_c. In addition, $\cos(2\pi f_c t)$ and $\sin(2\pi f_c t)$ are used as two elements on an orthogonal basis to construct a signal waveform. As a result, the transmitted bandpass signal is given by

$$s(t) = x_I(t) \cos(2\pi f_c t) - x_Q(t) \sin(2\pi f_c t)$$
$$= \Re\left\{ x_b(t) e^{j2\pi f_c t} \right\}$$

$$= \Re \left\{ x(t) \right\}, \tag{2.1}$$

where $x_I(t) = \Re\{x_b(t)\}$ and $x_Q(t) = \Im\{x_b(t)\}$, which are the in-phase and quadrature-phase components of $x_b(t)$, respectively, and $x(t) = x_b(t)e^{j2\pi f_c t}$.

At the receiver, a signal is received via multiple paths. The received signal is modeled as a weighted sum of multiple replicas of the transmitted signal with different weights and delays. Furthermore, background noise is added to the received signal. A model of the received bandpass signal is given as follows:

$$
\begin{aligned}
r(t) &= \Re \left\{ \sum_n a_n(t)x(t - \tau_n(t))e^{j\phi_{D_n}(t)} + z(t) \right\} \\
&= \Re \left\{ \left[\sum_n a_n(t)x_b(t - \tau_n(t))e^{-j(2\pi f_c \tau_n(t) - \phi_{D_n}(t))} + w(t) \right] e^{j2\pi f_c t} \right\}, \tag{2.2}
\end{aligned}
$$

where $a_n(t)$, $\tau_n(t)$, and $\phi_{D_n}(t)$ are the amplitude, delay, and Doppler phase shift of path n, $(n = 0, 1, \ldots)$, respectively, $z(t)$ is the background noise, and $w(t) = z(t)e^{-j2\pi f_c t}$. Here, $z(t)$ is usually modeled as a complex Gaussian process and so is $w(t)$. The Doppler phase shift is determined by the carrier frequency, the relative velocity of receiver, and the angle between the direction of arrival and the receiver's movement direction. Define $c_n(t) = a_n(t)e^{j\phi_n(t)}$ with

$$\phi_n(t) = -2\pi f_c \tau_n(t) + \phi_{D_n}(t). \tag{2.3}$$

Equation (2.2) becomes

$$
\begin{aligned}
r(t) &= \Re \left\{ \left[\int_{-\infty}^{\infty} \sum_n c_n(t)\delta(\tau - \tau_n(t))x(t - \tau)d\tau + w(t) \right] e^{j2\pi f_c t} \right\} \\
&= \Re \left\{ \left[\int_{-\infty}^{\infty} h(t, \tau)x(t - \tau)d\tau + w(t) \right] e^{j2\pi f_c t} \right\} \\
&= \Re \left\{ y(t)e^{j2\pi f_c t} \right\} \tag{2.4}
\end{aligned}
$$

where

$$h(t, \tau) = \sum_n c_n(t)\delta(\tau - \tau_n(t)), \tag{2.5}$$

which is the equivalent lowpass time-varying channel impulse response (CIR), and

$$y_b(t) = \int_{-\infty}^{\infty} h(t, \tau)x_b(t - \tau)d\tau + w(t), \tag{2.6}$$

9

which is the equivalent complex baseband representation of the received bandpass signal. From this, the bandpass signal model given in (2.2) is equivalent to the baseband signal model given in (2.6). As shown in (2.6), the baseband channel is a serial concatenation of a time-varying linear system and a white Gaussian noise addition. Note that the time-varying linear system is characterized by its CIR, i.e., $h(\tau, t)$, which is a function of two variables, time t and delay τ.

In studying the characteristics of the CIR, we have some important observations. First, the number of propagation paths could be very large due to a significant number of scatterers that presents in a scattering environment. In other words, there could be a large number of components in the sum of the right hand side of (2.5). Second, in (2.3), any small change of $\tau_n(t)$ can lead to a significant change of $\phi_n(t)$ as f_c is very high. Rapid phase changes of many paths result in a rapid fluctuation of $h(t, \tau)$ with t, know as *fading*. In the literature, two common assumptions are as follows [20, 21]: a) each of $c_n(t)$'s that are associated with non-light-of-sight (NLOS) paths is a stationary stochastic process; and b) $c_n(t)$'s are mutually independent for different values of n. The consequences of these assumptions are: i) with a fixed τ, $h(t, \tau)$ is a wide sense stationary (WWS) process in t; and ii) $h(t, \tau_1)$ and $h(t, \tau_2)$ are uncorrelated for $\tau_1 \neq \tau_2$. With these assumptions, a channel is referred to as a wide sense stationary uncorrelated scattering (WSSUS) channels [20]. Furthermore, due to a very large number of propagation paths, by invoking the central limit theorem, $h(t, \tau)$ can be modeled as a complex Gaussian random variable with independent real and imaginary parts for fixed t and τ. We commonly consider two cases for the mean of $h(t, \tau)$. The mean of $h(t, \tau)$ is zero for the case of no spectacular path associated with the delay τ. On the other hand, if there is at least a spectacular path associated with the delay τ that dominates other paths, $h(t, \tau)$ has a nonzero mean. Note that for the two cases above, zero and nonzero means of $h(t, \tau)$, the magnitudes of $h(t, \tau)$, i.e., $|h(t, \tau)|$, are Rayleigh and Rician distributed, respectively.

Under the WSSUS assumption, the most important characteristics of a channel are *power delay profile, coherence bandwidth, Doppler power spectrum*, and *coherence time* [19]. Let the autocorrelation function of $h(t, \tau)$ in t be

$$A_c(\Delta t, \tau) = \mathbb{E}\left[h^*(t, \tau)h(t + \Delta t, \tau)\right].$$

Note that $A_c(\Delta t, \tau)$ depends on the relative time difference, i.e., Δt, rather than the absolute time instants, i.e., t and $t + \Delta t$, as $h(t, \tau)$ is WSS in t. The function $A_c(\tau) \triangleq A_c(0, \tau)$ is known as the *power delay profile* of the channel, which shows the distribution of channel powers in the delay domain. Let $A_C(\Delta t, \Delta f)$ be the Fourier transform of $A_c(\Delta t, \tau)$ in τ, i.e.,

$$A_C(\Delta t, \Delta f) = \int_{-\infty}^{\infty} A_c(\Delta t, \tau) e^{-j2\pi \Delta f \tau} d\tau,$$

and let $A_C(\Delta f) \triangleq A_C(0, \Delta f)$. A value denoted by B_c where $A_C(\Delta f) \approx 0$ for all $\Delta f > B_c$ is called the *coherence bandwidth*, which shows how fast the channel gain varies with frequency. The difference between channel responses for different frequencies apart from each other further than the coherence bandwidth is quite significant. If the channel bandwidth is much greater than the coherence bandwidth, the channel is *frequency selective*. On the other hand, if the channel bandwidth is comparable to the coherence bandwidth, the channel is *frequency non-selective* or *frequency flat*. The reciprocal of B_c, denoted by T_m, is defined as the *delay spread* of the channel. Due to the fact that $A_C(\Delta t, \Delta f)$ and $A_c(\Delta t, \tau)$ in τ are in a Fourier transform pair, over the range $[0, T_m]$, $A_c(\tau)$ is essentially non-zero. By taking the Fourier transform of $A_C(\Delta t, \Delta f)$ in Δt, we have

$$S_C(\lambda, \Delta f) = \int_{-\infty}^{\infty} A_C(\Delta t, \Delta f) e^{-j2\pi \lambda \Delta t} d\Delta t.$$

The function $S_C(\lambda) \triangleq S_C(\lambda, 0)$ is called the *Doppler power spectrum*. The maximum value of λ for which $|S_C(\lambda)|$ is greater than zero is called the *Doppler spread* of the channel, which shows how fast the channel gain varies with time and we use D_s to denote this parameter. Its reciprocal is called the *coherence time* and is denoted by T_c. A channel having a property of that $T_m \ll T_c$ is an *underspread* channel. Note that typical wireless channels are underspread. More detailed discussions on characteristics of multipath fading channels can be found in [22, Chapter 14] and [19, Chapter 3].

2.2.2 Discrete-time channel model

Modern signal processing techniques often deal with discrete-time signals, i.e., signals that are discrete in time. In this subsection, we present a discrete-time channel model for a communication system.
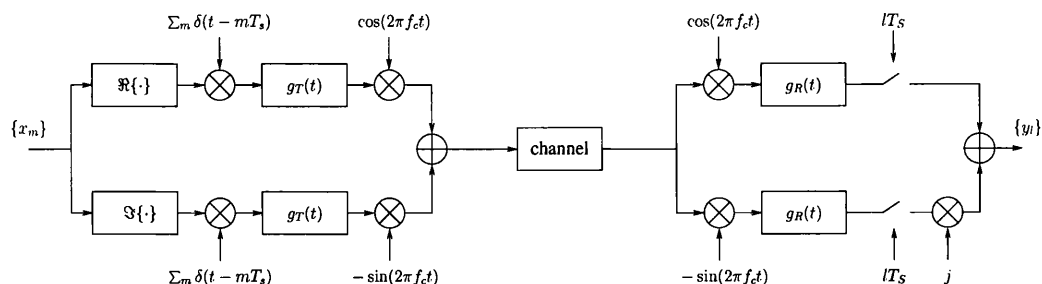
Figure 2.1: Block diagram of a system from baseband transmitted symbols to baseband received signals.

We consider a system whose block diagram is shown in Figure 2.1. In this system, the transmitter includes two identical pulse shape filters, which are used to convert a discrete sequence of symbols to a sequence of waveforms, and the receiver includes two identical lowpass filters before a sampler, which are used to obtain a sequence of discrete signals from an analog received signal. Let $\{x_m\}$ denote the sequence of symbols, where each symbol is selected from a *symbol alphabet*. The symbol alphabet is determined by the modulation method employed. For example, if quadrature phase shift keying (QPSK) signaling is used, the symbol alphabet is $\{-1/\sqrt{2}-j/\sqrt{2}, -1/\sqrt{2}+j/\sqrt{2}, 1/\sqrt{2}-j/\sqrt{2}, 1/\sqrt{2}+j/\sqrt{2}\}$. Let T_s and $g_T(t)$ be the sampling period and the transmitter's pulse shape function, respectively. The analog baseband signal is given by

$$x_b(t) = \sum_m x_m g_T(t - mT_s). \tag{2.7}$$

Note that if the bandpass signal is carried within a bandwidth of B, the bandwidth of $g_T(t)$ should be limited within $[-B/2, B/2]$ and the sampling period should be chosen such that $T_s > 1/B$. After the filtering and sampling at the receiver, a sequence of received signals, denoted by $\{y_l\}$, is obtained. Let $g_R(t)$ be the

12

impulse response of the filter at the receiver. Under the assumption of perfect timing synchronization, the lth element of the sampled signal sequence is given by

$$y_l = \int g_R(\xi) y_b(lT_s - \xi) d\xi. \tag{2.8}$$

Substituting (2.6) and (2.7) into (2.8), we have

$$
\begin{aligned}
y_l &= \int g_R(\xi) \left[\int h(lT_s - \xi, \tau) x_b(lT_s - \xi - \tau) d\tau \right] d\xi + \int g_R(lT_s - \xi) w(\xi) d\xi \\
&= \int g_R(\xi) \left[\int h(lT_s - \xi, \tau) \sum_m x_m g_T((l - m)T_s - \xi - \tau) d\tau \right] d\xi + w_l \\
&= \sum_m x_m \int g_R(\xi) \left[\int h(lT_s - \xi, \tau) g_T((l - m)T_s - \xi - \tau) d\tau \right] d\xi + w_l,
\end{aligned}
\tag{2.9}
$$

where $w_l = \int g_R(lT_s - \xi) w(\xi) d\xi$. If $\{g_R(lT_s - t)\}$ is a set of orthogonal functions, $\{w_l\}$ is an independent and identically distributed (iid) sequence of circularly symmetric complex Gaussian (CSCG) random variables. We generally assume an iid process sequence of CSCG elements for $\{w_l\}$. By letting $k = l - m$, (2.9) becomes

$$
\begin{aligned}
y_l &= \sum_k x_{l-k} \int g_R(\xi) \left[\int h(lT_s - \xi, \tau) g_T(kT_s - \xi - \tau) d\tau \right] d\xi + w_l \\
&= \sum_k h_{l,k} x_{l-k} + w_l,
\end{aligned}
\tag{2.10}
$$

which is the discrete-time channel model. In this model,

$$h_{l,k} = \int g_R(\xi) \left[\int h(lT_s - \xi, \tau) g_T(kT_s - \xi - \tau) d\tau \right] d\xi \tag{2.11}$$

is the response of a linear filter at time $l-k$ when the input is an impulse at time l. Since the coherence time is commonly much larger than the sampling period, i.e., $T_c \gg T_s$, we can approximate $h(lT_s - \xi, \tau) \approx h(lT_s, \tau), \forall \xi : |\xi| < T_s$. Furthermore, if all of the filters at both the transmitter and receiver are ideal lowpass filters, i.e., $g_T(t) = g_R(t) = \text{sinc}(t/T_s)$, where $\text{sinc}(t) \triangleq \frac{\sin \pi t}{\pi t}$, we have $h_{l,k} \approx h(lT_s, kT_s)$, which gives rise to a note that the number of essentially nonzero elements of $\{h_{l,k}\}$ approximates T_m/T_s. Because a filter with the *sinc* pulse shape is unrealizable,

13

other pulse shapes close to it can be used instead, e.g., raised cosine pulse, while the same principle can be applied. Besides, the filters' impulse responses should be chosen such that $g_R(t) = Cg_T(-t)$, where C is a constant, to maximize the useful signal energy.

Let P be the number of nonzero elements in $\{h_{l,k}\}$ and let $h_{l,k}$ be nonzero for $0 \le k \le P - 1$. Note that $P = 1$ if the channel is frequency flat, while $P > 1$ for a frequency selective channel. The discrete-time channel model in (2.10) can be written as

$$y_l = \sum_{k=0}^{P-1} h_{l,k} x_{l-k} + z_l. \tag{2.12}$$

As can be seen in (2.12), the current received signal is affected by an intersymbol interference (ISI) caused by the $P - 1$ previous transmitted symbols. If $P > 1$, the ISI should be mitigated in designing a wireless communication system.

2.3   Channel codes

It has been presented that a wireless channel, over which a sequence of symbols are transmitted, can be modeled as a serial concatenation of a discrete-time time-varying system and a noise addition. Note that the transmitter's input is a sequence of information bits and the receiver's output is a sequence of reconstructed versions of them. Then, the role of transmitter is to produce a transmitted symbol sequence, which becomes the discrete-time channel's input, from an information bit sequence, while the role of receiver is to recover a bit sequence from a received signal sequence, which is taken from the discrete-time channel's output. Below is the description of a possible way to fulfill the role of transmitter.

At the transmitter, suppose that a sequence of K information bits is encoded to be a sequence of L symbols, where the size of symbol alphabet is M. Each symbol conveys K/L information bits. This process can be performed in two steps as follows. In the first step, referred to as *channel encoding*, a sequence of K information bits is mapped into a sequence of N binary elements, where $N = L \log_2 M$. Each element in the resulting sequence is called a *coded bit*. In the

second step, known as *symbol mapping* or *modulation*, each group of $\log_2 M$ coded bits is mapped into a symbol. Here, M is the size of symbol alphabet. A system whose transmitter includes a concatenation of a channel encoder and symbol mapper is referred to as a *coded modulation* system and this kind of systems is mainly studied in this thesis. Note that there could be numerous ways to carry out channel encoding and symbol mapping. The performance of a system is hence decided by its channel characteristics, the selection of channel code and symbol mapping, and the decoding method employed.

The main aim of this section is to review two types of channel codes, namely *convolutional codes* and *turbo codes*. Both of them are in the family of linear channel codes. Convolutional codes, which have a relatively simple encoding structure, were introduced by Elias [23]. The maximum likelihood decoding algorithm for convolutional codes was proposed by Viterbi [16, 24]. Viterbi decoders[1] are known to be very efficient when convolutional encoders have relatively short memory lengths. However, in order to achieve a very good performance, i.e., close to the Shannon capacity [25], a large memory is required. A large memory of encoder results in a high decoding complexity. In 1993, Berrou, Glavieux, and Thitimajshima proposed turbo codes [7], which can provide surprisingly good performances with relatively simple structures of both of encoding an decoding. A turbo encoder is constructed by a parallel concatenation of two convolutional codes, while the turbo decoding is performed by iteratively exchanging information between two convolutional decoders. Even though good performances can be achieved, turbo codes still have an issue, which is that the number of decoding iterations may affect the decoding delay. Nevertheless, both convolutional codes and turbo codes are widely adopted in standards, e.g., a convolutional code with memory length of 6 is defined to be used in IEEE 802.11a [26] and a turbo code is optional in IEEE 802.16 [27].

---

[1]We refer to a decoder that uses the Viterbi algorithm as a Viterbi decoder. Similarly, a BCJR decoder is referred to a decoder that uses the BCJR algorithm, which will be described later.

2.3.1 Convolutional codes

Convolutional encoding

An information bit sequence of length K, denoted by $\mathbf{u} = [u_0 \; u_1 \; \ldots \; u_{K-1}]$, is encoded by a channel code $\mathcal{C}$ to become a coded bit sequence $\mathbf{c}$ of length N, i.e., $\mathbf{c} = \mathcal{C}(\mathbf{u})$. The code rate is defined as $R_c = K/N$. Note that R_c is always less than 1, i.e., $N > K$, as a redundancy is introduced by the channel code to protect the information bit sequence. For the sake of simplicity, we describe here convolutional codes of $R_c = 1/n_c$, where n_c is an integer. Other code rates can be obtained by puncturing from convolutional codes in such type [28, 29]. Let $\mathbf{u} + \mathbf{u}'$ be the binary sequence resulting from applying the modulo-2 addition to every pair of corresponding elements of $\mathbf{u}$ and $\mathbf{u}'$[1]. The linearity of a channel code implies that $\mathcal{C}(\mathbf{u}) + \mathcal{C}(\mathbf{u}') = \mathcal{C}(\mathbf{u} + \mathbf{u}')$.

An algebraic structure of a convolutional code is presented as follows. As a linear code is considered, the channel encoding is a linear mapping from the space of K-tuple binary vectors into the space of N-tuple binary vectors. The coded bit sequence is obtained by

$$\mathbf{c} = \mathbf{u}\mathbf{G}, \qquad (2.13)$$

where $\mathbf{G}$ is called the generator matrix. The range of this mapping is called the set of codewords and $\mathbf{c}$ is a codeword in this set. As $n_c = 1/R_c$ is assumed to be an integer, the coded bit sequence (codeword) can be presented as

$$\mathbf{c} = [c_0^{(1)} \; \ldots \; c_0^{(n_c)} \; \ldots \; c_{K-1}^{(1)} \; \ldots \; c_{K-1}^{(n_c)}].$$

For a convolutional code, the generator matrix has a special form given by

$$\mathbf{G} = \begin{bmatrix} \mathbf{g}_0 & \mathbf{g}_1 & \mathbf{g}_2 & \cdots & \mathbf{g}_{m-1} & & \\ & \mathbf{g}_0 & \mathbf{g}_1 & \cdots & \mathbf{g}_{m-2} & \mathbf{g}_{m-1} & \\ & & & \ddots & & & \ddots \end{bmatrix}, \qquad (2.14)$$

where $\mathbf{g}_j = [g_j^{(1)} \; g_j^{(2)} \; \ldots \; g_j^{(n_c)}]$, $j = 0, 1, \ldots, m-1$, and the blank positions in $\mathbf{G}$ are zeros. The name of convolutional codes is due to the fact that the $(kn_c + i)$th

---

[1] In describing operations of channel codes, we treat each information bit as an element in a finite field (the Galois field) of 2 elements.

coded bit is computed by taking a convolution as follows:

$$c_k^{(i)} = \sum_j g_j^{(i)} u_{k-j}. \tag{2.15}$$

From (2.15), we can see that $\{u_k\}$ and $\{c_k^{(i)}\}$ are respectively the input and output of a time-invariant linear filter whose impulse response is given by $\{g_k^{(i)}\}$. For convenience, in the literature, by letting $u(D) \triangleq \sum_k u_k D^k$, $c^{(i)}(D) \triangleq \sum_k c_k^{(i)} D^k$, and $g^{(i)}(D) \triangleq \sum_k g_k^{(i)} D^k$, which are the D-transforms of $\{u_k\}$, $\{c_k^{(i)}\}$, and $\{g_k^{(i)}\}$, respectively, the coding represented by the convolution in (2.15) becomes $c^{(i)}(D) = u(D)g^{(i)}(D)$ [30, 31]. The $g^{(i)}(D)$'s are called the generator functions of the convolutional code. Note that in general, we do not restrict $\{g_k^{(i)}\}$'s to be finite length and $g^{(i)}(D)$'s, therefore, can have infinite degrees. However, for a realizable convolutional code, $g^{(i)}(D)$'s must be polynomials or rationals in order to force the convolutional encoder to be a state machine with finite states [30].
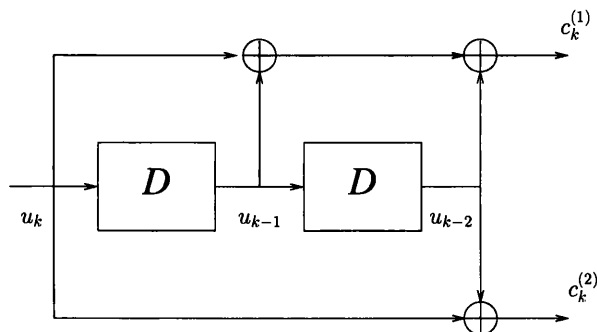
Figure 2.2: A convolutional encoder with $m = 3$, $\mathbf{g}_0 = [1\ 1]$, $\mathbf{g}_1 = [1\ 0]$, and $\mathbf{g}_2 = [1\ 1]$ (the (7,5) convolutional encoder).

To realize a convolutional code with generator polynomials of maximum $m-1$ degree, $m-1$ shift registers and some modulo-2 adders are required. For example, the block diagram of a half-rate convolutional code whose generator matrix is constructed from the set of three generator sequences given by $\mathbf{g}_0 = [1\ 1]$, $\mathbf{g}_1 = [1\ 0]$, and $\mathbf{g}_2 = [1\ 1]$, where $m = 3$, is illustrated in Figure 2.2. With this code, the D-transforms of impulse responses are $g^{(1)}(D) = 1 + D + D^2$ and $g^{(2)}(D) = 1 + D^2$, which are polynomials. In octals, the two coefficient sequences of generator polynomials are presented by 7 and 5, respectively. Therefore, the

convolutional code with the encoder shown in Figure 2.2 is referred to as the (7,5) convolutional code. In the block diagram of an encoder whose all of generator functions are polynomials, no feedback is required. This code is called a non-recursive convolutional code. If feedbacks are required to realize a convolutional code as one or some of its generator functions are rationals, the convolutional code is recursive. An example for the encoder of a recursive convolutional code is shown in Figure 2.6, in which the number of shift registers is given by the maximum degree of the generator functions' numerators and denominators. As the complexity of an encoder is decided by the number of shift registers, m becomes an important parameter and it is known as the *constraint length*.

Due to a structure with memory, a convolutional encoder is a finite state machine (FSM). In encoding a sequence of K information bits, a convolutional encoder experiences $K + 1$ states, each is defined as the sequence of information bits currently stored in the encoder's memory. As the size of the memory is $m - 1$ bits, the number of all possible values the memory can store is 2^{m-1}. For convenience, let the set of all the possible states be denoted by $\mathcal{S}$, where $|\mathcal{S}| = 2^{m-1}$. At time k, $k = 0, 1, \ldots, K - 1$, the input is u_k and the encoder is changed from the state $S_k = \{u_{k-1}, u_{k-2}, \ldots, u_{k-m+1}\}$ to the state $S_{k+1} = \{u_k, u_{k-1}, \ldots, u_{k-m+2}\}$. This transition produces a sequence of n_c coded bits given by $\{c_k^{(1)}, c_k^{(2)}, \ldots, c_k^{(n_c)}\}$.
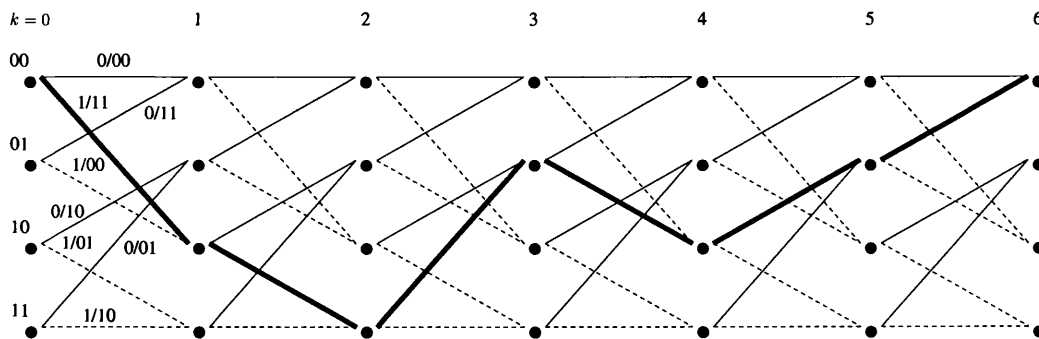
Figure 2.3: Trellis diagram for encoding operation of $\mathbf{u} = [1\ 1\ 0\ 1\ 0\ 0]$ using the (7,5) convolutional encoder.

To describe the operation of encoding an input sequence, a trellis diagram can

18

be used. In a trellis, there are $K+1$ stages, where K is the length of information bit sequence. The encoding of a sequence is presented by a path that consists of K transitions connecting states in $K+1$ stages. Note that the initial state must be the sequence of all zeros, which is called the zero state and denoted by S^0. As an example, the thicker path in a trellis diagram illustrated in Figure 2.3 presents the encoding of $\mathbf{u} = [1\ 1\ 0\ 1\ 0\ 0]$ by using the (7,5) convolutional encoder. Trellis presentations are very useful to describe convolutional decoding algorithms including the Viterbi [16] and Bahl-Cocke-Jelinek-Raviv (BCJR) [17] algorithms. Below are brief descriptions of these algorithms.

Covolutional decoding

In describing the decoding algorithms in this section, we assume a system model as follows. The symbol alphabet is a set of two elements given by $\{-1, +1\}$, i.e., binary phase shift keying (BPSK). Therefore, if the coded bit sequence is $\{c_k^{(i)}\}$, the transmitted symbol sequence is given by $\{x_k^{(i)}\}$, where $x_k^{(i)} = 1 - 2c_k^{(i)}$, $k = 0, 1, \ldots, K-1$, $i = 1, 2, \ldots, n_c$, . These symbols are transmitted over a flat fading channel. The $(kn_c + i)$th received signal is given by

$$y_k^{(i)} = h_k^{(i)} x_k^{(i)} + w_k^{(i)}. \tag{2.16}$$

where $h_k^{(i)}$ is the channel gain, $\{w_k^{(i)}\}$ is the background noise, and $w_k^{(i)} \sim \mathcal{CN}(0, N_0)$.

Viterbi decoding: The Viterbi algorithm is used to find the most likely information bit sequence from the received signal sequence based on the maximum likelihood (ML) criterion. In a trellis, the transition from state S_k to S_{k+1} is associated with a branch metric given by

$$M_k(S_k, S_{k+1}) = -\sum_{i=1}^{n_c} \left| y_k^{(i)} - h_k^{(i)} \tilde{x}_k^{(i)}(S_k, S_{k+1}) \right|^2, \tag{2.17}$$

where $\tilde{x}_k^{(i)}(S_k, S_{k+1}), i = 1, 2, \ldots, n_c$, is the ith transmitted symbol resulting from this transition. Finding the information bit sequence of which the likelihood function is maximized is equivalent to finding the state sequence of which the

path metric, which is defined as the sum of branch metrics of transitions between the states in this sequence, is maximized. To find such optimal state sequence, the Viterbi algorithm is described as follows. First, the decoder computes the branch metrics for all possible transitions in the trellis. Second, the decoder computes the path metrics for the most likely paths ending at all possible states at stage K. To reach stage K, the decoder starts from stage 0 and then subsequently goes through the K remaining stages. Let define the survival path for state S_k at stage k as the state sequence whose path metric is maximum among all possible paths starting at $S_0 = S^0$ and ending at S_k. Denote by $\hat{V}_l(S_k)$ the path metric of the survival path for S_k. Given the path metrics of survival paths for all states at stage $k-1$, the path metric of survival path for state $\hat{S}_k$ is computed recursively as

$$\hat{V}_k(\hat{S}_k) = \max_{S_{k-1} \in \mathcal{P}^s(\hat{S}_k)} \left[\hat{V}_{k-1}(S_{k-1}) + M_{k-1}\left(S_{k-1}, \hat{S}_k\right) \right], \qquad (2.18)$$

where $\mathcal{S}^s(\hat{S}_k)$ is the set of all possible states that can transit to $\hat{S}_k$. In addition, the decoder keeps tracking the previous state in the survival path for each state. Finally, the decoder traces from stage K back to stage 0 to find the optimal state sequence. In practice, the encoding is forced to end at the zero state and such codes are referred to as terminated convolutional codes. In this case, the decoder starts tracing from S^0 in stage K. Once the optimal state sequence is found, the transmitted information bit sequence can be uniquely decoded. Note that according to [32], the Viterbi algorithm is seen as a simplified version of the dynamic programming.

BCJR decoding: An alternative method for decoding is based on the BCJR algorithm. In applying the BCJR algorithm, the maximum *a posteriori* (MAP) criterion is used to decode each bit in the coded bit sequence. In addition, if iterative decoding (ID) is employed and at least a convolutional decoders is used as a constituent component in the ID receiver, this convolutional decoder needs to exploit *a priori* information for information and/or coded bits provided by the other receiver's component to produce *a posteriori* information. In this case, BCJR algorithm is applicable. Receivers with iterative structure will be discussed in more details in Subsections 2.3.2 and 2.4.2.

Assume that *a priori* information for the information bits is necessary to be exploited by a convolutional decoder. For a convenient implementation, *a priori* and *a posteriori* information for information bit sequences are represented by log likelihood ratios (LLRs). Denote by $\{\Lambda_k^{u,I}\}$ and $\{\Lambda_k^{u,O}\}$ the *a priori* and *a posteriori* LLR sequences, respectively. The *a posteriori* LLR for the kth information bit is given by

$$\Lambda_k^{u,O} = \log \frac{\sum_{\{(S_k, S_{k+1})|\Im((S_k,0)\rightarrow S_{k+1})=1\}} \exp\left[\alpha_k\left(S_k\right) + \gamma_k\left(S_k, S_{k+1}\right) + \beta_{k+1}\left(S_{k+1}\right)\right]}{\sum_{\{(S_k, S_{k+1})|\Im((S_k,1)\rightarrow S_{k+1})=1\}} \exp\left[\alpha_k\left(S_k\right) + \gamma_k\left(S_k, S_{k+1}\right) + \beta_{k+1}\left(S_{k+1}\right)\right]}, \tag{2.19}$$

where

$$\Im((S_k, b) \longrightarrow S_{k+1}) = \begin{cases} 1 & \text{if } S_{k+1} \text{ is transited from } S_k \text{ when the input is } b, \\ 0 & \text{otherwise.} \end{cases}$$

with $b \in \{0, 1\}$,

$$\gamma_k\left(S_k, S_{k+1}\right) = \sum_{i=1}^{n_c} \left[-\frac{\left|y_k^{(i)} - h_k^{(i)}\tilde{x}_k^{(i)}(S_k, S_{k+1})\right|^2}{N_0} + \tilde{x}_k^i(S_k, S_{k+1})\Lambda_k^{u,I} \right], \tag{2.20}$$

$$\alpha_k\left(S_k\right) = \log \sum_{S_{k-1} \in \mathcal{S}^s(S_k)} \exp\left[\alpha_{k-1}\left(S_{k-1}\right) + \gamma_{k-1}\left(S_{k-1}, S_k\right)\right], \tag{2.21}$$

and

$$\beta_k\left(S_k\right) = \log \sum_{S_{k+1} \in \mathcal{S}^e(S_k)} \exp\left[\beta_{k+1}\left(S_{k+1}\right) + \gamma_k\left(S_k, S_{k+1}\right)\right], \tag{2.22}$$

where $\mathcal{S}^s(S_k)$ and $\mathcal{S}^e(S_k)$ denote the sets of states that can transit to and be transited from S_k, respectively.

From this, a BCJR decoder can be performed as follows. First, the decoder computes $\gamma_k\left(S_k, S_{k+1}\right)$'s for all the transitions based on (2.20). Second, the decoder forwardly and backwardly computes $\alpha_k\left(S_k\right)$'s and $\beta_k\left(S_k\right)$'s for all the states based on (2.21) and (2.22), respectively. Then, the decoder computes the *a posteriori* LLRs for all the information bits based on (2.19). For a computational efficiency, an approximation can be used for the logarithms of sums of

exponential functions in these equations, e.g., the log-max approximation (i.e., $\log \sum_i \exp(z_i) \approx \max_i z_i$). Finally, the decoder decodes all the information bits based on the MAP principle, i.e., the decoder decides the kth decoded information bit as

$$\hat{u}_k = \begin{cases} 0 & \text{if } \Lambda_k^{u,O} \geq 0, \\ 1 & \text{otherwise.} \end{cases} \tag{2.23}$$
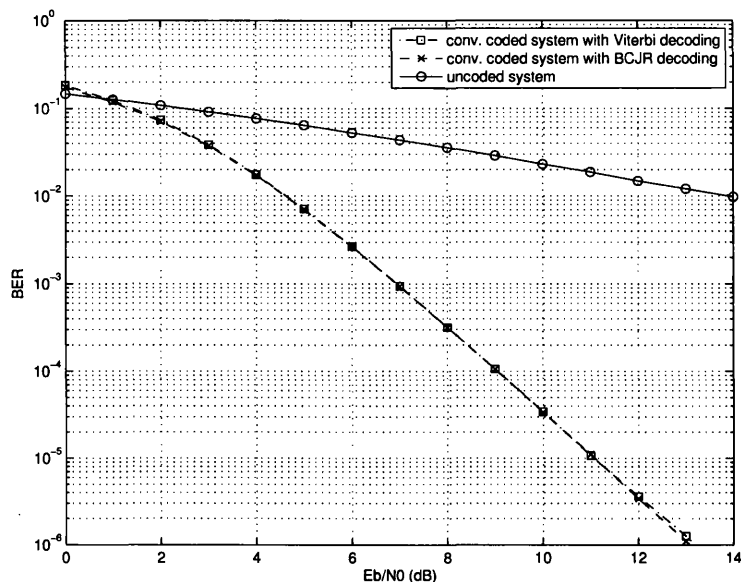
Figure 2.4: BER performance of the (7,5) convolutional code, Rayleigh fading channel.

We carry out simulations to demonstrate the performances of two systems employing the (7,5) convolutional code in conjunction with BPSK signaling, one system uses the Viterbi algorithm and the other uses the BCJR algorithm for decoding. The bit error rate (BER) is the performance index. The performances are compared in different values of E_b/N_0, where E_b denotes the average energy per information bit. In simulations, we assume modulated symbols are transmitted over a flat fading channel whose channel coefficient sequence is assumed to be an iid sequence of CSCG random variables, i.e., Rayleigh fading channel. For comparison purposes, we include a system in which no channel code is employed in our simulations. We refer to the systems with and without convolutional codes as the convolutional coded and uncoded systems, respectively.

In comparison with the uncoded system, as shown in Figure 2.4, the coded systems perform better due to fact that they can exploit time diversity gains. Over the Rayleigh fading channel, the diversity order is represented by the slope of the BER curve, which is determined by the minimum Hamming distance between two codewords in the codeword alphabet, known as the *free distance*.

In addition, it can be seen in Figure 2.4 that the Viterbi and BCJR decoding can provide almost the same performances. Without an iterative structure at the receiver, Viterbi decoding is preferred due to its lower decoding complexity compared to BCJR decoding. On the other hand, a BCJR decoder is suited to be a component in an iterative receiver such as a turbo decoder or a bit-interleaved coded modulation with iterative decoding (BICM-ID) receivers.

2.3.2 Turbo codes

As mentioned earlier, convolutional codes have a relatively simple encoding structure. In order to improve the performance, we can increase the memory length of the encoder. By doing so, the minimum Hamming distance between codewords can be increased. However, increasing the memory length too much may not be welcome since the decoding complexity is also increased.

Turbo codes, also known as parallel concatenated convolutional codes, represent a very promising encoding/decoding method. Before this, concatenations of channel codes were known to be efficient approaches to improve *coding gains* [33]. An advanced feature of turbo codes is that the decoding is performed iteratively by exchanging information between two convolutional decoders so that the performance is improved.

Turbo encoding

A turbo encoder consists of two convolutional encoders, called the constituent encoders, a bitwise interleaver, and an optional puncturer as illustrated in Figure 2.5. The two constituent codes are normally identical with the same code

rate $R_c = 1/n_c$. Let $\mathbf{u} = [u_0, u_1, \ldots, u_{K-1}]$ be an information bit sequence. The first constituent encoder encodes $\mathbf{u}$ to produce a binary coded sequence given as

$$\check{\mathbf{c}}_1 = [\check{c}_{1,0}^{(1)}, \ldots, \check{c}_{1,0}^{(n_c)}, \ldots, \check{c}_{1,K-1}^{(1)}, \ldots, \check{c}_{1,K-1}^{(n_c)}].$$

In addition, $\mathbf{u}$ is permuted by the interleaver to become

$$\check{\mathbf{u}} = \Pi(\mathbf{u}) = [\check{u}_0, \check{u}_1, \ldots, \check{u}_{K-1}]$$

before entering to the second constituent encoder. The output of the second constituent encoder is given by

$$\check{\mathbf{c}}_2 = [\check{c}_{2,0}^{(1)}, \ldots, \check{c}_{2,0}^{(n_c)}, \ldots, \check{c}_{2,K-1}^{(1)}, \ldots, \check{c}_{2,K-1}^{(n_c)}].$$

Both the constituent codes are usually chosen to be recursive, systematic convolutional codes. Figure 2.6 shows an encoder of a half-rate recursive, systematic convolutional code whose transfer functions are 1 and $(1 + D^2)/(1 + D + D^2)$. Note that for two identical convolutional codes that are systematic, $\check{c}_{1,k}^{(1)} = u_k$ and $\check{c}_{2,k}^{(1)} = u_k'$ for all k from 0 to $K - 1$. At the output of a systematic convolutional encoder, the part that is identical to the input is called the systematic part while the remaining is called the parity part. As the systematic parts of the two encoder's outputs convey the same information, it is not necessary to transmit the systematic part of the second encoder's output. Furthermore, to reduce the lengths of parity parts in order to achieve a desired code rate, a puncturer can be used.

Turbo decoding

A turbo decoder is constructed by two constituent BCJR decoders as illustrated by Figure 2.7. The turbo decoding is iteratively performed in some iterations. In each iteration, the first constituent decoder produce the extrinsic information for the information bits. If the *a priori* and *a posteriori* information are represented by LLR sequences, the extrinsic information is obtained by subtracting the *a priori* LLR sequence from the *a posteriori* LLR sequence. The second constituent decoder uses the first decoder's extrinsic information as its *a priori* information to
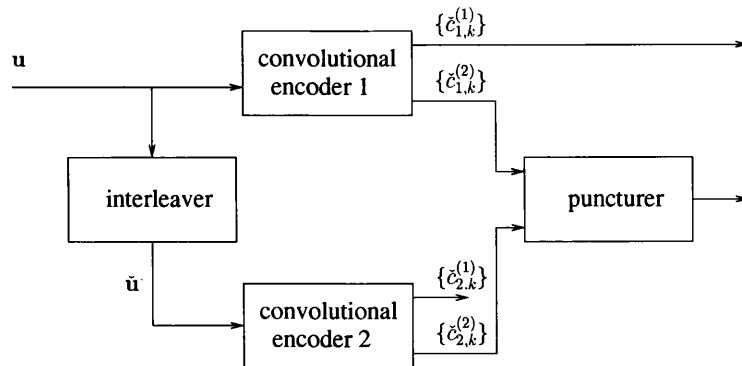
Figure 2.5: Block diagram of a turbo encoder.
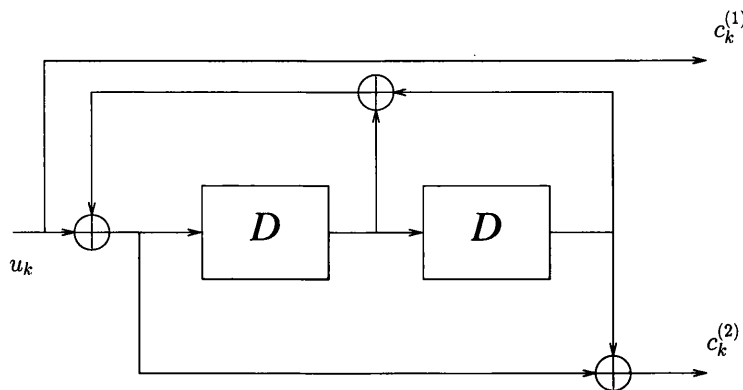
Figure 2.6: A recursive, systematic convolutional encoder

produce its extrinsic information, which is then fed back to the first decoder. After a number of iterations, the information bits are detected from the *a posteriori* information provided by the second constituent decoder.

The BER performance of a turbo code is illustrated in Figure 2.8. In simulations, we use a turbo encoder constituted by two convolutional encoder, which is presented in Figure 2.6. Inside the turbo encoder, the interleaver is assumed to be randomly changed from a codeword to another to average the effect of interleaving. A puncturer is used to achieve a code rate of 1/2. We refer the system employing turbo code to as the turbo coded system. Furthermore, BPSK signaling is also used for modulation. Modulated signals are transmitted over a
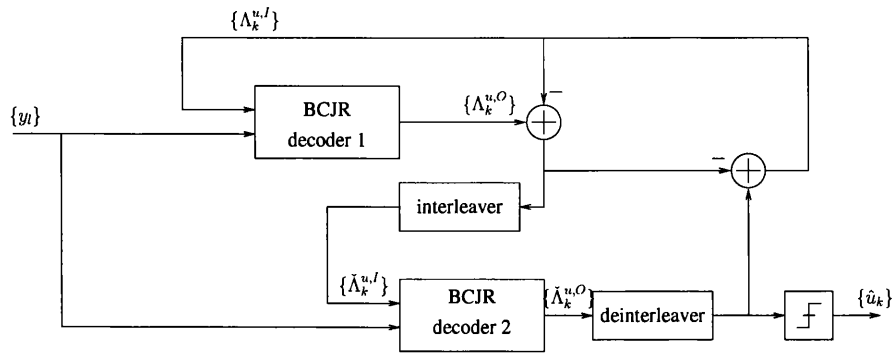
Figure 2.7: Block diagram of a turbo decoder.
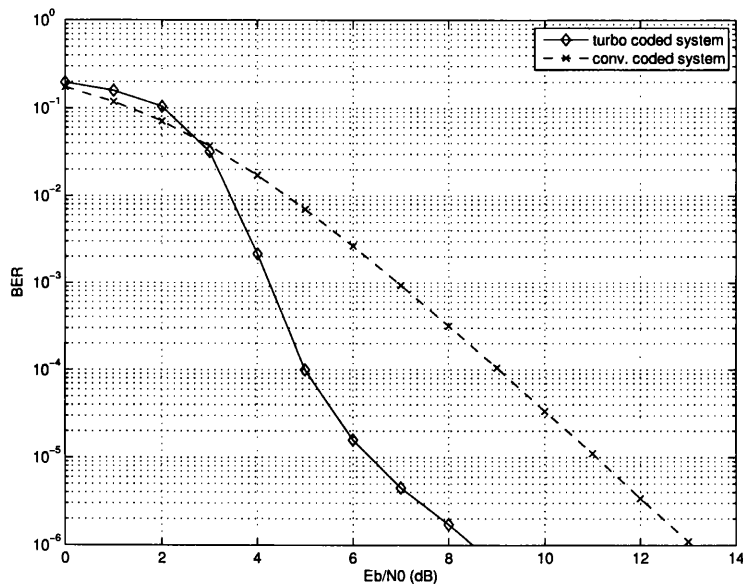
Figure 2.8: BER performance of the turbo code constructed by the two recursive, systematic $(1, (1+D^2)/(1+D+D^2))$ convolutional codes, Rayleigh fading channel.

Rayleigh fading channel. Turbo decoding is performed with 6 iterations. The simulated BER in Figure 2.8 shows that the employed turbo code can easily achieve a good performance. In particular, the turbo code requires 6.5 dB E_b/E_0 to achieve 10^{-5} BER, while the $(7,5)$ convolutional code requires 11 dB E_b/E_0 to achieve the same performance.

Turbo codes are very good in exploiting coding gains rather than diversity gains. In fact, a turbo code has a free distance lower than a convolutional code with a comparable complexity [34]. However, when consulting the two Hamming distance spectra, the convolutional code's spectrum is denser in the low Hamming distance region, while the frequencies of low Hamming distances for the turbo code are much lower. Consequently, the turbo code has a relatively short waterfall region. In addition, there must be an error floor in the BER performance of the turbo code due to a low diversity order. Since the error floor is at very low BER, it is not exhibited in Fig 2.8.

2.4 Coded modulation

In the previous section, we have considered systems that achieve spectral efficiencies less than 1 bps/Hz. For those data rates, required SNR values are low and this region of SNR is known as the power-limited region. In this region, BPSK signaling should be used to achieve a good performance. In the other extreme, when the SNR is sufficiently high, a higher order modulation can be used to improve the spectral efficiency. This region of SNR is known as the band-limited region. Note that using a higher order modulation may lead to a higher error probability due to smaller Euclidean distances between different transmitted symbols. Therefore, Euclidean distances should be considered in designing an effective coded modulation system working in the band-limited region.

2.4.1 Trellis coded modulation

In [35], Ungerboeck introduced an approach for jointly designing channel coding and symbol mapping. For the additive white Gaussian noise (AWGN) channel, the Ungerboeck's approach is better than that for designing a system in which the channel coding and symbol mapping are performed independently and the channel decoding and symbol demapping are operated separately. Such enhancement of Ungerboeck's approach is due to the fact that a system is designed to exploit a coding gain. The structure based on the Ungerboeck's approach is called

trellis coded modulation (TCM). This had been further extended to multidimensional modulations [36] and multiple-input multiple-output (MIMO) systems [12]. In designing a TCM system, instead of the minimum Hamming distance as for the case of considering a channel code only, the metric to be maximized is the minimum Euclidean distance between two codewords.

information bits   coded bits
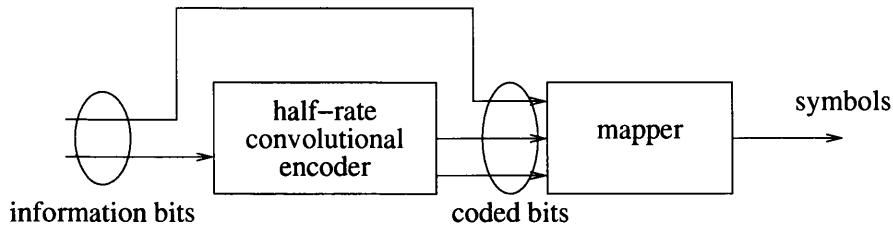
Figure 2.9: A TCM structure.

An example of TCM is illustrated in Figure 2.9. In this example, the odd bits of information bit sequences are left uncoded, while the even bits are encoded by a half rate convolutional code. The resulting channel code becomes a rate-2/3 systematic code. Next, every group of three output bits is mapped into a symbol in an symbol alphabet of 8 elements, e.g., 8 phases Phase Shift Keying (8-PSK) signaling. The spectral efficiency of resulting system is 2 bps/Hz. Since the first bit in each group of three bits at the input of the symbol mapper is unprotected by the channel code, two groups of three bits that are identical except the first bits is expected to be mapped into two different symbols between which the Euclidean distance is as large as possible. This expectation drives a heuristic approach named as *mapping by set partitioning* for symbol mapping design.

Figure 2.10 illustrates a set partitioning for 8-PSK. In this examples, the set partitioning is performed in three levels. At each level, each symbol set or subset is further divided into two subsets of equal number of symbols such that the intra Euclidean distances within each divided subset are increased. At the lowest level, each subset consists of two symbols. Note that the Euclidean distance of two symbols in each subset in the lowest level is equal to the maximum Euclidean distance of the symbol mapping alphabet of 8-PSK. Two symbols in such pairs are labeled by two groups of three bits that are identical except their first bits.
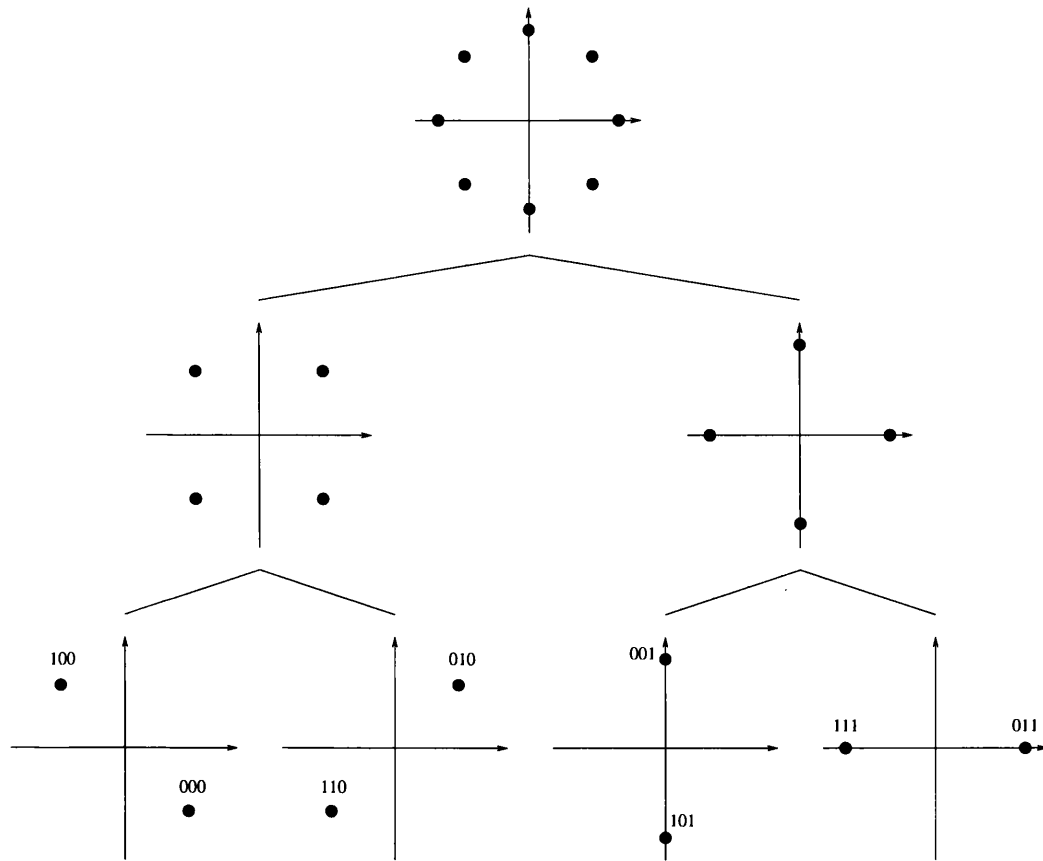
Figure 2.10: Set partitioning for 8-PSK.

As a convolutional code is used in a TCM system, the Viterbi algorithm based on a trellis can be used for the ML decoding.

2.4.2 Bit-interleaved coded modulation.

TCM can improve coding gains. Therefore, TCM performs well over the AWGN channel. However, the AWGN channel may not commonly happen in wireless communications because of the fading phenomenon. If the channel condition varies sufficiently fast, besides the coding gains, improving diversity gains is also essential. TCM, in fact, does not exploit the full diversity gain given by a channel code, as a sacrifice for a coding gain.
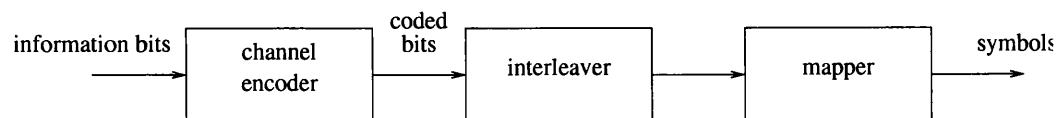
Figure 2.11: Block diagram of a BICM transmitter.

To exploit the full diversity gain given by a channel code, a technique of employing a bitwise interleaver immediately following a channel code can be used. Figure 2.11 illustrates a transmitter structure that employs a bitwise interleaver between a channel code and a symbol mapper. The resulting system is referred to as bit-interleaved coded modulation (BICM). BICM was introduced by Zehavi in [37] and extensively studied by Caire et al. in [5]. Comprehensive discussions on BICM can be found in [6]. In a BICM transmitter, the channel code can be any linear channel code such as a convolutional code or turbo code to produce a sequence of coded bits. The symbol mapper is a M-ary modulator, where M is the size of symbol alphabet, that map each group of $\log_2 M$ interleaved bits into a symbol. Note that there is an important difference between a TCM transmitter and a BICM transmitter, which is that the bitwise interleaving is introduced in BICM transmitter to break the correlations between consecutive coded bits in order to make the coded bits in a group labeling a transmitted symbol fairly uncorrelated. Under an assumption of ideal interleaving, elements in a group of consecutive coded bits are mapped into different symbols and those symbols are transmitted over different fading paths. Therefore, the diversity order of the free distance of channel code can be achieved.

For BICM, the optimal receiver could be the one based on maximizing the likelihood function of transmitted information bit sequence for a given received signal sequence. However, due to the bitwise interleaving, the optimal receiver is very complicated and a sub-optimal approach of separating symbol demapping and channel decoding can be used instead. In addition, a deinterleaver is used between a symbol demapper and channel decoder. In particular, a BICM receiver consists of a demapper, a deinterelaver, and a channel decoder. The demapper produces soft information for coded bits, normally represented by a sequence of

30

extrinsic LLRs, and the channel decoder uses the deinterleaved version of this sequence as it *a priori* information for coded bits to perform decoding.
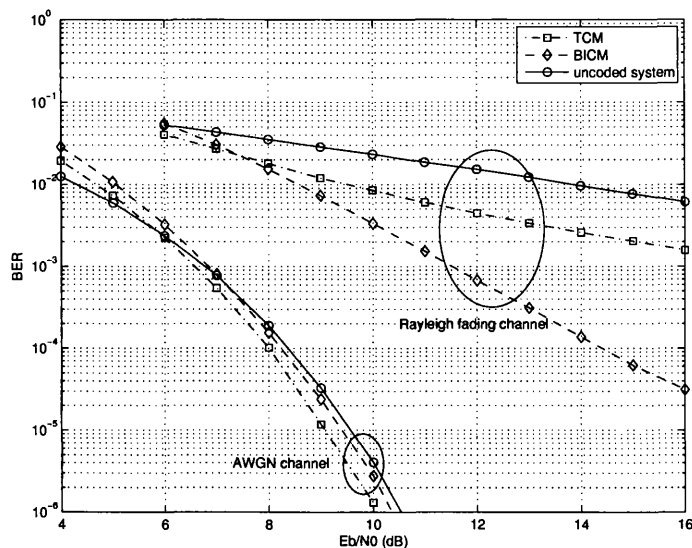
Figure 2.12: BER performances of TCM and BICM over the AWGN and Rayleigh fading channels.

Although a BICM system has a relatively simple structure, it was shown to be a very effective approach to cope with fading [5, 6]. As discussed earlier, in comparison with TCM, BICM can achieve a higher diversity gain since the diversity order of a BICM system is equal to the free distance of channel code while the diversity order of a TCM system is determined by the maximum number of distinct symbols between two symbol sequences into which two different codewords are mapped. This is confirmed by simulation results shown in Figure 2.12. In our simulations, both the TCM and BICM systems use 8-PSK modulation. The TCM system is of structure illustrated in Figure 2.9, where channel codes are the (7,5) convolutional codes. In the BICM system, a puncturer is used to obtain an overall code rate of 2/3. Set partitioning (SP) mapping is used in TCM while Gray mapping is used in BICM.

In order to improve the performance of BICM, an iterative structure at the receiver was proposed by Li and Ricey [8, 38] based on the turbo principle. The

31
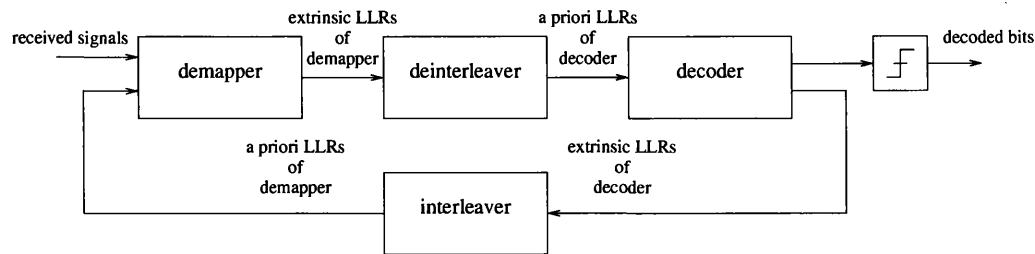
Figure 2.13: BICM-ID receiver structure.

resulting system is known as BICM with iterative decoding (BICM-ID). In the BICM-ID receiver, illustrated in Figure 2.13, a demapper and a channel decoder exchange their extrinsic information for coded bits in some iterations. In particular, let $\mathcal{X}$ denote the symbol alphabet. In each iteration, the LLR representing the extrinsic information for the ith bit in the lth symbol is computed by the symbol demapper as

$$\Lambda_{l,i}^{c,O,dem} = \log \frac{\sum_{x \in \mathcal{X}_0^i} \exp \left(-\frac{|y_l - h_l x|^2}{N_0} + \sum_{j=1, j \neq i}^{m} \frac{(1 - 2\ell^j(x)) P_{l,j}^{c,I,dem}}{2} \right)}{\sum_{x \in \mathcal{X}_1^i} \exp \left(-\frac{|y_l - h_l x|^2}{N_0} + \sum_{j=1, j \neq i}^{m} \frac{(1 - 2\ell^j(x)) P_{l,j}^{c,I,dem}}{2} \right)}, \qquad (2.24)$$

where $\ell^i(x)$ is the ith bit in the label of x, $\mathcal{X}_b^i$, $b \in \{0, 1\}$, indicates a subset of symbols whose ith bit in its label is b, i.e., $\mathcal{X}_b^i = \{x : \ell^i(x) = b\}$, and $\Lambda_{l,i}^{c,I,dem}$ is the *a priori* LLR for the ith bit in the symbol l provided by the channel decoder. Note that in (2.24), l denotes the symbol index. After going through a deinterleaver, $\{\Lambda_{l,i}^{c,O,dem}\}$ becomes $\{\Lambda_{l,i}^{c,I,dec}\}$, the *a priori* LLR sequence for coded bits used by the channel decoder. The channel decoder then processes $\{\Lambda_{l,i}^{c,I,dec}\}$ to produce an extrinsic LLR sequence $\{\Lambda_{l,i}^{c,O,dec}\}$, which, after interleaved, becomes *a priori* LLR sequence used by the symbol demapper in the next iteration. After a number of iterations, the channel demapper computes a sequence of *a posteriori* LLRs for information bits, which is used to decode the information bit sequence. In computing the extrinsic/*a posteriori* LLRs for coded/information bits, the decoder can use a modified BCJR algorithm given in [39, 40].

Without iterative decoding, Gray mapping, shown in Figure 2.14(a), is normally the best choice for symbol mapping since it maximizes the Euclidean be-

0010	0110	1110	1010	1101	1110	1001	1010
0011	0111	1111	1011	0100	0111	0000	0011
0001	0101	1101	1001	0001	0010	0101	0110
0000	0100	1100	1000	1000	1011	1100	1111

(a)   (b)
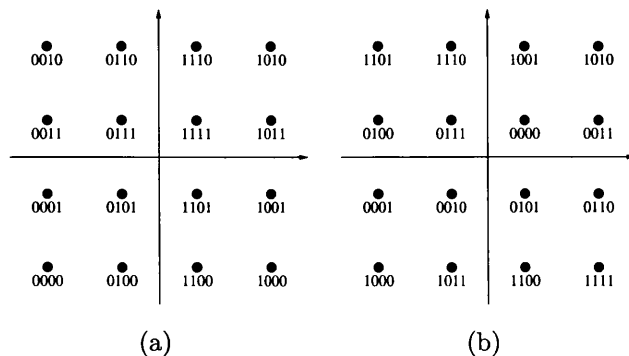
Figure 2.14: Gray and MSP mappings: (a) Gray, (b) MSP.

tween subsets of symbols in which two symbols in two different subsets are labeled by two groups of bits that differs in a bit position [5]. On a contrary, for BICM-ID, other mapping rules could provide better performances than Gray mapping. The reason is that from the second iteration, the demapper can exploit a knowledge on the other bits to compute the extrinsic information for a specific bit in a label so that maximizing the intra-subset Euclidean distances is no longer optimal. Due to the important role of symbol mapping for BICM-ID, there was an extensive list of research works on symbol mapping design, including but not limited to [9, 13, 14]. For example, in [9], Chindapol et al. proposed a criterion for symbol mapping design that aims to maximize the minimum Euclidean distance between two symbols whose labels are identical except in only one bit position under assumption that the demapper can have perfect knowledge on the other bits after a large number of iterations. A mapping proposed in [9] is called modified set partitioning (MSP), whose the labeling rule is shown in Figure 2.14(b). Simulation results in Figure 2.15 show an advantage of MSP over Gray mapping in the BICM-ID setup.

2.5 Orthogonal frequency division multiplexing

As mentioned earlier, frequency selectivity commonly happens in a wideband system. Note that a wide bandwidth is required for transmitting a high data rate
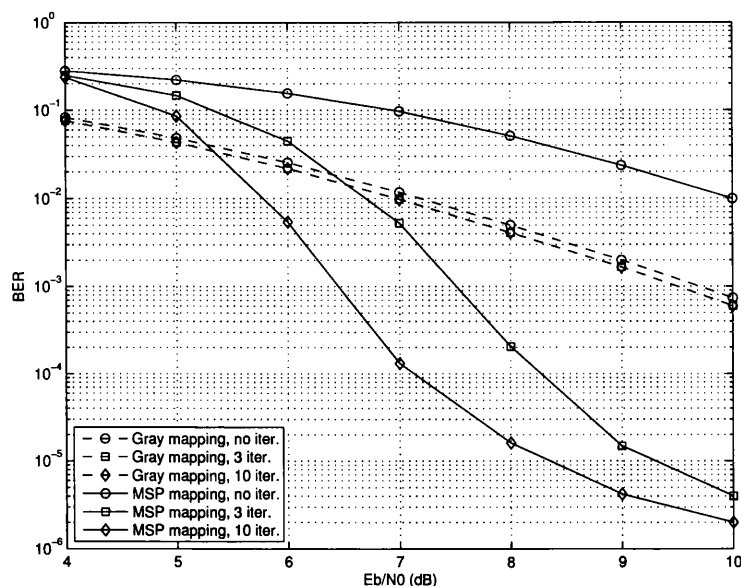
Figure 2.15: BER performances of BICM-ID systems with Gray and MSP mappings over the Rayleigh fading channel.

information stream. Due to frequency selectivity, the discrete channel in (2.12) can have a relatively large values of P, which causes an ISI from a symbol to another. To mitigate the ISI, equalizers can be used. However, the complexity required to equalize a channel with a relatively large P could be high, which might be undesirable in practice [41].

Orthogonal frequency division multiplexing (OFDM), introduced by Chang et al. [10], is an effective technique for transmitting signals in a frequency selective fading channel while it overcomes an issue of using a high complexity equalizer. In OFDM, a high data rate stream is divided into multiple sub-streams of lower data rates, which are transmitted over narrow bandwidth flat fading channels, each is carried by a subcarrier, without interference from one subcarrier to another. As each channel is flat fading, a one-tap equalizer can be used for detection/decoding.

Fig 2.16 illustrates the operation of OFDM. At the transmitter side, a stream of mapped symbols goes through a serial to parallel converter (S/P) to become a sequence of L size symbol vectors, where L is the number of subcarriers and each
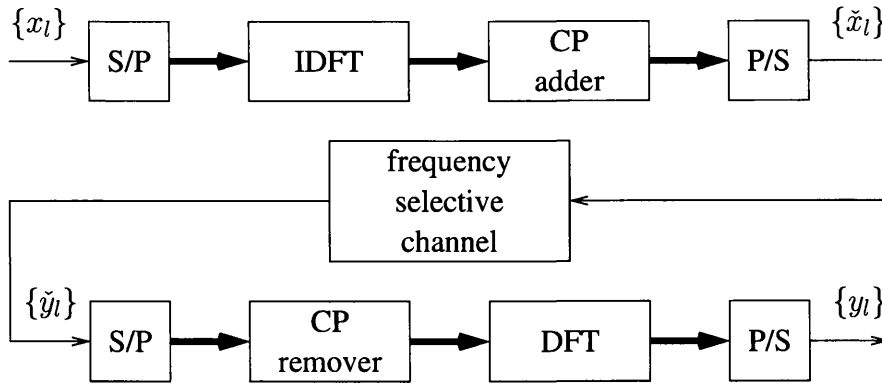
Figure 2.16: Orthogonal frequency division multiplexing.

vector is an OFDM symbol[1]. In an OFMD symbol, each symbol is carried by one of L subcarriers. An inverse discrete Fourier transform (IDFT) operator is used to convert OFDM symbols from the frequency domain to the time domain. In order to completely remove the interference from an OFDM symbol to another, a cyclic prefix (CP) is usually inserted in front of each OFDM symbol. The CP is simply a copy of some samples at the end of the OFDM symbol. At the receiver side, the received signals are processed inversely by the receiver, which comprises a concatenation of a CP remover, a discrete Fourier transform (DFT) operator, and a parallel to serial converter (P/S), before being detected/decoded. As channels are typically underspread, channel coefficients are usually assumed to be unchanged during a transmission of an OFDM symbol.

A system model for OFDM is described as follows. Under the assumption of unchanged channel coefficients during a transmission an OFDM symbol, we can drop the OFDM symbol index for simplicity. Let $\mathbf{h} = [h_0 \ h_1 \ \ldots \ h_{P-1}]^T$ be the CIR vector of length P, where P is the channel delay. Let $\breve{\mathbf{x}} = [\breve{x}_0 \ \breve{x}_1 \ \ldots \ \breve{x}_{L-1}]^T$ be the output vector of the IDFT operator. Let $\bar{P}$ is the length of CP, where $\bar{P} \geq P - 1$. The transmitted symbol vector of length $L + \bar{P}$ obtained by adding

---

· [1]In this thesis, "symbol"refers to a PSK/QAM symbol and "OFDM symbol"refers to a vector of L PSK/QAM symbols.

35

CP to $\breve{\mathbf{x}}$ is given as

$$\underbrace{[\breve{x}_{L-\bar{P}}\ \breve{x}_{L-\bar{P}+1}\ \ldots\ \breve{x}_{L-1}}_{\bar{P}\text{ samples}}\ \underbrace{\breve{x}_0\ \breve{x}_1\ \ldots\ \breve{x}_{L-1}]^T}_{L\text{ samples}}.$$

Let $\breve{\mathbf{y}} = [\breve{y}_0\ \breve{y}_1\ \ldots\ \breve{y}_{L-1}]^T$ be the received signal vector after removing CP. The lth element of this vector is given by

$$\breve{y}_l = \sum_{p=0}^{P-1} h_p \breve{x}_{(l-p) \pmod{L}} + \breve{w}_l,\ l = 0, 1, \ldots, L-1, \qquad (2.25)$$

where $\{\breve{w}_l\}$ is the sequence of independent background noise signals and $\breve{w}_l \sim \mathcal{CN}(0, N_0), \forall l$. Let $\breve{\mathbf{w}} = [\breve{w}_0\ \breve{w}_1\ \ldots\ \breve{w}_{L-1}]^T$. Note that $\breve{\mathbf{w}} \sim \mathcal{CN}(\mathbf{0}_{L,1}, N_0\mathbf{I}_L)$. Eq. (2.25) can be rewritten in a vector/matrix form as

$$\breve{\mathbf{y}} = \mathbf{H}\breve{\mathbf{x}} + \breve{\mathbf{w}}, \qquad (2.26)$$

where

$$\mathbf{H} = \begin{bmatrix} h_0 & 0 & \ldots & 0 & h_{P-1} & h_{P-2} & \ldots & h_1 \\ h_1 & h_0 & \ldots & 0 & 0 & h_{P-1} & \ldots & h_2 \\ \vdots & \vdots & \vdots & \vdots & \vdots & \vdots & \vdots & \vdots \\ 0 & 0 & \ldots & h_{P-1} & h_{P-2} & h_{P-3} & \ldots & h_0 \end{bmatrix}.$$

Since $\mathbf{H}$ is a circulant matrix, we have $\mathbf{H} = \mathbf{U}^{-1}\mathbf{\Lambda}\mathbf{U}$, where $\mathbf{U}$ is the DFT matrix of size $L \times L$ whose (l, l')th element is given by $[\mathbf{U}]_{l,l'} = \frac{1}{\sqrt{L}}\exp\left(-\frac{j2\pi ll'}{L}\right), l, l' \in \{0, 1, \ldots, L-1\}$, and $\mathbf{\Lambda}$ is a diagonal matrix of size $L \times L$ whose (l, l)th element is given by $[\mathbf{\Lambda}]_{l,l} = \breve{h}_l = [\sqrt{L}\mathbf{U}\mathbf{h}]_l, l \in \{0, 1, \ldots, L-1\}$. By multiplying both the sides of (2.26) by $\mathbf{U}$, we have

$$\mathbf{U}\breve{\mathbf{y}} = \mathbf{\Lambda}\mathbf{U}\breve{\mathbf{x}} + \mathbf{U}\breve{\mathbf{w}}$$

$$\mathbf{y} = \mathbf{\Lambda}\mathbf{x} + \mathbf{w}, \qquad (2.27)$$

where $\mathbf{y} = [y_0\ y_1\ \ldots\ y_{L-1}]^T = \mathbf{U}\breve{\mathbf{y}}$, $\mathbf{x} = [x_0\ x_1\ \ldots\ x_{L-1}]^T = \mathbf{U}\breve{\mathbf{x}}$, and $\mathbf{w} = [w_0\ w_1\ \ldots\ w_{L-1}]^T = \mathbf{U}\breve{\mathbf{w}}$. We also have $\mathbf{w} \sim \mathcal{CN}(\mathbf{0}_{L,1}, N_0\mathbf{I}_L)$ since $\mathbf{U}$ is a unitary matrix. Because $\mathbf{\Lambda}$ is diagonal, (2.27) can be presented by a set of L equations given as

$$y_l = \breve{h}_l x_l + w_l,\ l = 0, 1, \ldots, L-1, \qquad (2.28)$$
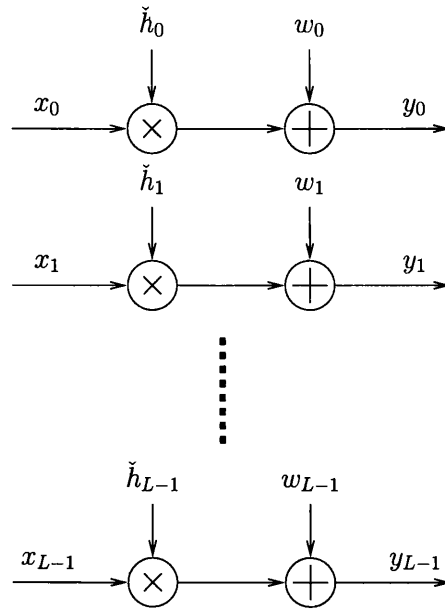
Figure 2.17: Equivalent parallel channels for OFDM.
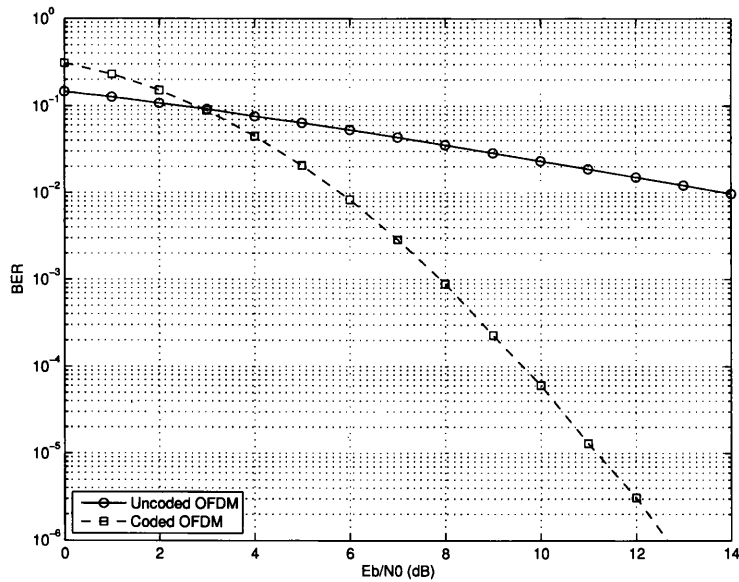
Figure 2.18: BER performances of coded OFDM and uncoded OFDM systems.

where $z_l \sim \mathcal{CN}(0, N_0)$. From (2.28), an OFDM channel is equivalent to a set of L parallel flat fading channels as illustrated in Figure 2.17.

Since the channel is frequency selective fading, the channel gain varies from a subcarrier to another. Channel coding in conjunction with bitwise interleaving can be used to exploit a frequency diversity. An OFDM system in which BICM is employed is referred to as a coded OFDM system. For demonstration purposes, Figure 2.18 shows a comparison between performances achieved by a coded OFDM and a uncoded OFDM systems. In both the systems, BPSK signaling is used for modulation and the number of subcarriers is 64. The coded OFDM system uses a half-rate convolutional code with generator (171,133) in octal as a channel code. Channels are frequency selective fading and the CIR vector of 16 independent elements independently changes from an OFDM symbol to another. The power delay profile is assumed as follows:

$$h_p \sim \mathcal{CN}\left(0, \frac{\exp(-\alpha p)}{1 - \exp(-\alpha)}\right), p = 0, 1, \ldots, 16,$$

with $\alpha = 1/3$. Channel coefficients are assumed to be estimated at the receiver perfectly. As shown in Figure 2.18, by exploiting the frequency diversity, the coded OFDM system outperforms the uncoded OFDM system.

2.6 Multiple-input multiple-output

Multiple-input multiple-output (MIMO) refers to a communication system in which both the transmitter and receiver can transmit and receive multiple data streams. Most of MIMO applications are in wireless communications, which is the scope limited in this thesis. In a wireless MIMO system, both the transmitter and receiver are equipped with multiple antennas. Special cases of MIMO are single-input multiple-output (SIMO) and multiple-input single-output (MISO), where the transmitter and the receiver are only equipped with a single antenna, respectively. Note that in a system with multiple transmit antennas, a symbol stream transmitted by an antenna at the transmitter can be interfered by other streams transmitted by other transmit antennas. In addition, signals also can

be received by multiple receive antennas in SIMO or MIMO systems. A MIMO system is able to use interferences as benefits in order to increase the data rate and/or improve the reliability. Due to its advantages, MIMO is included in modern standards such as IEEE 802.11n [26], IEEE 802.16 [27], and 3GPP long term evolution advanced (LTE-Advanced) [3].

MIMO systems can increase data rates since the capacity of MIMO channels, theoretically, linearly increases with the number of antennas [42, 43, 44]. The capacity increases, without any additional power consumption, is due to the fact that the numbers of dimensions increase at both the sides of a MIMO channel. Schemes that attempt to increase data rates are referred to as schemes for exploiting multiplexing gains, of which vertical Bell laboratories layered space time (V-BLAST) is a practically implementable approach [42, 45].

Since replicas of a signal can go through different paths, i.e., transmitted from and/or received by multiple antennas, which are fairly uncorrelated, antenna diversities, including transmit diversities and receive diversities, can be exploited and BER performances can be improved [12, 46]. Note that while a multiplexing gain requires both sides to be multidimensional, a diversity gain can be exploited from the multidimensionality at either transmit or receive sides. To exploit a transmit diversity gain, i.e, multiple antennas at the transmitter, space-time codes (STCs) [12] can be used. In [12], it was proved that the maximum diversity gain can be achieved in a MIMO system is equal to the product of the numbers of transmit and receive antennas. Among STCs, the Alamouti scheme [18], applied to the case of two transmit antennas, can be seen as a very simple but effective one, which, in fact, can achieve the full diversity while the code rate is 1 symbol per channel use. The Alamouti scheme falls into the family of orthogonal space-time block codes (O-STBC), for which a linear processing can be used at the receiver to deal with the multidimensionality [47]. It is noteworthy that as both the types of schemes, to exploit multiplexing and diversity gains, are based on the dimensional expansion in a MIMO system, we can exploit either a multiplexing gain or a diversity gain or both of them. If both of them are exploited in a system, there must be a trade-off between them. Comprehensive discussions on the fundamental trade-offs can be found in [48].

To demonstrate how a transmit diversity gain can be exploited, let us discuss the Alamouti scheme [18] for a 2×1 MIMO system as follows. Assume that the channel gains are kept unchanged in every two consecutive time slots. In each of the two time slots, the transmitter transmits an Alamouti codeword via its two transmit antennas. Let us drop the codeword index for simplicity. Denote by $[h_1 \ h_2]^T$ the channel vector in two consecutive time slots, where h_1 and h_2 are the channel gains from the first and second transmit antennas to the receive antenna, respectively. Assume that the system wants to transmit a symbol vector given by $[x_1 \ x_2]^T$ in this pair of time slots. In order to do that, an Alamouti codeword is formed as $\begin{bmatrix} x_1 & -x_2^* \\ x_2 & x_1^* \end{bmatrix}$. Let $[y_1 \ y_2]^T$ be the received signal vector, where $y_i, i = 1, 2$, is the signal received in the ith time slot. A system model for the 2×1 MIMO system is given by

$$[y_1 \ y_2] = [h_1 \ h_2] \begin{bmatrix} x_1 & -x_2^* \\ x_2 & x_1^* \end{bmatrix} + [w_1 \ w_2], \tag{2.29}$$

where w_1 and w_2 are two independent noise signals and $w_i \sim \mathcal{CN}(0, N_0), i = 1, 2$. After a simple algebraic manipulation, we have

$$\begin{bmatrix} y_1 \\ y_2^* \end{bmatrix} = \begin{bmatrix} h_1 & h_2 \\ h_2^* & -h_1^* \end{bmatrix} \begin{bmatrix} x_1 \\ x_2 \end{bmatrix} + \begin{bmatrix} w_1 \\ w_2^* \end{bmatrix}. \tag{2.30}$$

In (2.30), if h_1 and h_2 are independent, each transmitted symbol, i.e., $x_j, j = 1, 2$, is replicated and transmitted through two independent fading paths. Therefore, a diversity gain of order of two can be achieved. In addition, the detection problem for (2.30) can be seen as solving a set of two linear equations of two variables. Since $\mathbf{H} = \begin{bmatrix} h_1 & h_2 \\ h_2^* & -h_1^* \end{bmatrix}$ is an orthogonal matrix (two columns of the matrix are orthogonal), the interference from a transmitted symbol to the other can be canceled out by projecting the vector $[y_1 \ y_2^*]^T$ on a column of $\mathbf{H}$. Therefore, only linear signal processing is required for detection. Furthermore, for the general case of multiple antennas at the receiver, a further receive diversity gain can be exploited by performing a maximal ratio combining (MRC) after the cancellation process [18, 47].

Fig 2.19 shows the BER performances for 2×1 MISO and 2×2 MIMO systems that use Alamouti scheme. It confirms that 2×1 MISO and 2×2 MIMO systems
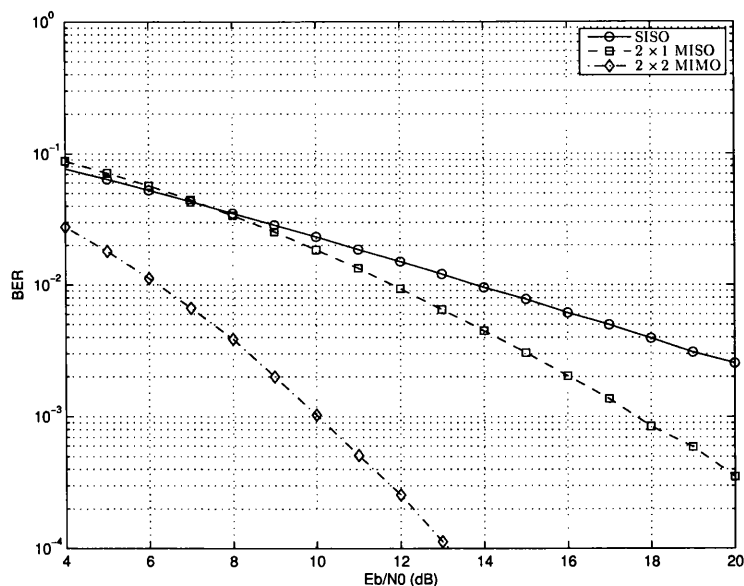
Figure 2.19: BER performances of 1×1 single-input single-output, 2×1 MISO, and 2×2 MIMO systems.

can achieve diversity orders of two and four, respectively. Note that no diversity gain is achieved in a uncoded single-input single-output system, in which both the transmitter and receiver are equipped with single antennas.

2.7 Two-way relay networks and physical-layer network coding

To achieve a good performance, a system certainly requires a sufficient SNR. Sometimes, due to a number of system constraints, such as a transmission power limitation or a large distance from the transmitter to the receiver, a direct communication might not be possible. In such the cases, relays can be used to help establish a communication from a transmitter to a receiver. Note that with the presences of relays, network topologies could be more complicated. For some specific networks with relays, especially for the ones that serve one directional transmissions, network capacities could be found according to the max-flow min-

41

cut theorem [49, Chapter 15, Section 15.7].
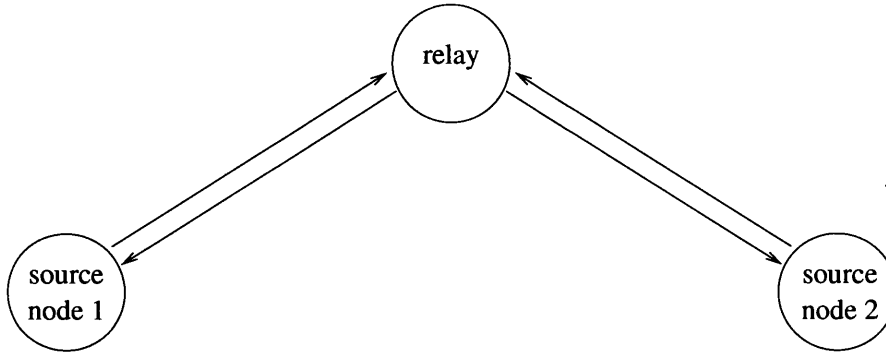
Figure 2.20: A two-way relay network.

In this section, we consider a relay network consisting of there nodes, two source nodes and a relay, and four directional links between the source nodes and the relay. The two source nodes want to simultaneously exchange their information between each other. In the network, no direct link between two source nodes is assumed and if a source node want to communicate with the other, it must be assisted by the relay. This network is called a two-way relay network (TWRN) and is illustrated in Figure 2.20. In addition, we assume that the transmission and reception of signals can not be operated at the same time due to a high interference from a transmit antenna to a receive antenna. Therefore, all the nodes, including the source nodes and relay, operate in the half-duplex mode. It can be observed that, in this network, to complete a cycle of exchanging a pair of symbols between two source nodes, the simplest operational method requires four time slots.

As wireless channels are considered, it is possible that the relay can receive signals transmitted by the two source nodes simultaneously. In addition, both the two source nodes (which become two sink nodes while receiving) can receive a signal broadcasted by the relay nodes. Therefore, the number of time slots required for exchanging a pair of symbols can be reduced from four to three or even two. By reducing the number of required time slots, the exchanging data rate can be increased. In order to achieve the rate of one symbol per time slot in two-way exchange, the relay must be able to decode a desired function of

information sent by two source nodes and then broadcast this function to the two source nodes. Furthermore, each source node must be able to decode the information sent by the other based on the function received from the relay and its own information. A function with the roles described above is called a *network code*.

The method of *network coding* was introduced by Ahlswede et al. in [50]. In this seminal work, network coding, carried out in bottleneck relays, has been shown to be an effective approach to achieve the network capacity. Note that in many research works including [50, 51, 52, 53], network coding is performed at the network layer in order to increase throughputs. In these works, networks are considered to have error-free links. That means, each link in a network is assigned a number of capacity units and throughputs are analyzed under the assumption that each link can be used to transmit with transmission rate equal to its capacity.

Network coding can be performed at the physical layer. In this case, the term physical-layer network coding (PNC) [11, 54] is used to define a function of information sent by two source nodes. By allowing the relay to broadcast the PNC function, we can save the time slots required for information exchange in a TWRN. Interestingly, there were some protocols in an independent work in [55], which were proposed to increase the achievable exchanging data rate in a TWRN. In [55], although the term PNC is not used, the proposed idea is very similar to that in [11, 54], where the ability of performing coding at the relay node was shown as an advantage.

A simple PNC is presented as follows. We assume that uncoded BPSK signals are transmitted by the two source nodes. Let x_1 and x_2, where $x_1, x_2 \in \{-1, 1\}$, be the two symbols the source nodes want to exchange. A cycle of exchanging information is carried out in two time slots. In the first time slot, both the two source nodes transmit their signals simultaneously. Under the assumption of perfect synchronization, the relay receives a signal given by

$$r = h_1 x_1 + h_2 x_2 + w_R, \qquad (2.31)$$

where h_1 and h_2 are the channel gains for the channels from the first and second source nodes to the relay, respectively, and w_R, $w_R \sim \mathcal{CN}(0, N_{0,R})$, is the background noise at the relay. The relay attempts to decode a function of x_1 and x_2, which is defined as $z = x_1 x_2$. Let $\hat{z}$ denote the decoded version of z at the relay. In the second time slot, the relay broadcast $\hat{z}$ to both the two sinks, which play the roles of sources in the previous time slot. The ith sink, $i = 1, 2$, receives

$$y_i = g_i \hat{z} + w_i, \qquad (2.32)$$

where g_i is the channel gain for the channel from the relay to the ith sink and w_i, $w_i \sim \mathcal{CN}(0, N_{0,i})$, is the background noise at the ith sink. The ith sink then decode $\hat{z}$ from it received signal, i.e., y_i. In this node, the symbol sent by the other node is detected by performing a multiplication between the decoded symbol sent by the relay and its own symbol transmitted in the first time slot. In particular, let $\check{z}_i$ be the decoded version of $\hat{z}$ in the ith sink. The two detected symbols are respectively given by $\check{x}_2 = \check{z}_1 x_1$ and $\check{x}_1 = \check{z}_2 x_2$.
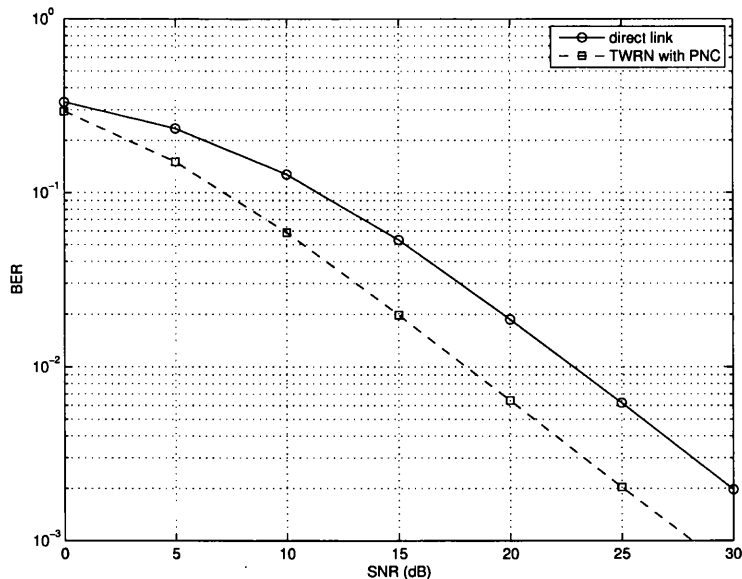
Figure 2.21: BER performance of Two-Way Relay Systems.

Figure 2.21 shows the performance of the system described above. The channels are assumed to be Rayleigh fading. All of nodes are assumed to have a

identical SNR. For comparison purposes, we include a system of direct link in simulations. The distance between two nodes in the direct link system is assumed to be twice as the distance between each source node and the relay in TWRN. A path loss exponent of 3 is assumed. Therefore, the SNR at the destination/sink node in the direct link system is 1/8 of that of each node in TWRN. Note that in completing an exchange of two bits sent by two source nodes, both systems require two time slots. For such the type of channels, we can see the advantage of the relay system over the direct link system, i.e., a two-way system without relay.

2.8 Summary

In this chapter, main characteristics of wireless channels were presented. Wireless channels suffer from fading, i.e., the channel state vary with time. Over a fading channel, diversity techniques can be used to achieve a better reliability. This chapter also presented *state-of-the-art* coded systems. In such systems, coding plays very important roles, which can allow the systems exploit diversity gains. With channel coding in conjunction with bitwise interleaving, time diversities can be exploited. For a system with a wide bandwidth, a frequency selectivity can potentially provide a frequency diversity. Coded OFDM is a practical approach to exploit frequency diversity gains provided by frequency selective channels. In a system with multiple antennas at the transmitter, space-time codes could be used to exploit antenna diversities. Finally, physical-layer network coding in bidirectional networks with relay (two-way relay networks) was introduced in this chapter. In a two-way relay network, the conventional approach requires four time slots for exchanging a pair of symbols. To achieve a higher spectral efficiency, physical-layer network coding was shown to be an efficient approach.

3

Symbol mapping design based on parameterized EXIT function

3.1 Introduction

Bit-interleaved coded modulation (BICM) can provide good performances over fading channels with a relatively simple structure [37, 5, 6]. In order to further improve the performance, iterative decoding (ID) has been employed in [8]. The resulting system is called BICM with iterative decoding (BICM-ID). With non-iterative decoding, Gray mapping is known to be optimal in terms of providing the lowest bit error rate (BER) for most signal-to-noise ratio (SNR) values [5]. However, in the BICM-ID paradigm, as reported in [9, 13, 14], Gray mapping is not optimal and the symbol mapping can be optimized to improve the performance after convergence. Due to the importance of mapping rules, it is desirable to find an optimal mapping rule in conjunction with a channel code employed in a BICM-ID system. This chapter addresses a problem of symbol mapping design in a BICM-ID system.

For iterative receivers, extrinsic information transfer (EXIT) charts have been widely used to understand convergence properties and performance [15, 56]. Under the binary erasure channel (BEC) model for *a priori* information, it was shown in [57] that the area under an EXIT function of a demapper is decided

by the coded modulation (CM) capacity [5], (the area property). Furthermore, it implies that we can design a capacity-achieving scheme by matching the two EXIT functions of the demapper and channel decoder under the BICM-ID setup.

Motivated by the area property, curve-fitting approaches have been used to meet matching criteria for code designs [58, 59, 60] and symbol mapping designs [61, 62, 63]. By using curve-fitting approaches, capacity-achieving schemes can be found under certain conditions (e.g., ergodic channels, sufficiently long codewords, an unlimited number of iterations for convergence). However, two scenarios should be considered: i) fast fading channels with a limited number of iterations; and ii) slow fading channels with an unlimited number of iterations. Under these scenarios, the required SNR should be higher than the threshold SNR for convergence. Therefore, we deem that there should be a gap between the two EXIT functions under such scenarios.

As the gap between the two EXIT functions is considered, the matching criterion may no longer be suitable. Therefore, we propose a design criterion, which we call the *maximum flatness criterion*, for a constant difference between the EXIT function of the demapper and decoder, i.e., flat tunnel. Based on this criterion, the following advantages can be achieved: i) a faster convergence over fast fading channels; ii) a lower outage probability over slow fading channels. Note that the meaning of flatness in this thesis is different from the flattening idea mentioned in [64]. That is, while the term flatness in this thesis is applied to the function of difference between the two EXIT functions of the demapper and decoder (tunnel function), the design procedure in [64] attempts to flatten only the detector's EXIT function when a capacity-achieving channel code, (e.g., turbo code, low-density parity-check (LDPC) code), whose EXIT function is already sufficiently flat, is used. To apply the proposed flatness criterion, a curve-fitting approach may not be directly applicable since the two EXIT curves can no longer be matched. Therefore, we propose to adopt a parametric approach for design purposes.

It will be shown that the EXIT function of the demapper is a weighted sum of binomial functions, where the weights are the average mutual information (MI) between a received signal and a coded bit in a transmitted symbol under the

47

assumption that some of other bits in the group of labeling the transmitted symbol are explicitly known. Therefore, we can parameterize the EXIT function of the demmaper by the coefficients for the binomial basis. The number of parameters is equal to the number of bits in the label of a transmitted symbol. Interestingly, these parameters only depends on the mapping rule employed and the channel characteristics. Therefore, a numerical method can be used to compute the EXIT function's parameters. For a function in the space spanned by the binomial functions, representing it by a weighted sum of elements in an orthonormal basis, whose first element is a constant function, allows us to see the flatness of this function. The orthonormal basis can be obtained from the binomial basis via the Gram-Schmidt (GS) procedure [65]. The flatness of the difference between the EXIT functions of the demapper and decoder (the tunnel function) is maximize. Note that to obtain the tunnel function we need to know both the EXIT functions of the demmaper and decoder. While the parameters for the EXIT function of the demapper can be obtained by a numerical method, those for the decoder is obtained by simulations. Nevertheless, given a fixed channel code and channel characteristics, the tunnel function depends on the mapping rule employed via its coefficients in representing it with the orthogonal basis. Finally, once the problem is formulated, a search algorithm modified from the binary switching algorithm (BSA) proposed in [13] can be used to find a desired mapping rule.

The remainder of this chapter is organized as follows. Section 3.2 presents the system model. In Section 3.3, we develop a parameterization of the EXIT function of the demapper. Section 3.4 comprises the main contributions of this chapter, where motivations is presented, the flatness criterion for symbol mapping design is formally stated, a design problem is formulated, and an illustrative example is provided to demonstrate the proposed approach. Simulation results are shown in Section 3.5. Finally, this chapter is summarized in Section 3.6.

3.2   System model

A block diagram for the overall system is illustrated in Figure 3.1. At the transmitter, we employ BICM [5] to transmit coded sequences over a fading channel.
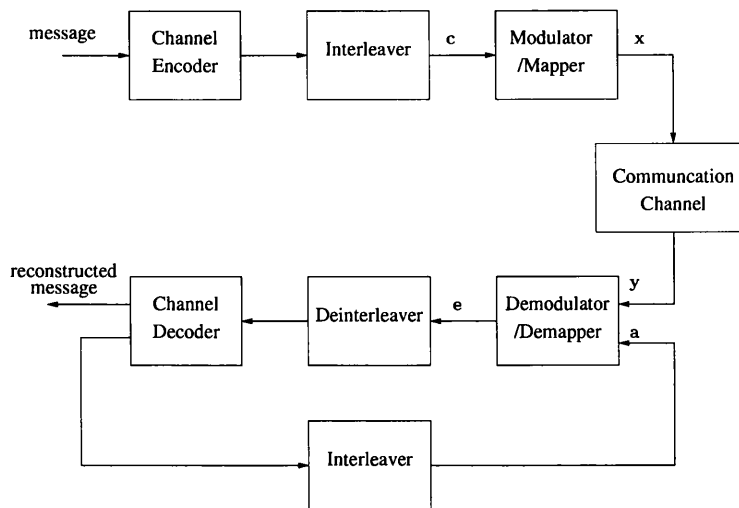
Figure 3.1: Block diagram of a BICM-ID system.

A binary message of K bits is encoded by a channel encoder to obtain a binary codeword consisting of N coded bits, where the code rate is $R_c = K/N$. A random bitwise interleaver is used to break the correlation between consecutive bits in a codeword. The interleaved sequence of coded bits is divided into a number of chunks, each of them consists of m bits. Note that N is assumed to be an integer multiple of m. Denote by $\mathbf{c}_l = [c_l^{(1)}, c_l^{(2)}, \ldots, c_l^{(m)}]^T$, $0 \le l \le N/m - 1$, the vector presenting the lth chunk of bits. This vector is further mapped onto symbol $x_l \in \mathcal{X}$ by a mapping rule, denoted by μ, i.e., $\mu(\mathbf{c}_l) = x_l$, where $\mathcal{X}$ is the symbol alphabet of size $|\mathcal{X}| = 2^m$. Here, $\mathcal{X} \subset \mathbb{C}$, where $\mathbb{C}$ denotes the set of complex numbers, is assumed. The average energy of symbols in $\mathcal{X}$ is normalized as $\frac{1}{2^m} \sum_{x \in \mathcal{X}} |x|^2 = 1$.

Mapped symbols are transmitted over a block-fading channel [66]. A block-fading model is commonly assumed for a correlated slow fading channel, e.g., in a multi-carrier orthogonal frequency division multiplexing (OFDM) system. In particular, the duration of transmitting every codeword, which has the length of N/m symbols, is divided into B blocks of equal lengths. The length of each block, which is given by $T = N/(mB)$, is assumed to be an integer. Here, B is called the fading degrees of freedom [67]. We assume that channel coefficients

49

remain constant within a block, but different from a block to another. In order to see the impact of B, we will consider two different cases of large and small B for fast and slow fading channels, respectively. The received signal is given by

$$y_l = \sqrt{\bar{\gamma}} h_t x_l + w_l,$$

where $t = \lfloor l/T \rfloor$, $\bar{\gamma}$ is the average SNR, h_t is the channel coefficient in the tth block, and n_t is the background noise with $w_l \sim \mathcal{CN}(0, 1)$. Under the block-fading model, $\{h_t\}$ is an independent and identically distributed (iid) sequence of circularly symmetric complex Gaussian (CSCG) elements and $h_t \sim \mathcal{CN}(0, 1)$ (Rayleigh fading). Furthermore, the channel state information (CSI) is assumed to be perfectly known to the receiver. The instantaneous SNR of block t is defined as $\gamma_t = \bar{\gamma} |h_t|^2$. Note that the instantaneous SNR varies from a block to another independently. With this model of $\{h_t\}$, the channel is characterized by a probability density function (pdf) of SNR given by $p_\gamma(\gamma) = \frac{1}{\bar{\gamma}} \exp\left(-\frac{\gamma}{\bar{\gamma}}\right)$.

At the receiver, the maximum *a posteriori* (MAP) symbol detection and channel decoding are iteratively performed with exchanging extrinsic information [8]. In both constituent components, which are a demapper and a channel decoder, the log likelihood ratio (LLR) is used as the soft information for each (input or output) coded bit. In particular, for a given received signal sequence, i.e., $\{y_l\}$, and *a priori* information sequence, denoted by $\{a_l^{(i)}\}$, the demapper produces an extrinsic information sequence, denoted by $\{e_l^{(i)}\}$. The channel decoder, in turn, uses the deinterleaved version of $\{e_l^{(i)}\}$ as its *a priori* information to compute its extrinsic information, which is then fed back to the input of the demapper through an interleaver. Note that in the first iteration, no prior knowledge on the coded bit sequence is available to the demapper, i.e., $\{a_l^{(i)}\}$ is an all-zero sequence in the first iteration. The values of $\{a_l^{(i)}\}$ and $\{e_l^{(i)}\}$ are iteratively updated after every iteration.

3.3 Parameterized EXIT functions

In this section, we focus on the parameterization of EXIT functions to derive a mapping design approach in Section 3.4.

3.3.1 Types of EXIT functions
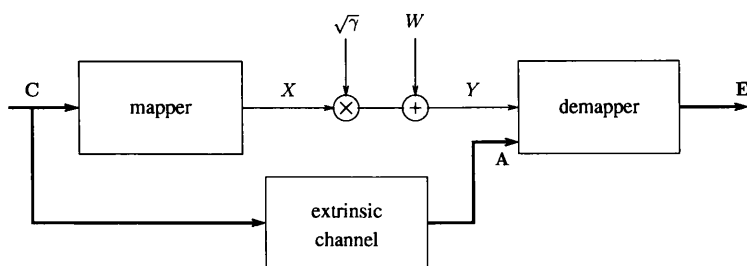
Figure 3.2: A model for *a priori* information.

In order to see how an EXIT function of the demapper is constructed, let us consider an abstract model introduced by Ashikhmin in [57] illustrated in Figure 3.2. In this model, a coded bit vector $\mathbf{C} = [C^{(1)} \ C^{(2)} \ \ldots \ C^{(m)}]^T$ is mapped onto a symbol $X \in \mathcal{X}$ by a mapper according to a mapping rule $X = \mu(\mathbf{C})$. Here, $C^{(1)}, C^{(2)}, \ldots, C^{(m)}$ are the output of an interleaver. Under the assumption of ideal interleaving, $C^{(1)}, C^{(2)}, \ldots, C^{(m)}$ are identically and uniformly distributed over $\{0, 1\}$. X is thus uniformly distributed over $\mathcal{X}$. This symbol is transmitted over a communications channel modeled by

$$Y = \sqrt{\gamma}X + W,$$

where Y is the received signal, γ is the SNR, and W is the white Gaussian noise. Note that in this model, $C^{(i)}, i = 1, 2, \ldots, m$, X, W, and Y are considered as random variables, while γ is firstly considered as a parameter of the communications channel. The demapper is a soft-input soft-output processor, which produce an extrinsic LLR vector $\mathbf{E} = [E^{(1)} \ E^{(2)} \ \ldots \ E^{(m)}]^T$ for the coded bit vector based on the MAP principle. In the model shown in Figure 3.2, a dummy channel, called the extrinsic channel, uses $\mathbf{C}$ to produce a vector $\mathbf{A} = [A^{(1)} \ A^{(2)} \ \ldots \ A^{(m)}]^T$. Since $\mathbf{A}$ is considered as *a priori* information for the demapper, the *a priori* MI of the demapper is defined as

$$I_A = \frac{1}{m} \sum_{i=1}^{m} I(A^{(i)}; C^{(i)}).$$

Note that instead of considering $\mathbf{A}$ as the output of channel decoder, we consider it as the output of the extrinsic channel, which is characterized by a single parameter I_A, for convenience. By defining extrinsic MI of the demapper as

$$I_E = \frac{1}{m} \sum_{i=1}^{m} I(E^{(i)}; C^{(i)}),$$

we can see that I_E depends on μ, γ, and I_A. In representing I_E as a function of μ, γ, and I_A, we have the EXIT function of the demapper written as follows:

$$I_E = f_{dem}(I_A, \mu, \gamma). \tag{3.1}$$

To distinguish with other EXIT functions defined later, $f_{dem}(I_A, \mu, \gamma)$ is referred to as the instantaneous EXIT function for a given γ.

Now, if we consider γ is a random variable, which is distributed according to a pdf $p_\gamma(\gamma)$, $f_{dem}(I_A, \mu, \gamma)$ becomes a random function. Define the ergodic EXIT function as

$$
\begin{aligned}
I_E &= \bar{f}_{dem}\left(I_A, \mu, p_\gamma(\gamma)\right) \\
&\stackrel{\triangle}{=} \mathbb{E}\left[f_{dem}(I_A, \mu, \gamma)\right],
\end{aligned} \tag{3.2}
$$

where the expectation is taken with respect to $p_\gamma(\gamma)$. According to the definitions in (3.1) and (3.2), $f_{dem}(I_A, \mu, \gamma)$ is considered as the EXIT function for an AWGN channel, while $\bar{f}_{dem}\left(I_A, \mu, p_\gamma(\gamma)\right)$ is considered as the EXIT function for an ergodic fading channel. As we assume $p_\gamma(\gamma)$ is an exponential function characterized by a single parameter $\bar{\gamma}$, i.e., a Rayleigh fading channel is assumed, we compactly rewrite the ergodic EXIT function as $\bar{f}_{dem}\left(I_A, \mu, \bar{\gamma}\right)$.

For a block-fading channel with B degrees of freedom, let $\mathbf{\Gamma} = [\gamma_0 \; \gamma_1 \; \ldots \; \gamma_{B-1}]^T$ denote a vector of B elements of SNRs. Since the elements of $\mathbf{\Gamma}$ are iid, the MI between the input of the mapper and the output of the demapper become the average of MI for all the elements of $\mathbf{\Gamma}$. Define the average EXIT function as

$$
\begin{aligned}
I_E &= f_{dem-bf}(I_A, \mu, \mathbf{\Gamma}) \\
&= \frac{1}{B} \sum_{t=0}^{B-1} f_{dem}(I_A, \mu, \gamma_t).
\end{aligned} \tag{3.3}
$$

When $B \to \infty$, $f_{dem-bf}(I_A, \mu, \mathbf{\Gamma})$ converges to the ergodic EXIT function. Here, $B \to \infty$ in the sense that m and T are fixed and $N \to \infty$, i.e., infinite codeword length.

3.3.2   Parameterized EXIT functions

To parameterize the EXIT functions defined above, we use a model introduced in [57] for the extrinsic channel in Figure 3.2. In particular, we assume that the extrinsic channel is a parallel concatentation of m independent and identical memoryless BECs. Under the BEC model, $X^{(i)} \in \{0, 1\}, A^{(i)} \in \{0, \Omega, 1\}$ for $i = 1, 2, \ldots, m$, where Ω represents the erasure. Through the extrinsic channel, an erasure event happens when $A^{(i)} = \Omega$, i.e., $A^{(i)} \neq X^{(i)}$. Let δ denote the erasure probability for each BEC, which is defined as $\delta \overset{\triangle}{=} \Pr(A^{(i)} = \Omega | X^{(i)} = 0) = \Pr(A^{(i)} = \Omega | X^{(i)} = 1)$. For given I_A, the MI between the input and output of the extrinsic channel, the erasure probability is obtained by $\delta = 1 - I_A$.

Let
$$\mathbf{A}^{[i]} \overset{\triangle}{=} \left[A^{(1)} \ldots A^{(i-1)}, A^{(i+1)} \ldots A^{(m)} \right]^T.$$

Denote by $\mathcal{B}_k^{(i)}$, where $0 \leq k \leq m - 1$, the event that k bits in $\mathbf{A}^{[i]}$ are known, i.e., $m - 1 - k$ elements in $\mathbf{A}^{[i]}$ are equal to Ω. The probability of $\mathcal{B}_k^{(i)}$ for given I_A becomes

$$
\begin{aligned}
\Pr\left(\mathcal{B}_k^{(i)}\right) &= \binom{m-1}{k}(1 - \delta)^k \delta^{(m-1-k)} \\
&= \binom{m-1}{k}(I_A)^k(1 - I_A)^{(m-1-k)} \\
&\overset{\triangle}{=} \alpha_k(I_A).
\end{aligned}
\tag{3.4}
$$

Note that $\alpha_k(I_A)$ does not depend on i, the bit posistion of interest.

Based on the BEC model, a derivation of $f_{dem}(I_A, \mu, \gamma)$ can be written as

follows:

$$
\begin{aligned}
f_{dem}(I_A, \mu, \gamma) &= \frac{1}{m} \sum_{i=1}^{m} I\left(X^{(i)}; E^{(i)}\right) \\
&\stackrel{\text{(a)}}{=} \frac{1}{m} \sum_{i=1}^{m} I\left(X^{(i)}; Y, \mathbf{A}^{[i]}\right) \\
&\stackrel{\text{(b)}}{=} \frac{1}{m} \sum_{i=1}^{m} I\left(X^{(i)}; Y | \mathbf{A}^{[i]}\right) \\
&\stackrel{\text{(c)}}{=} \frac{1}{m} \sum_{i=1}^{m} \sum_{k=0}^{m-1} \left[\Pr\left(\mathcal{B}_k^{(i)}\right) I\left(X^{(i)}; Y | \mathcal{B}_k^{(i)}\right) \right] \\
&\stackrel{\text{(d)}}{=} \frac{1}{m} \sum_{k=0}^{m-1} \left[\alpha_k(I_A) \sum_{i=1}^{m} I\left(X^{(i)}; Y | \mathcal{B}_k^{(i)}\right) \right],
\end{aligned}
\tag{3.5}
$$

where (a) is due to the fact that the MAP demapper is used, (b) is due to the fact that $X^{(i)}$ and $\mathbf{A}^{[i]}$ are independent, (c) is derived based on the definition of conditional MI, and (d) is a direct substitution from (3.4). Let the average extrinsic MI for given other k bits known be

$$
I_E^k(\mu, \gamma) = \frac{1}{m} \sum_{i=1}^{m} I(X^{(i)}; Y | \mathcal{B}_k^{(i)}).
\tag{3.6}
$$

Here, $I(X^{(i)}; Y | \mathcal{B}_k^{(i)})$ can be obtained by a Monte Carlo numerical integration method [68, 69]. Note that $I_E^k(\mu, \gamma)$ is independent of the amount of prior information represented by I_A. Substituting (3.6) into (3.5), we have

$$
f_{dem}(I_A, \mu, \gamma) = \sum_{k=0}^{m-1} I_E^k(\mu, \gamma) \alpha_k(I_A).
\tag{3.7}
$$

From this, the average and ergodic EXIT functions, defined in (3.3) and (3.2), respectively, are given by

$$
f_{dem-bf}(I_A, \mu, \mathbf{\Gamma}) = \sum_{k=0}^{m-1} I_{E-bf}^k(\mu, \mathbf{\Gamma}) \alpha_k(I_A)
\tag{3.8}
$$

$$
\text{and } \bar{f}_{dem}(I_A, \mu, \bar{\gamma}) = \sum_{k=0}^{m-1} \bar{I}_E^k(\mu, \bar{\gamma}) \alpha_k(I_A),
\tag{3.9}
$$

respectively, where

$$I_{E-bf}^{k}(\mu, \mathbf{\Gamma}) = \frac{1}{B} \sum_{t=0}^{B-1} I_{E}^{k}(\mu, \gamma_t) \qquad (3.10)$$

$$\text{and } \bar{I}_{E}^{k}(\mu, \bar{\gamma}) = \mathbb{E}\left[I_{E}^{k}(\mu, \gamma)\right]. \qquad (3.11)$$

Consequently, the ergodic EXIT function of the demapper can be parameterized as a weighted sum of binomial functions. In other words, given μ and $\bar{\gamma}$, the set of m parameters for $f_{dem}(I_A, \mu, \bar{\gamma})$ are $\bar{I}_{E}^{k}(\mu, \bar{\gamma})$'s, $0 \le k \le m-1$. While the ergodic EXIT function of the demapper is represented by discrete values of I_A in [68], the parametric model here can provide the ergodic EXIT function for any value of $I_A \in [0, 1]$. Note that, based on the chain rule of MI, the parameters have the following property:

$$\sum_{k=0}^{m-1} \bar{I}_{E}^{k}(\mu, \bar{\gamma})) = I\left(X^{(1)}, X^{(2)}, \ldots, X^{(m)}; Y\right)$$
$$= I(X; Y)$$
$$\triangleq C_{cm}(\bar{\gamma}), \qquad (3.12)$$

which is referred to as the ergodic CM capacity [5].

Similar to the EXIT functions of the demapper, the EXIT function of the decoder is defined as

$$I_E = f_{dec}(I_A), \qquad (3.13)$$

where I_A is the MI between *a priori* LLRs of decoder and a coded bits and I_E is the MI between extrinsic LLRs of decoder and coded bits. Note that the decoder has only one input, which is the *a priori* LLR sequence provided by the demapper, the EXIT function of the decoder is independent of SNR.

Although the EXIT function of the decoder can be parameterized in some special cases (for mainly LDPC codes and repeat accumulate (RA) codes [57, 58, 59, 70]), there is no analytical approach to derive EXIT functions of decoders in general yet. We thus use a simulation based approach to find $f_{dec}(I_A)$ for a convolutional code that will be used in an illustrative example.

3.4 Symbol mapping design based on parameterized EXIT function

3.4.1 Motivations

In an EXIT chart, which is a 2-D plane where the EXIT functions of the demapper and channel decoder are plotted in, the decoding process can be represented by the evolution of the trajectory through the tunnel bounded by the two EXIT functions. If the input MI of the demapper and the output MI of the channel decoder are both represented in the horizontal axis (the x-axis), the vertical axis will represent $f_{dem-bf}(x, \mu, \Gamma)$ and $f_{dec}^{-1}(x)$ for the demapper and decoder, respectively. The trajectory cannot pass over the intersection point of the two EXIT curves. If an early intersection occurs, the performance is very poor. On the other hand, if the intersection point is sufficiently close to 1 (the maximum MI at bit level), we deem that a reasonable performance can be achieved. We often say that the decoding process does not converge in the former case, and converges in the latter case.

Note that the possibility of successful decoding discussed above is for single codeword and it could vary from a codeword to another. It is because while the EXIT function of the channel decoder, i.e., $f_{dec}^{-1}(x)$, does not depend on the channel state and is fixed for any channel realization (Γ), the EXIT function of the demapper ($f_{dem-bf}(x, \mu, \Gamma)$), depends on the channel realization, which is assumed to be changed for different transmissions of codewords. There are certainly different shapes of tunnels for different $f_{dem-bf}(x, \mu, \Gamma)$. Recall that the expectation of $f_{dem-bf}(x, \mu, \Gamma)$ is $\bar{f}_{dem}(x, \mu, \bar{\gamma})$. If we consider a specific mapping μ, the tunnel between $\bar{f}_{dem}(x, \mu, \bar{\gamma})$ and $f_{dec}^{-1}(x)$ is deterministic for a fixed $\bar{\gamma}$. In the following, we will explain why this tunnel with the flatness property is desirable for both the two cases: i) fast fading, i.e., a large B, and ii) slow fading, i.e., a small B.

For a fast fading channel, $f_{dem-bf}(x, \mu, \Gamma)$ is almost identical to $\bar{f}_{dem}(x, \mu, \bar{\gamma})$. Therefore, if the number of iterations is not restricted, as long as the tunnel between $\bar{f}_{dem}(x, \mu, \bar{\gamma})$ and $f_{dec}^{-1}(x)$ is open, ID can converge as explained earlier.

However, we can observe that the number of iterations required for convergence increases if the tunnel has a narrow gap section. While a small number of iterations for convergence provides a significant advantage for delay and/or computing constrained receivers, it is always desirable to avoid possible narrow gap sections between the two EXIT functions.

For a slow fading channel, we need to consider $f_{dem-bf}(x, \mu, \mathbf{\Gamma})$ as it could be different of $\bar{f}_{dem}(x, \mu, \bar{\gamma})$. Even thought the mean of $f_{dem-bf}(x, \mu, \mathbf{\Gamma})$ is given by $\bar{f}_{dem}(x, \mu, \bar{\gamma})$, a smaller B leads to the larger variation of $f_{dem-bf}(I_A, \mu, \mathbf{\Gamma})$ from one realization of $\mathbf{\Gamma}$ to another. In this case, considering the outage probability is more meaningful [71]. Note that if ϵ is chosen such that a low (codeword or bit) error rate is achieved when the two EXIT functions $f_{dem-bf}(x, \mu, \mathbf{\Gamma})$ and $f_{dec}^{-1}(x)$ intersect at any $x \in [0, 1 - \epsilon]$, the outage event is defined as an event when the intersection falls inside this region. From our simulations, we found that the distributions of $f_{dem-bf}(x, \mu, \mathbf{\Gamma})$ are almost identical for all $x \in [0, 1 - \epsilon]$. Under the assumption of identical distributions, the outage probability can be written as follows:

$$P_{out} = \Pr\left(f_{dem-bf}(x^*, \mu, \mathbf{\Gamma}) < f_{dec}^{-1}(x^*)\right), \tag{3.14}$$

where $x^* = \arg\min_{0 \le x \le 1-\epsilon} \left|\bar{f}_{dem}(x, \mu, \bar{\gamma}) - f_{dec}^{-1}(x)\right|.$

If B is not too small (larger or equal to 10), supported by the central limit theorem, we can model the variation of $f_{dem-bf}(x^*, \mu, \mathbf{\Gamma})$ as a Gaussian random variable. Note that the variance of $f_{dem-bf}(x^*, \mu, \mathbf{\Gamma})$ is equal to $\frac{1}{B}$ of that of $f_{dem}(x^*, \mu, \gamma)$. The outage probability can be predicted based on this variance. As the area under $\bar{f}_{dem}(x, \mu, \bar{\gamma})$ is a constant for any μ, a mapping of flatter tunnel between $\bar{f}_{dem}(x, \mu, \bar{\gamma})$ and $f_{dec}^{-1}(x)$ results in a lower outage probability.

Our aim is to design a symbol mapping rule such that it can provide the maximum flatness between the two EXIT functions, $\bar{f}_{dem}(x, \mu, \bar{\gamma})$ and $f_{dec}^{-1}(x)$, in order to achieve a less number of iterations required for convergence or a lower outage probability. We will formulate a problem accordingly below.

3.4.2 Maximum flatness criterion

For a fixed $\bar{\gamma}$, let $f_1(x;\mu) = \bar{f}_{dem}(x,\mu,\bar{\gamma})$ and $f_2(x) = f_{dec}^{-1}(x)$. Define the tunnel function, which is the difference between the two EXIT functions, as

$$D(x;\mu) = f_1(x;\mu) - f_2(x), \ 0 \leq x \leq 1, \tag{3.15}$$

where $f_2(x)$ is fixed. Here, $f_1(x;\mu)$ is parameterized as

$$f_1(x;\mu) = \sum_{k=0}^{m-1} w_k(\mu)\alpha_k(x), \tag{3.16}$$

where the weights $w_k(\mu)$'s $(w_k(\mu) = \bar{I}_E^k(\mu,\bar{\gamma}))$ are constrained as follows:

$$\sum_{k=0}^{m-1} w_k(\mu) = C_{cm}(\bar{\gamma});$$
$$\text{and } 0 < w_0(\mu) \leq w_1(\mu) \leq \ldots \leq w_{m-1}(\mu) < 1. \tag{3.17}$$

We propose a symbol mapping design criterion to find the symbol mapping rule μ whose $w_k(\mu)$'s can provide the maximum flatness of $D(x;\mu)$ to achieve the desired properties as discussed earlier. The resulting criterion is called the maximum flatness criterion.

To this end, we transform the basis of binomial functions to form an orthonormal basis. Let

$$\mathcal{S} = \{1, \alpha_0(x), \alpha_1(x), \ldots, \alpha_{m-1}(x)\},$$

where the last element linearly depends on the others. Using the GS procedure, we can find a set of m orthonormal functions from $\mathcal{S}$. Let $\phi_k(x)$, $k = 0, 1, \ldots, m-1$, denote such orthonormal functions. Let $\phi_0(x) = 1$ for convenience. For illustration purposes, the orthonormal basis for the case of $m = 4$ is shown in Figure 3.3. It can be seen that $\phi_0(x)$ corresponds to a DC component while the other functions correspond to AC components. For any tunnel function represented by an element in the function space spanned by

$$\{\phi_0(x), \phi_1(x), \ldots, \phi_{m-1}(x)\},$$
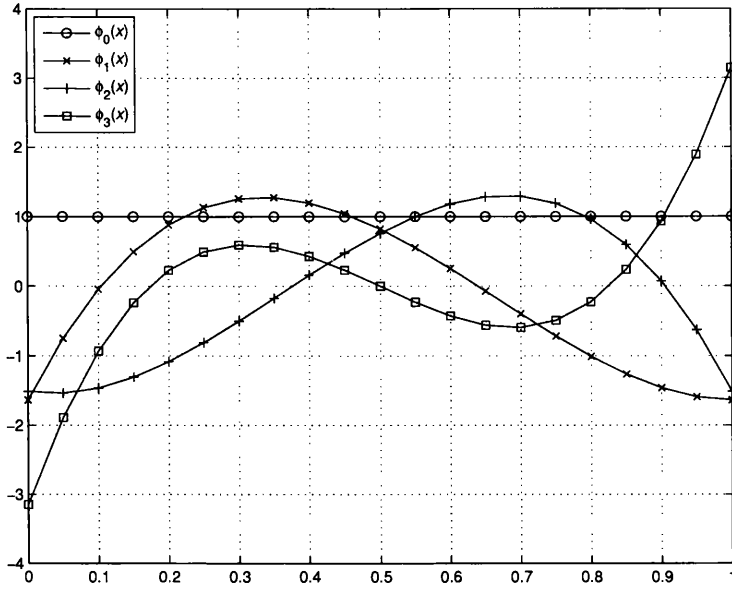
Figure 3.3: Orthonormal basis for the case of $m = 4$ (the number of bits in the label of a transmitted symbol).

a flatter tunnel can be achieved if the coefficients of AC components are all smaller.

With the new basis, $f_1(x; \mu)$ can be represented by

$$f_1(x; \mu) = \sum_{k=0}^{m-1} f_{1,k}(\mu) \phi_k(x), \qquad (3.18)$$

where $f_{1,k}(\mu) = \int_0^1 \phi_k(x) f_1(x; \mu) dx$. Note that $f_{1,0}(\mu) = C_{cm}(\bar{\gamma})$. For $f_2(x)$, we can consider the projection onto the subspace spanned by

$$\{\phi_0(x), \phi_1(x), \dots, \phi_{m-1}(x)\}$$

as follows:

$$\tilde{f}_2(x) = \sum_{k=0}^{m-1} f_{2,k} \phi_k(x), \qquad (3.19)$$

where $f_{2,k} = \int_0^1 \phi_k(x) f_2(x) dx$. Note that $f_{2,0} \approx R_c$ due to the area property [57].

59

The tunnel function becomes

$$D(x;\mu) = (f_{1,0}(\mu) - f_{2,0})\phi_0(x) + \sum_{k=1}^{m-1}(f_{1,k}(\mu) - f_{2,k})\phi_k(x) + (\tilde{f}_2(x) - f_2(x)).$$

(3.20)

It can be seen that the first term on the right hand side in (3.20), which is the difference between two DC components of the EXIT functions, remains constant for $x \in [0,1]$, while the other terms fluctuate. Furthermore, the difference between $f_2(x)$ and its projection represented by the last term does not depend on the mapping rule. For the maximum flatness of $D(x;\mu)$ over $x \in [0,1]$, it is desirable to minimize the squared variation given by

$$F(\mu) \triangleq \int_0^1 \left| \sum_{k=1}^{m-1}(f_{1,k}(\mu) - f_{2,k})\phi_k(x) \right|^2 dx$$

$$= \sum_{k=1}^{m-1}(f_{1,k}(\mu) - f_{2,k})^2,$$

(3.21)

which is defined as the cost function. The optimal (maximum flatness) mapping rule becomes

$$\mu^* = \arg\min_\mu F(\mu).$$

(3.22)

Although an exhaustive search can be used to find the best mapping rule that minimizes the cost in (3.21), it is computationally prohibitive. Thus, sub-optimal, but low complexity, search methods are preferred. Among them, we modify the binary switching algorithm (BSA) in [13]. Note that since the cost in (3.21) cannot be decomposed into multiple sub-costs for each symbol, the BSA in [13] cannot be directly applied. With an initial mapping rule (which is randomly chosen), denoted by μ_0, we build a set of mapping rules by swapping pairs of labels, which is denoted by $\mathcal{M}_1$ (with $M(M-1)/2$ elements for M-QAM). From this set, we choose the mapping rule that has the smallest cost, which is denoted by $\mu_1 \in \mathcal{M}_1$. With μ_1, we also generate another set of mapping rules, denoted by $\mathcal{M}_2$. The same procedure is repeated until the cost of μ_n is not less than that of μ_{n-1}. Iteratively performing a number of searches started from different random mapping rules can achieve a better result.

3.4.3 Illustrative example for 16-QAM constellation

In this example, the system employs a half-rate 64-state convolutional code with $(171, 133)$ octal generator. We consider the following 16-QAM constellation:

$$x^q = \frac{1}{\sqrt{10}} \left\{ \left[2 \left\lfloor q/\sqrt{16} \right\rfloor - (\sqrt{16} - 1) \right] + \sqrt{-1} \left[2(q \pmod{\sqrt{16}}) - (\sqrt{16} - 1) \right] \right\},$$

$$q = 0, \ldots, 15,$$

and $\mathcal{X} = \{x^0, \ldots, x^{15}\}$.

Table 3.1: Orthonormal weights and costs (at $E_b/N_0 = 6.35$ dB).

	Weights	Cost
64-state convolutional code	[0.5000 −0.0383 0.0420 0.0596]	
MF16-C64	[0.6187 −0.0435 0.0491 0.0451]	2.88×10^{-4}
MSP [9]	[0.6187 −0.0813 0.0638 0.0675]	23.87×10^{-4}
Gray [5]	[0.6187 −0.0021 0.0023 0.0020]	62.04×10^{-4}

The decoder weights for the orthonormal basis (obtained by a simulation) are given in the first row of Table 3.1. Note that $f_{2,0}$ is close to $R_c = 1/2$. At an E_b/N_0 of 6.35 dB, the modified BSA produces the following label list:

$$\{8, 10, 11, 1, 7, 14, 15, 9, 2, 6, 5, 12, 13, 4, 0, 3\},$$

which is referred to as MF16-C64. In this list, the qth element, $q = 0, 1, \ldots, 15$, is used to label x^q. With MF16-C64, the demapper weights for the orthonormal basis and the resulting cost are given in the second row of Table 3.1. For comparison purposes, the weights and costs for the modified set partitioning (MSP) [9] and Gray [5] are also provided in this table, which shows that the cost of MF16-C64 is much lower than that of MSP or Gray. As shown in the EXIT chart in Figure 3.4, MF16-C64 has a wider tunnel gap than that of Gray or MSP.

3.5 Simulation results

We carry out simulations with the symbol mapping rules corresponding to the EXIT functions in Figure 3.4. The same channel code used in Subsection 3.4.3
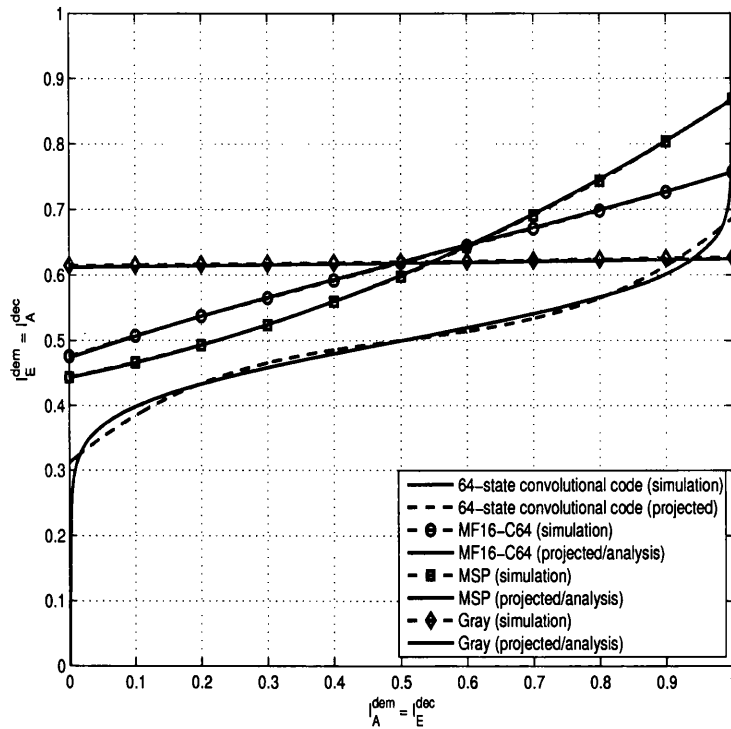
Figure 3.4: EXIT functions of the demapper with different mapping rules and the $(171, 133)_8$ convolutional decoder. The EXIT functions of the demappers are obtained at $E_b/N_0 = 6.35\text{dB}$, Rayleigh fading.

is employed. Two different fading channels are considered as follows. Channel A is a fast fading channel with $B = 10,000$ over which long codewords of $40,000$ bits are transmitted. Channel B is a slow fading channel with $B = 10$ over which shorter codewords of $4,000$ bits are transmitted. The bit error rate (BER) and codeword error rate (CWER) are the performance indices for Channels A and B, respectively.

Figure 3.5 shows the convergence behavior of ID over Channel A at $E_b/N_0 = 6.35$ dB. This shows that for a sufficiently low target BER (say 10^{-4}), which cannot be achieved by Gray mapping, MF16-C64 requires 4 iterations, which exhibits a faster convergence rate than MSP in the case of fast fading. Figure 3.6 shows the CWER results over Channel B, in which we can see that MF16-C64 outperforms MSP and Gray as expected in a slow fading channel.
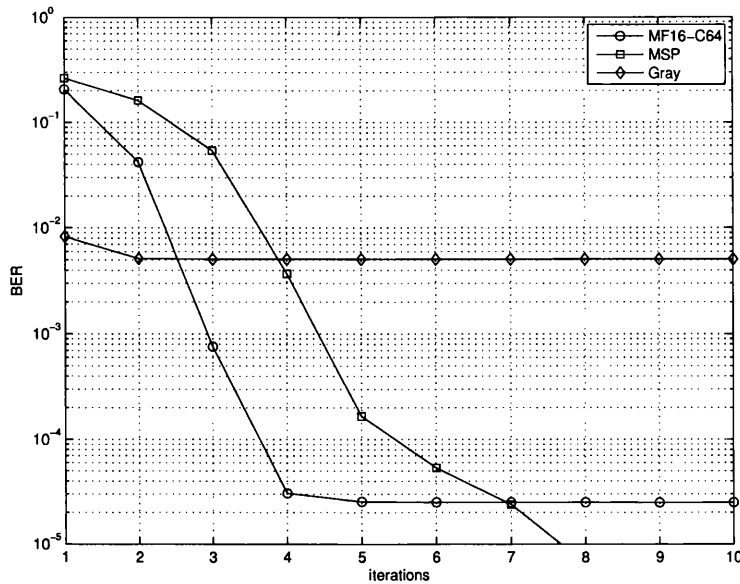
Figure 3.5: Simulated BERs vs number of iterations over a fast Rayleigh fading channel, i.e., Channel A, at $E_b/N_0 = 6.35\text{dB}$.

3.6 Summary

The EXIT chart was used as a design tool in deriving a good symbol mapping. Two main contributions of this chapter are as follows. First, on the EXIT chart, we proposed the maximum flatness criterion in order to achieve the following desirable properties: i) a fast convergence rate for fast fading channels and ii) a low outage probability for slow fading channels. This proposed criterion requires a flat tunnel between the ergodic EXIT function of the demmaper and the EXIT function of the decoder. Second, to apply the flatness criterion, we proposed to adopt a new approach based on the parameterization of the EXIT function of the demapper. From the parameterized EXIT function, a least square problem was formulated and an algorithm modified from the binary switching algorithm (BSA) was used to find a good mapping rule in conjunction with a specific channel code. The simulation results confirmed that the mapping rule obtained by the proposed criterion can provide the desirable properties and good performance with a (64-state) convolutional code.
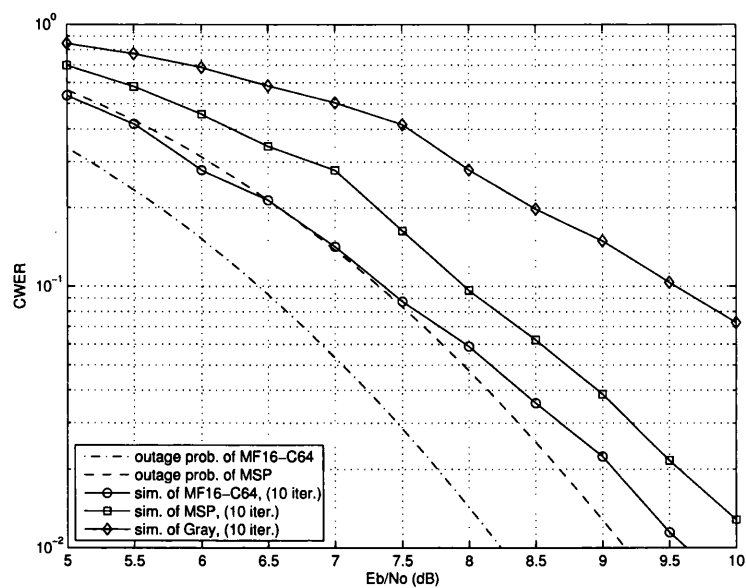
Figure 3.6: Simulated CWERs over a slow Rayleigh fading channel, i.e., Channel B.

64

4

Power allocation for multiband coded OFDM systems with limited feedback

4.1 Introduction

As introduced in Chapter 2, orthogonal frequency division multiplexing (OFDM) in conjunction with simple one-tap equalizers is an effective technique to combat frequency selective fading. In OFDM, mapped symbols are transmitted over parallel channels, which are called subcarriers, in different frequencies. There is no interference between symbols transmitted over different subcarriers since they are weighted by orthogonal column vectors in an inverse discrete Fourier transform (IDFT) matrix before transmitted. In addition, no intersymbol interference between symbols transmitted over the same subcarrier since this channel is flat fading. As there is a variation of channel gains for different subcarriers, coding over the frequency domain can exploit a frequency diversity. As mentioned earlier, a scheme that employs a channel code followed by a bitwise interleaver is referred to as coded OFDM, which has been widely used in various standards, e.g., IEEE 802.11a [26] and IEEE 802.16 [27].

In a practical OFDM system, the average transmitted power is often limited.

As such, according to the water-filling theorem, a higher power level should be allocated to the subcarrier that experiences a better channel gain so that it can carry signals of a higher data rate to maximize the overall throughput [72, 49]. The method of allocating power levels and assigning data rates for different sub-carriers is referred to as the adaptive bit-loading technique. Based on this technique, various adaptive modulation and coding (AMC) systems were proposed in [73, 74, 75, 76]. In these systems, feedback links of high data rate are required to provide the transmitter with all the subcarrier gains. Excessive feedback loads may lead to a difficulty in practical implementation. In order to reduce the amount of feedback information, a more realistic system called OFDM with symbol-level adaptive modulation and coding (symbol-level AMC) was proposed in [77]. In this symbol-level scheme, the signals transmitted by all the subcarriers of an OFDM symbol (which is a codeword) are encoded and modulated by a single pair of encoder and modulation scheme, which is adaptively decided by the receiver based on a prediction of channel state information (CSI). This scheme was further discussed in [78] for channels with relatively short delay spreads. Note that in symbol-level AMC, since no feedback information on each subcarrier is available, adaptive bit-loading is not possible and an optimal performance is not achieved, which is the price of limited feedback.

For an ultra-wideband (UWB) system, which is supported with a very wide bandwidth, signals can be transmitted over multiple OFDM bands. The resulting system is called multiband OFDM UWB which has been defined in IEEE 802.15.3a standard [79]. Due to the frequency selectivity of the channel, different OFDM bands can experience different channel conditions. Furthermore, the whole bandwidth consisting of multiple OFDM bands can share a fixed amount of power budget. Motivated by these conditions and inspired by the approach in [77, 78], we propose a new and efficient power allocation method over OFDM bands based on the greedy and dynamic programming principles. In this method, the receiver predicts the CSI of all OFDM bands and then accordingly allocates suitable transmission power levels and corresponding modulation and coding schemes[1]. The advantages of the proposed method are as follows: i) Since

---

[1]This method could be applied to single band OFDM systems where the power allocation

the receiver only needs to feedback a transmission power level and a pair of modulation format and coding for each OFDM band, the total amount of feedback information can be kept significantly lower than that of a conventional system which provides feedback for all subcarriers; ii) Rather than equally allocating power for all OFDM symbols in the conventional symbol level AMC approach in [77, 78], the proposed method allows us to enjoy more freedom in allocating transmission power over multiple OFDM symbols. Therefore, the average throughput is improved because an OFDM band in a better condition will be assigned with a higher power level and can transmit in a higher data rate effectively. Simulation results show that the proposed power allocation method achieves a significant SNR gain compared with the system with equal power allocation.

The remainder of this chapter is organized as follows. Section 4.2 presents the system model and the proposed power allocation method. This method is then mathematically formulated by an optimization problem in Section 4.3. Section 4.4 shows simulation results. Finally, Section 4.5 summarizes this chapter.

4.2 Power allocation for multiband OFDM systems

In this section, we first describe the signal model for multiband OFDM systems and then propose a new method for power allocation over multiple OFDM bands.

4.2.1 Multiband OFDM system model

The block diagram of a coded OFDM system is illustrated in Figure 4.1. There are N OFDM bands in this system sharing a fixed power budget to transmit OFDM signals. For each band, the transmitter has a chain of a channel encoder, a bitwise interleaver, a modulator, and an inverse discrete Fourier transform (IDFT) operator. Let us consider the signals which are transmitted in the nth

---

is carried out over groups of OFDM symbols (in the time domain) provided that the CSI of future OFDM symbols are predicted.

OFDM band, where $n = 1, 2, \ldots, N$. After going through a channel encoder, an interleaver, and a symbol mapper/modulator where Gray mapping is used, the transmitted message becomes a symbol sequence of length L, which is denoted by $\mathbf{x}_n = [x_{n,0} \; x_{n,1} \; \ldots \; x_{n,L-1}]^{\mathrm{T}}$. We make the following assumptions: i) the average energy of transmitted symbols is unit; ii) the channel remains unchanged during each OFDM symbol interval but varies from one symbol to another; iii) no ISI is observed due to cyclic prefix (CP); and iv) for simplicity, each OFDM symbol consists of only one codeword, i.e., the number of subcarriers is L.
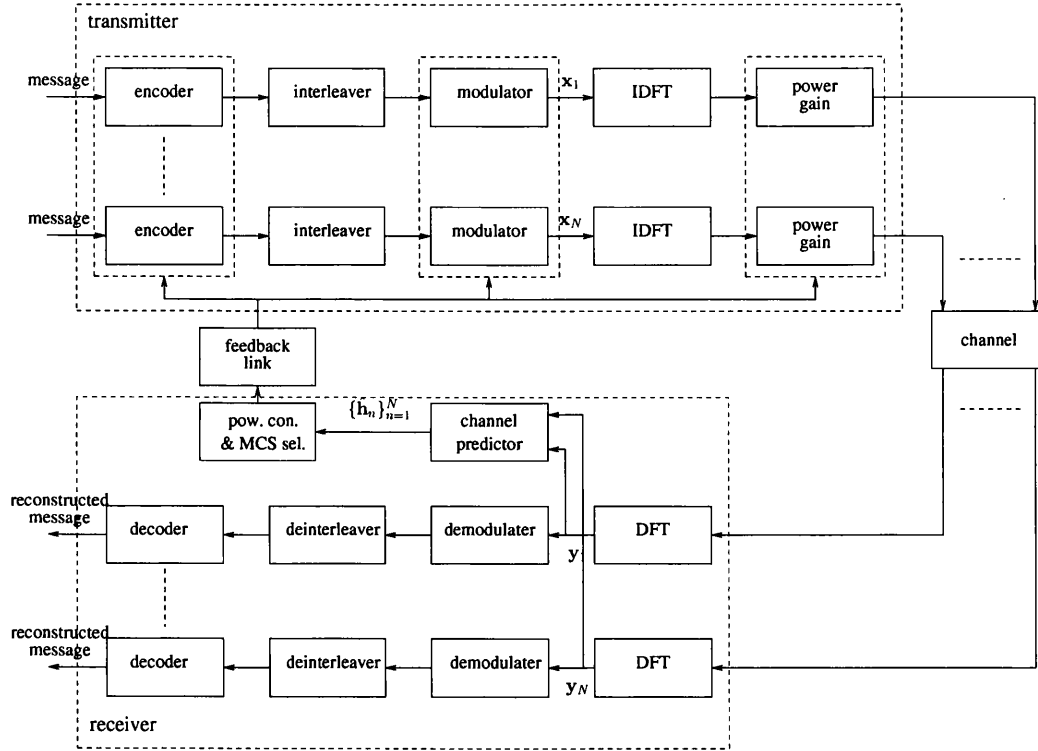
Figure 4.1: Proposed system.

Let $\mathbf{h}_n = [h_{n,0} \; h_{n,1} \; \ldots \; h_{n,P-1}]^{\mathrm{T}}$ be the channel impulse response (CIR) vector for the considered OFDM symbol transmitted in the nth OFDM band. Note that $\mathbf{h}_n$'s are different for different bands. The received signal at the lth subcarrier after taking the discrete Fourier transform (DFT) is given by

$$y_{n,l} = \sqrt{E_n} g_{n,l} x_{n,l} + w_{n,l}, \quad l = 0, 1, \ldots, L - 1, \tag{4.1}$$

where E_n is the transmission power allocated for the nth OFDM band, $g_{n,l}$ is the lth subcarrier's gain, which is obtained by

$$g_{n,l} = \sum_{p=0}^{P-1} h_{n,p} \exp\left(-\frac{j2\pi lp}{L}\right), \quad l = 0, 1, \ldots, L-1, \tag{4.2}$$

and $\{w_{n,l}\}$ is an independent and identically distributed (iid) background noise sequence of circularly symmetric complex Gaussian (CSCG) random variables with variance σ^2, i.e., $w_{n,l} \sim \mathcal{CN}(0, \sigma^2)$. For convenience, let $E[\|\mathbf{h}_n\|^2] = 1$ and $\sigma^2 = 1$. The average signal-to-noise ratio (SNR) for the OFDM symbol transmitted in this band, called OFDM symbol SNR (OS-SNR), is therefore given by E_n. At the receiver, the received signal vector $\mathbf{y}_n = [y_{n,0} \; y_{n,1} \; \cdots \; y_{n,L-1}]^{\mathrm{T}}$, is used as the input of a soft-output demodulator. The output of the demodulator is fed into a channel decoder which then reconstructs the original message.

4.2.2 Power allocation over multiple OFDM bands

A new power control method for a multiband coded OFDM system is proposed as follows. In the system, there is a set of predefined modulation and coding pairs with each being referred to as a modulation and coding scheme (MCS) candidate. To transmit an OFDM symbol in an OFDM band, the transmitter can select one of the MCS candidates in this set and a suitable power level. Importantly, in our proposed method, the MCS assignment and power allocation are decided by the receiver. In performing a power control policy, the following steps are carried out:

Step 1: The receiver first predicts the CIR vectors for all N bands.

Step 2: Based on predicted CIR vectors for the given OFDM bands, the receiver then allocates power levels for all the bands so as to maximize the total data rate subject to the constraints that i) the sum of allocated powers does not exceed a predefined power level and ii) a certain bit error rate (BER) target is achieved for the assigned MCS to each band. The predefined power level is called the power budget. The BER target is the parameter to control the quality of service (QoS).

69

Step 3:   Finally, the allocated power levels and assigned MCSs are sent to the transmitter via a feedback link.

In our proposed method, deriving an effecient algorithm in Step 2 plays an essential role and this will be discussed in Section 4.3.

4.3   Power allocation policy: Problem formulation and algorithms

In this section, we first formulate the optimization problem for our proposed power allocation method and then discuss two low-complexity algorithms based on the greedy and dynamic programming principles.

4.3.1   Problem formulation

We assume that the system uses a set $\mathcal{M}$ of M MCS candidates with the data rates $\eta^{(m)}$, $m = 1, 2, \ldots, M$, where $0 = \eta^{(1)} < \eta^{(2)} < \ldots < \eta^{(M)}$. Each MCS candidate is represented by an index in the set $\{1, 2, \ldots, M\}$. In order to perform a power allocation policy, it is assumed that the predicted CIR vectors for all N OFDM bands are available, which are denoted by $\hat{\mathbf{h}}_1, \hat{\mathbf{h}}_2, \ldots, \hat{\mathbf{h}}_N$. Furthermore, for a given CIR vector, it is also assumed that the receiver can estimate the BER performance corresponding to a specific MCS. Let $P_b(E; m, \mathbf{h})$ denote the estimated BER function, where E is the transmission power, m is the index for the MCS candidates in $\mathcal{M}$, and $\mathbf{h}$ is the CIR vector[1]. Since the data rate corresponding to the MCS index 1 is zero, $P_b(E; 1, \mathbf{h}) = 0$, $\forall E \geq 0$, i.e, if the data rate is zero, there is no error for any transmission power level.

Let E_T and $\bar{P}_b$ be the power budget and the target BER, respectively. Note that we set the same target BER for all the OFDM bands. In addition, $\bar{P}_b$ is chosen to be sufficiently low such that the system can achieve a good performance. The problem is to assign MCSs and allocate power levels for transmitting OFDM

---

[1]An example of BER estimate, i.e., $P_b(E; m, \mathbf{h})$, will be given in Section 4.4.

symbols over N OFDM bands constrained on the conditions that the sum of power levels does not exceed E_T and the estimated BERs are not greater than $\bar{P}_b$. In an efficient power allocation policy, we expect that an OFDM band suffering from a worse channel condition is allocated a lower power level or even no power in order to save the power for the other bands which are in better conditions. Note that if no power is allocated for an OFDM symbol, the data rate is zero as the MCS index 1 is chosen. The problem is formulated as follows:

$$\max_{\substack{m_1,\dots,m_N \\ E_1,\dots,E_N}} \sum_{n=1}^{N} \eta^{(m_n)}, \tag{4.3}$$

subject to $E_n \geq 0, \ \forall k : 1 \leq n \leq N,$

$$\sum_{k=1}^{N} E_n \leq E_T,$$

$$m_n \in \{1, 2, \dots, M\}, \ \forall n : 1 \leq n \leq N,$$

$$P_b(E_n; m_n, \hat{\mathbf{h}}_n) \leq \bar{P}_b, \ \forall n : 1 \leq n \leq N,$$

where E_n and m_n, $n = 1, 2, \dots, N$, are the allocated power level and assigned MCS index for the nth OFDM band, respectively. Note that there are $2N$ variables to be controlled in (4.3). However, because of the QoS constraint, the selection of an MCS index, say m_n, strongly depends on the corresponding power level, i.e, E_n. Assuming that E and $\hat{\mathbf{h}}$ are given for an OFDM band, we can not choose the MCS index for this band with a value greater than

$$m_n^*(E) = \max_{\substack{m \in \{1,2,\dots,M\} \\ P_b(E;m,\hat{\mathbf{h}}) \leq \bar{P}_b}} m \tag{4.4}$$

since $P_b(E; 1, \mathbf{h}) \leq P_b(E; 2, \mathbf{h}) \leq \dots \leq P_b(E; M, \mathbf{h})$ (performance is always a nondecreasing function with data rate). Therefore, to achieve the maximum total data rate, we should always select $m_n^*(E)$ for OFDM band n if E power is assigned for this band. From the discussions above and by letting

$$\eta_n^*(E) = \eta^{m_n^*(E)}, \tag{4.5}$$

the problem in (4.3) becomes

$$\max_{E_1,\ldots,E_N} \sum_{n=1}^{N} \eta_n^*(E_n), \tag{4.6}$$

$$\text{subject to } E_n \geq 0, \ \forall n : 1 \leq n \leq N,$$

$$\sum_{n=1}^{N} E_n \leq E_T.$$

This problem can be seen as an application of water-filling theorem to multiple OFDM symbols as the sum rate is to be maximized with power constraint. The main difference is that we consider practical coding with a (coded) BER constraint. Thus, this formulation is generic and applicable to other problems where the power allocation is required to multiple codewords.

The solution to (4.6) can be found by an exhaustive search as follows. Firstly, we list all possible combinations of MCS candidates for N OFDM bands. (There are M^N possible combinations). Secondly, for each combination, where $\hat{m}_n$ is supposed to be used in OFDM band n, $n = 1, 2, \ldots, N$, find the set of power levels $\hat{E}_n$, $n = 1, 2, \ldots, N$, such that $\hat{m}_n = m_n^*(\hat{E}_n)$. The value of $\hat{E}_n$ is certainly unique since $P_b(E; \hat{m}_n, \hat{\mathbf{h}}_n)$ is always a decreasing function in E. If this set of power levels satisfies the power budget constraint, this selection of MCS candidates and power levels is a feasible solution. Lastly, among the feasible solutions, the optimal solution is decided by the one that can achieve the highest total data rate. However, since the complexity of an exhaustive search grows exponentially with N and becomes prohibitively high if N is relatively large, searching algorithms of lower complexity are preferred[1]. In the following, we will discuss two low complexity algorithms to derive good power allocation policies based on the greedy and dynamic programming principles.

4.3.2 Greedy algorithm

An algorithm based on the greedy principle is described as follows. The algorithm is performed in a number of steps. In the first step, all the OFDM bands are

---

[1]Throughout this thesis, the complexity of an algorithm is roughly represented by the number of steps required to carry out the algorithm.

assigned with MCS of $\eta^{(1)}$ and are allocated by no transmission power. In each subsequent step, the MCS index for one of N OFDM bands is increased by 1. The OFDM band chosen to be reassigned is the one which requires the lowest amount of increasing power for a unit of increasing data rate to achieve the target BER constraint. Each step takes an amount of power from the power budget to allocate for the OFDM band that is reassigned with a new data rate. The algorithm is performed iteratively until the remaining power budget is not enough to increase the data rate for any band. This algorithm is very similar to the bit-loading technique found in the literature, e.g., [80, 81].

The advantage of the greedy algorithm is that its complexity is relatively low ($\mathcal{O}(MN)$). However, there are some issues open for discussion. First, the necessary condition for the greedy algorithm to be optimal is that for two different data rate levels, the higher one always requires a larger amount of power to increase a unit of data rate than the other [82]. In practice, this condition may not be satisfied. For example, the MCS candidates with indices 2, 3, and 4 in Table 4.1 have diversity of orders 10, 5, and 6, respectively, Therefore, if the set of MCS candidates given in Table 4.1 is used, for some CIR realizations, increasing the data rate from 2 bps/Hz to 3 bps/Hz requires more additional amount of power than that used to increase from 3 bps/Hz to 4 bps/Hz. Due to the fact that the occurrence of this behavior is not often, the greedy algorithm can be seen as a very effective algorithm provided that the power levels are unquantized, i.e., no constraint on the number of feedback bits for power levels. Second, if the number of bits assigned to the feedback of the power levels is limited, the amount of power taken from the power budget in each step should be in quantized levels. In this case, the greedy algorithm is certainly no longer optimal. Therefore, we next develop another algorithm based on dynamic programming, which is optimal if only discrete levels of feedback power are considered.

4.3.3 Dynamic programming

Let the positive integer Q be the number of power steps, which allows $Q + 1$ possible power levels to be allocated from 0 to E_T. We assume that these possible

power levels are uniformly quantized. Therefore, $E_T = QE_0$, where E_0 is the identical changing step of power. Let $d_n, d_n \in \mathbb{Z}^+$, denote the multiple of E_0 allocated for the nth OFDM band, i.e., $E_n = d_n E_0$. In the power allocation problem, a set of integers $\{d_1, d_2, \ldots, d_N\}$ constrained by $\sum_{n=1}^{N} d_n \leq Q$ that maximizes the throughput needs to be found. Thus, the problem for the case of discrete power levels become

$$\max_{\{d_n\}_{n=1}^{N}} \sum_{n=1}^{N} \eta_n^*(d_n E_0),$$

$$\text{subject to } d_n \in \mathbb{Z}^+, \ \forall n : 1 \leq n \leq N;$$

$$\sum_{n=1}^{N} d_n \leq Q, \tag{4.7}$$

where $Q = E_T/E_0$ and $\eta_n^*(\cdot)$ is defined in (4.5).
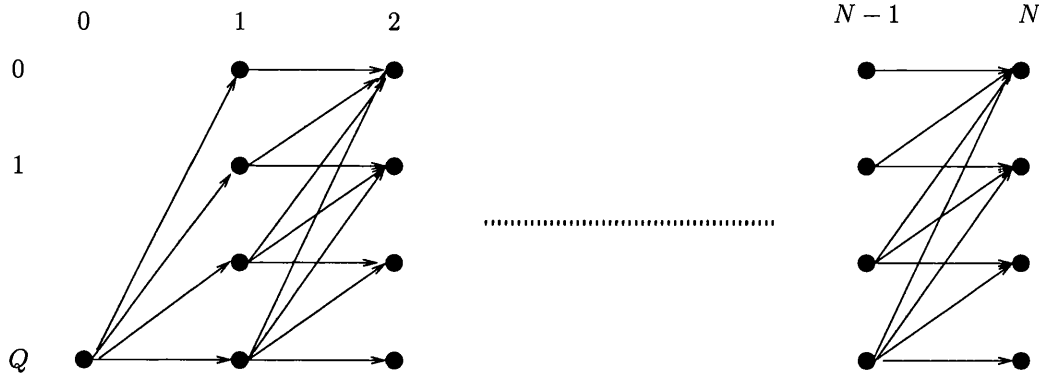
Figure 4.2: Trellis presentation for power allocation.

To apply a dynamic programming technique to this optimization problem, the process of allocating power levels can be presented in a trellis that includes $N + 1$ stages from 0 to N. At stage n, there are $Q + 1$ possible states from 0 to Q, where each state represents the remaining number of unit powers that can be used to allocate for the OFDM bands from $n + 1$ to N. Note that the initial state at $n = 0$ must be Q. From state q at stage n, the next state at stage $n + 1$ cannot be greater than q. The output of a transition from q to q' is given by $f_n(q, q') = \eta_n^*((q - q')E_0)$, which is defined as the cost of a transition.

Furthermore, the metric of a path through a sequence of states is defined by the sum of costs. Figure 4.2 illustrates a graphical representation of the trellis. The optimization problem is to find the best path that has the maximum path metric. As the cost of a transition is based only on the starting and ending states, an algorithm based on dynamic programming can provide the optimal solution with a lower complexity. In particular, through the stages from 1 to N, a state at each stage keeps the previous state, which in fact stores the path that maximizes the sum of the costs up to the current state. The optimal path over all $N + 1$ stages then can be found by tracing back from the state with highest path metric at stage N.

Note that the complexity of this dynamic programming is $\mathcal{O}((Q+1)N)$, which could be higher than that of the greedy algorithm. However, with the discrete power constraint, i.e., $E_n \in \{0, E_0, , \ldots, QE_0\}$, the dynamic programming provides the optimal solution. Furthermore, this solution is an approximation for the original problem in (4.3) and this approximation can be improved by increasing Q. Through simulations in the next section, we can see that the dynamic programming is preferred for a relatively small value of Q.

4.4 Simulation results

In all simulations, we choose $N = 8$ and $L = 1024$. We assume that CIR vectors are independent from one OFDM band to another. In each band, the CIR vector has $P = 128$ independent tap coefficients and an identical exponential power delay profile, i.e.,

$$h_{n,p} \sim \mathcal{CN}\left(0, \frac{\exp(-pT_s/T_{rms})}{1 - \exp(-T_s/T_{rms})}\right), \forall n : 1 \leq n \leq N,$$

where T_s is the sampling period, and T_{rms} is the root mean square delay spread, which is assumed that $T_{rms} = 6T_s$.

For modulation and coding, the set of MCS candidates in Table 4.1 is used. For the MCS candidates with the code rate of half, the convolutional code of $(171, 133)$ octal generator is used, and it is defined as the mother code. For

MCS index	Modulation format	Code rate	Data rate (bps/Hz)
1			0
2	QPSK	1/2	1
3	16-QAM	1/2	2
4	16-QAM	3/4	3
5	64-QAM	2/3	4
6	64-QAM	3/4	4.5

Table 4.1: List of employed modulation and coding schemes.

the MCS candidates with code rates higher than half, the channel codes are obtained by puncturing from the mother code, where the puncturing patterns, the minimum Hamming distances, and the total input weights of error events for each Hamming distance are found in [83]. For BER estimation, i.e., $P_b(E; m, \mathbf{h})$, we use the derivation in [77]. In particular, assume that a MCS candidate of index m uses a pair of code $\mathcal{C}$ and modulation μ. Here, μ can be QPSK, 16-QAM, and 64-QAM (with Gray mapping). Let $d_f(\mathcal{C})$ denote the minimum Hamming distance (free distance) of $\mathcal{C}$. Let $a(d)$ denote the total input weight of error events at Hamming distance d of $\mathcal{C}$. Let $d_m(\mu)$ denote the minimum Euclidean distance in the constellation of μ, which are given by $\sqrt{2}$, $\sqrt{2/5}$, and $\sqrt{2/21}$ for QPSK, 16-QAM, and 64-QAM, respectively. The estimated BER is obtained by

$$P_b(E; m, \mathbf{h}) = \sum_{d=d_f(\mathcal{C})}^{5} a(d) \left(P_e(E; \mu, \mathbf{h}) \right)^d,$$

where

$$P_e(E; \mu, \mathbf{h}) = \frac{1}{L} \sum_{l=0}^{L-1} \left[b_1(\mu) Q \left(\sqrt{\frac{E|h_l|^2 d_m(\mu)}{4\sigma^2}} \right) + b_2(\mu) Q \left(\sqrt{\frac{E|h_l|^2 d_m(\mu)}{2\sigma^2}} \right) \right]$$

with $[b_1(\mu) \; b_2(\mu)]^{\mathrm{H}}$'s for QPSK, 16-QAM, and 64-QAM are $[1 \; 1]^{\mathrm{H}}$, $[6/8 \; 9/8]^{\mathrm{H}}$, and $[28/48 \; 49/48]^{\mathrm{H}}$, respectively. Here, $Q(\cdot)$ is the Gaussian Q-function [22, Equation 2-1-97].

For comparison purposes, we include in our simulations the symbol-level adaptive modulation and coding system with equal power control policy as in [77]. We

assume that the channel estimation and prediction are perfect. Furthermore, an error-free feedback link is assumed. The target BER is set by $\bar{P}_b = 10^{-4}$. To measure the performance, we only count the codewords that can be decoded without any bit errror to compute the average successful bits per each subcarrier and refer to the measurement index as goodput. In our simulations, the greedy algorithm is performed in discrete power levels that are identical to that used by the dynamic programming. When $Q = 31$ is used, Figure 4.3 shows the advantage of the system with our proposed power control method over the system with equal power control. For example, about 2 dB SNR gap at 2.5 bps/Hz goodput is exhibited. In addition, it can be seen that the dynamic programming can provide a slightly better performance than the greedy algorithm.

To have a finer comparison between the dynamic programming and greedy algorithms, we carry out simulations for different values of Q at 20 dB OS-SNR. Figure 4.4 shows that the dynamic programming always outperforms the greedy algorithm. However, the performance gap is relatively small. Therefore, for a high value of Q, i.e., the number of bits for the feedback of power levels is sufficiently large, the greedy algorithm could be a better choice due to its low complexity.
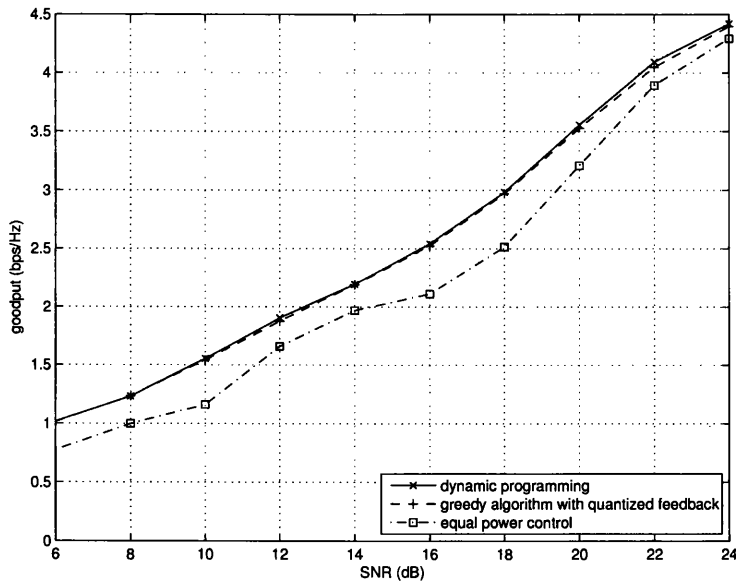
Figure 4.3: System performances for different power control policies, $Q = 31$.
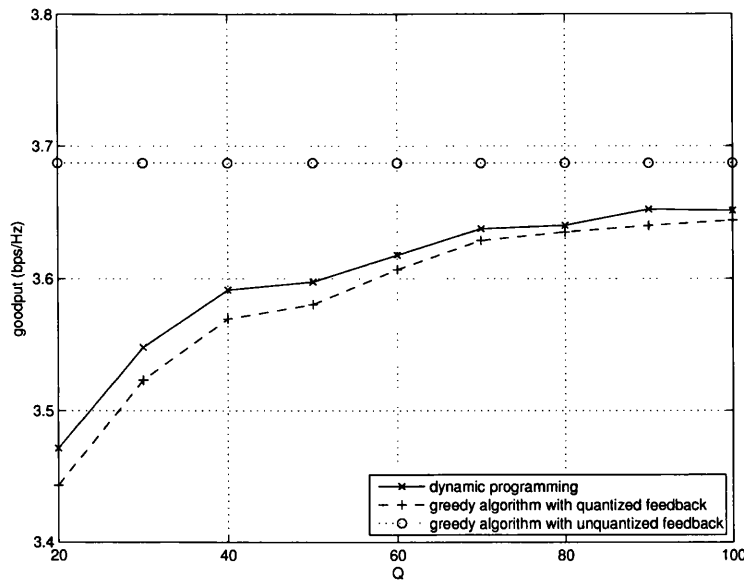
Figure 4.4: Average goodput versus Q (the number of discrete power levels for power allocation), SNR = 20 dB.

4.5 Summary

In this chapter, we proposed a power control method for multiband coded OFDM systems based on the greedy principle and dynamic programming. It can be seen that the proposed power control is an application of water-filling theorem to multiple OFDM symbols, where each OFDM symbol is a codeword of possibly different code rate. Through the simulations, it was confirmed that the proposed method can increase the system throughput. The dynamic programming is optimal under the discrete power levels constraint. This algorithm is suitable for the case of a small number of feedback bits for power control, while the greedy algorithm is more promising due to its low complexity for the case of a sufficiently large number of feedback bits.

5

PNC in TWRNs: Low-complexity decoding at relays in networks using channel codes

5.1 Introduction

As introduced in Chapter 2, due to the broadcast nature of wireless channels, it can be useful to perform network coding [50] in the physical layer. Physical-layer network coding (PNC) was proposed by Zhang et al. [11] as a protocol for information exchange between two nodes with the help of a relay in a two-way relay network (TWRN). The information exchange consists of two phases, multiple access control (MAC) and broadcast (BC) phases. In the MAC phase, two source nodes simultaneously transmit signals to a relay node. Then, in the BC phase, the relay node broadcasts an XORed codeword, which is encoded from the two source nodes' messages, to two source nodes, which become the sink nodes when receiving signals. It was also reported in [55] that using protocols with two phases in TWRNs can achieve a higher spectral efficiency than using three or four phases. In [54], the notion of PNC was refined to demonstrate that how to

obtained an XORed codeword by PNC. Note that there could be various ways to represent the XORed codeword, e.g. superimposed XOR was used in [84]. In terms of practical design, there has been extensive research activities on designing effective modulation and coding schemes for PNC. In [85], when no channel code is considered, an adaptive scheme is proposed to decide detection regions in the MAC phase and to choose a proper constellation in the BC phase. With channel coding, in [86], PNC is performed at message level and the decoding algorithm is redesigned for repeat accumulate (RA) code to decode XORed messages. Although proposed in [86], whether the proposed decoding methods are optimal or not were not discussed. In addition, to the best of our knowledge, there has been no work considering the diversity analysis for PNC in conjunction with channel codes, e.g., convolutional codes and turbo codes, where codewords can be decoded based on trellises, yet. Note that convolutional and turbo decoding can be performed by using the Viterbi [16] and BCJR [17] algorithms, respectively. These decoding algorithms based on trellises have complexities proportional to the number of states on a trellis. In designing decoding methods at the relay node, we expect that the decoding can be performed with low complexities.

In this chapter, PNC is performed at message level as in [86]. This scheme is referred to as the link-by-link coded PNC scheme. We focus on the decoding algorithms based on trellises at the relay node. At the relay node, the Viterbi or BCJR algorithms based on a full-state trellis can be used for decoding similar to a classical MAC [87], where the complexity is approximately square of that for point-to-point channels. Since the relay node only needs to decode XORed message rather than two individual messages, we show that the decoding can be performed based on a reduced-state trellis, an approach has been widely used for the sequence detection in frequency-selective channels [88]. Exploiting the reduced-state trellis, the decoding complexity is decreased while the diversity order is kept unchanged if the encoders at the source nodes are identical. Simulation results show that even though there are performance gaps between full-state and reduced-state decoding, which is a cost for reduced complexity, when convolutional or turbo codes are used, no loss in the diversity order is confirmed.

The remainder of this chapter is organized as follows. Section 5.2 presents

the system model. In Section 5.3, we discuss decoding algorithms based on the full-state trellis. A reduced-trellis structure for decoding with a lower complexity at the relay node is proposed in Section 5.4. Simulation results are provided in Section 5.5. Section 5.6 summarizes this chapter.

5.2 System model

The system model is illustrated in Figure 5.1, where two source nodes S_1 and S_2 exchange their messages with the assist of relay node R using the PNC protocol consisting of MAC and BC phases. In the MAC phase, S_1 and S_2 encode their messages and transmit coded signals simultaneously. Then, R decodes the XORed version of the two signals at message level and forwards its coded signals to both the source nodes during the BC phase. Since each source node knows its own message, it can decode the message sent by the other node from the XORed message.
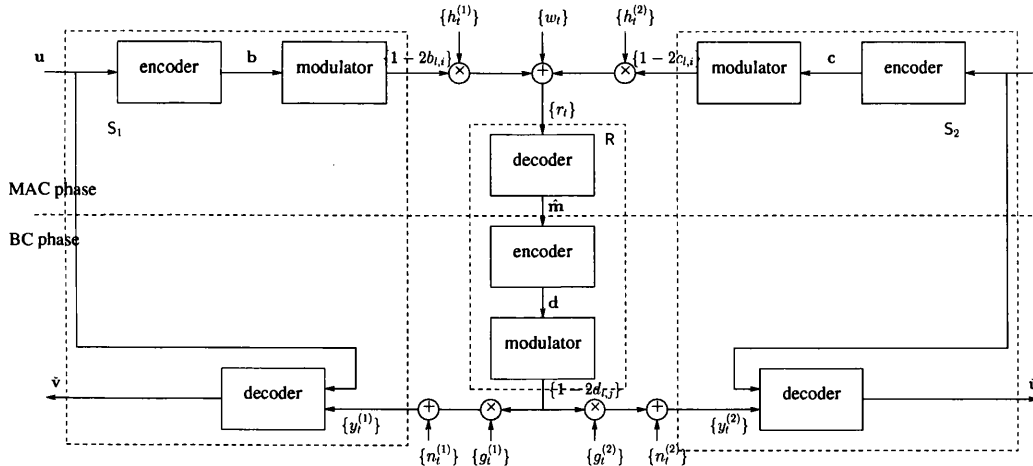
Figure 5.1: System model of PNC in conjunction with channel code in a TWRN.

Let $\mathbf{u} = \{u_1, u_2, \ldots, u_L\}$ and $\mathbf{v} = \{v_1, v_2, \ldots, v_L\}$ be two binary message sequences of the same length L, which are generated by S_1 and S_2, respectively. At the two source nodes, they are encoded by two channel encoders, denoted by $\mathcal{C}_1$ and $\mathcal{C}_2$. Throughout this chapter, only convolutional codes and turbo codes

are considered for channel coding. We assume that $\mathcal{C}_1$ and $\mathcal{C}_2$ are in the same type and have the same code rate r. In addition, assume that $r = 1/N$, where N is a positive integer for the sake of simplicity. Let $\mathbf{b}$ and $\mathbf{c}$ be the coded sequences encoded by $\mathcal{C}_1$ and $\mathcal{C}_2$ from $\mathbf{u}$ and $\mathbf{v}$, respectively. Note that $\mathbf{b}$ and $\mathbf{c}$ have the same length LN. Then, we have

$$\mathbf{b} = \{b_{1,1} \ldots, b_{1,N}, \ldots, b_{L,1}, \ldots, b_{L,N}\} = \mathcal{C}_1(\mathbf{u})$$
$$\mathbf{c} = \{c_{1,1} \ldots, c_{1,N}, \ldots, c_{L,1}, \ldots, c_{L,N}\} = \mathcal{C}_2(\mathbf{v}).$$

At all the nodes, including source nodes and relay node, binary phase shift keying (BPSK) is used for modulation, where coded bits 0 and 1 are modulated to be the binary data symbols "+1" and "−1", respectively. Although our proposed decoding algorithms can work with higher order modulation, we use BPSK to demonstrate the algorithm and, importantly, to simplify diversity analyses. As a consequence, the signal sequences transmitted by S_1 and S_2 can be represented by $\{1 - 2b_{l,i}\}$ and $\{1 - 2c_{l,i}\}$, respectively.

In the MAC phase consisting of LN-symbol duration, both the source nodes transmit their coded signals simultaneously and the those signals are assumed to be perfectly synchronized at that relay node. In particular, if the time index is denoted by $t = (l-1)N + i$, $1 \leq l \leq L$, $1 \leq i \leq N$, during the MAC phase, the received signal at R is given by

$$r_t = h_t^{(1)} \sqrt{E_1} \left(1 - 2b_{l,i}\right) + h_t^{(2)} \sqrt{E_2} \left(1 - 2c_{l,i}\right) + w_t,$$
$$t = 1, 2, \ldots, LN, \tag{5.1}$$

where E_k and $\{h_t^{(k)}\}$, $k = 1, 2$, are the transmission power and the sequence of channel gains from S_k to R, respectively, and $\{w_t\}$ is the background noise sequence at R, which is assumed to be an independent and identically distributed (iid) sequence of circularly symmetric complex Gaussian (CSCG) random variables with zero mean and variance σ_R^2, i.e., $w_t \sim \mathcal{CN}(0, \sigma_\mathsf{R}^2)$. For the additive white Gaussian noise (AWGN) channel, it is assumed that $h_t^{(k)} = 1 \forall t$, while $\{h_t^{(k)}\}$ is an iid random sequence[1] for fading channels.

---

[1] This is not necessary to derive decoding algorithms, but we consider this assumption to see the diversity gain over fading channels.

At the relay node, network coding is performed at message level as in [86], which is referred to as link-by-link coded PNC scheme. Let $\mathbf{m} = \{m_1, m_2, \ldots, m_L\}$ be the element-wise XORed message sequence from $\mathbf{u}$ and $\mathbf{v}$. That is, the lth element of $\mathbf{m}$ is given by $m_l = u_l \oplus v_l$, where $\oplus$ denotes the binary XOR operator. For convenience in notations, let us write $\mathbf{m} = \mathbf{u} \oplus \mathbf{v}$. Denote by $\hat{\mathbf{m}}$ the decoded version of $\mathbf{m}$ at R. We assume that the channel state information (CSI), i.e., $\{h_t^{(k)}\}$, $k = 1, 2$, are perfectly known to the relay node. Let $\mathcal{D}_R(\cdot)$ denote the decoding function at R. The decoded XORed message is given by

$$\hat{\mathbf{m}} = \mathcal{D}_R(\{r_t\}). \tag{5.2}$$

In (5.2), although not explicitly expressed, the decoding rule implicitly relies on the known CSI (i.e., coherent detection).

Next, $\hat{\mathbf{m}}$ is encoded by a channel encoder, denoted by $\mathcal{C}_R$, to form the coded sequence $\mathbf{d} = \mathcal{C}_R(\hat{\mathbf{m}})$. Assume that the code rate of $\mathcal{C}_R$ is $r' = 1/N'$, where N' is a positive integer. Therefore, the length of $\mathbf{d}$ is LN'.

In the BC phase consisting of LN'-symbol duration, R broadcasts the coded signals to both the source nodes. In particular, at $t = (l-1)N'+j$, $l = 1, 2, \ldots, L$ and $j = 1, 2, \ldots, N'$, in the BC phase, S_k, $k = 1, 2$, receives the following signal:

$$y_t^{(k)} = g_t^{(k)} \sqrt{E_R} \left(1 - 2d_{l,j}\right) + n_t^{(k)}, \ t = 1, 2, \ldots, LN', \tag{5.3}$$

where E_R and $\{g_t^{(k)}\}$ are the transmission power and the sequence of channel gains from R to S_k, respectively, and $\{n_t^{(k)}\}$ is the background noise sequence at S_k which is an iid sequence of CSCG random variables, i.e., $n_{l,j}^{(k)} \sim \mathcal{CN}(0, \sigma_k^2)$. For the additive white Gaussian noise (AWGN) channel, it is assumed that $g_t^{(k)} = 1 \ \forall t$, while $\{g_t^{(k)}\}$ is iid for fading channels.

Let $\mathcal{D}_1(\cdot)$ and $\mathcal{D}_2(\cdot)$ denote the decoding functions for XORed message at S_1 and S_2, respectively. The outputs of decoders are given by

$$\check{\mathbf{m}}^{(k)} = \mathcal{D}_k(\{y_t^{(k)}\}), \ k = 1, 2. \tag{5.4}$$

Finally, S_1 decodes $\mathbf{v}$, the message sent by S_2, by taking the XOR operation of $\mathbf{u}$ and $\check{\mathbf{m}}^{(1)}$, i.e., $\check{\mathbf{v}} = \mathbf{u} \oplus \check{\mathbf{m}}^{(1)}$. Similarly, $\mathbf{u}$ is found at S_2 as $\check{\mathbf{u}} = \mathbf{v} \oplus \check{\mathbf{m}}^{(2)}$.

Since the model in the BC phase is analogous to a standard point-to-point channel, any channel code can be used in this phase and decoding algorithms used in a point-to-point system can be applied to decode the network coded message directly without modification. For example, if the maximum likelihood (ML) criterion is considered for decoding in the BC phase, with known $\{g_t^{(k)}\}$, the ML decoding function is given by

$$\mathcal{D}_k^{\mathrm{ML}}(\{y_t^{(k)}\}) = \arg\min_{\hat{\mathbf{m}}} W_{\mathrm{bc}}^{(k)}\left(\mathcal{C}_{\mathsf{R}}(\hat{\mathbf{m}})\right), \qquad (5.5)$$

where

$$W_{\mathrm{bc}}^{(k)}(\mathbf{d}) = \sum_{t=1}^{LN'} \left| \frac{y_t^{(k)}}{\sigma_k} - g_t^{(k)}\sqrt{\gamma_{\mathrm{bc},k}}\,(1 - 2d_{l,i}) \right|^2$$

with $\gamma_{\mathrm{bc},k} = E_{\mathsf{R}}/\sigma_k^2$. Note that when (5.4) is the ML decoding, i.e., as given in (5.5), since for given $\mathbf{u}$ (resp. $\mathbf{v}$), the mapping from $\mathbf{v}$ (resp. $\mathbf{u}$) to $\mathbf{m}$ is an one-to-one mapping, $\check{\mathbf{v}}$ and $\check{\mathbf{u}}$ are the ML decoding results. If a convolutional code is used at the relay node, the ML decoding in (5.5) can be performed using the Viterbi algorithm as same as that at the receiver of a point-to-point system. On the other hand, although the model in the MAC phase is very similar to a classical multiple access channel, there is a major difference between them, which is that the relay node only needs to decode XORed message rather than two individual messages. Therefore, we focus on decoding algorithms at the relay node, i.e., $\mathcal{D}_{\mathsf{R}}(\cdot)$. while the ML decoders are assumed to be used at both the sinks.

5.3   Full-state decoding

In this section, first, we will present a method of trellis based decoding for the XORed message, which requires two steps. The first step is that two individual messages sent by the two source nodes are decoded jointly. The second step is taking XOR operation on two decoded messages resulting from the first step. Although this method is trivial, we will show that it in fact can provide an approximate ML performance. The first step is simply as same as the decoding

in a classical MAC. In performing this step, a two-user trellis, also named as full-state trellis, is described and the Viterbi and BCJR algorithms based on this trellis are discussed. It can be seen that a decoding based on the full-state trellis requires the complexity of square of that for single-user decoding in point-to-point channels. Then, for the case of convolutional codes, based on the Hamming distance analysis in a full-state trellis, we will show that the achieved diversity is decided by the minimum free distance of the two channel codes used in two source nodes.

5.3.1 Full-state decoding

If we consider the ML criterion for decoding at the relay node, the decoding function is given by

$$\mathcal{D}_R^{ML}(\{r_t\}) = \arg\max_{\mathbf{m}} \log \sum_{\mathbf{u},\mathbf{v}: \ \mathbf{m}=\mathbf{u}\oplus\mathbf{v}} \exp\left(W_{mac}\left(\mathcal{C}_1(\mathbf{u}), \mathcal{C}_2(\mathbf{v})\right)\right), \qquad (5.6)$$

where

$$W_{mac}(\mathbf{b}, \mathbf{c}) = -\sum_{t=1}^{LN} \left| r_t/\sigma_R - h_t^{(1)}\sqrt{\gamma_{mac,1}}\left(1 - 2b_{l,i}\right) - h_t^{(2)}\sqrt{\gamma_{mac,2}}\left(1 - 2c_{l,i}\right) \right|^2$$
$$(5.7)$$

with $\gamma_{mac,k} = E_k/\sigma_R^2$, $k = 1, 2$. Certainly, an exhaustive search can be performed. However, the decoding complexity could be prohibitively high. Therefore, it is desirable to use algorithms with lower complexity rather than the method of exhaustive search.

In (5.6), the objective function, known as the original ML decoding metric, is a logarithm of a sum of exponential functions. With this presentation, the decoding metric cannot be decomposed into a number of sub-metrics, e.g. branch metrics, and Viterbi and BCJR algorithms therefore cannot be directly applied to decoding. Fortunately, if we modify the original ML decoding metric by using the log-max approximation, we can show that the decoding process can be decomposed into two steps, and one of them is actually joint decoding, namely two-user decoding. The Viterbi and BCJR algorithms are applicable for two-user

decoding. Note that, while two users can transmit at arbitrary rates in general MACs, the two source nodes should have the same rate in a TWRN with PNC.

By using the log-max approximation (i.e., $\log \sum_i \exp(z_i) \approx \max_i z_i$), the modified decoding function is given by

$$\mathcal{D}_{\mathsf{R}}^{\mathrm{ML-apx}}(\{r_t\}) = \arg \max_{\mathbf{m}} \max_{\mathbf{u,v: \ m=u\oplus v}} W_{\mathrm{mac}}\left(\mathcal{C}_1(\mathbf{u}), \mathcal{C}_2(\mathbf{v})\right). \tag{5.8}$$

The log-max approximation is a good approximation for sufficiently high $\gamma_{\mathrm{mac},1}$ and $\gamma_{\mathrm{mac},2}$. We observe that the decoding process based on the decoding function given in (5.8) can be carried out by two following steps: i) the two message sequences are jointly decoded as

$$\{\hat{\mathbf{u}}, \hat{\mathbf{v}}\} = \arg \max_{\{\mathbf{u,v}\}} W_{\mathrm{mac}}\left(\mathcal{C}_1(\mathbf{u}), \mathcal{C}_2(\mathbf{v})\right); \tag{5.9}$$

and ii) the XORed message sequence is obtained by

$$\hat{\mathbf{m}} = \hat{\mathbf{u}} \oplus \hat{\mathbf{v}}. \tag{5.10}$$

It is critical to derive a decoding algorithm for step i). To this end, we present below a two-user trellis for encoding if two convolutional codes are used at two source node. For the case of turbo codes, since each constituent code of the turbo code is a convolutional code, the two-user trellis also can be used for presenting the encoding by two corresponding constituent convolutional encoders, each is at a source node. In order to distinguish with another trellis structure with lower number of states proposed for a low complexity decoding in the next section, the trellis presented in this section is referred to as the full-state trellis while the other presented in the next section is referred to as reduced-state trellis.

Full-state trellis

Provided that $\mathbf{u}$ and $\mathbf{v}$ are transmitted, the state at the lth stage is represented by

$$S_l = \left\{u_{l-1}, \ldots, u_{l-\nu_1}, v_{l-1}, \ldots, v_{l-\nu_2}\right\},$$

where ν_k, $k = 1, 2$, is the memory length of $\mathcal{C}_k$. From S_l, if the joint input is (u_l, v_l), the next state is

$$S_{l+1} = \{u_l, \ldots, u_{l-\nu_1+1}, v_l, \ldots, v_{l-\nu_2+1}\}.$$

The transition from S_l to S_{l+1} generates a joint output sequence of length N given by $\{(b_{l,1}, c_{l,1},), \ldots, (b_{l,N}, c_{l,N})\}$. For convenience, denote by $\mathcal{S}$ the state alphabet. Its size is given by $|\mathcal{S}| = 2^{\nu_1+\nu_2}$.

Viterbi algorithm

The Viterbi algorithm is used to search the optimal pair of messages. Since each pair of messages corresponds to a unique path through a sequence of states, finding the optimal pair of messages becomes a search for the optimal path associated with maximum path metric. The path metric of state sequence $\{S_l\}$ whose elements are indexed from 0 to L is given by

$$V_{\text{mac}}(\{S_l\}) = \sum_{l=1}^{L} M_l(S_l, S_{l+1}), \tag{5.11}$$

In (5.11), $M_l(S_l, S_{l+1})$ is the branch metric for the transition from S_l to S_{l+1}, which is given by

$$M_l(S_l, S_{l+1}) = -\sum_{i=1}^{N} \left| r_{(l-1)N+i}/\sigma_{\mathsf{R}} - h^{(1)}_{(l-1)N+i}\sqrt{\gamma_{\text{mac},1}}\left(1 - 2\tilde{b}_{l,i}(S_l, S_{l+1})\right) \right.$$
$$\left. - h^{(2)}_{(l-1)N+i}\sqrt{\gamma_{\text{mac},2}}\left(1 - 2\tilde{c}_{l,i}(S_l, S_{l+1})\right) \right|^2, \tag{5.12}$$

where $\tilde{b}_{l,i}(S_l, S_{l+1})$ and $\tilde{c}_{l,i}(S_l, S_{l+1})$ are the $(2i)$th and $(2i+1)$th bits in the joint output sequence generated by the transition from S_l to S_{l+1}. Note that the path metric $V_{\text{mac}}(\{S_l\})$ is actually the decoding metric $W_{\text{mac}}(\mathcal{C}_1(\mathbf{u}), \mathcal{C}_2(\mathbf{v}))$ in (5.9), when $\mathbf{u}$ and $\mathbf{v}$ are the two message sequences associated with $\{S_l\}$.

BCJR algorithm

The BCJR algorithm is used to compute *a posteriori* information for every pair information bits based on the maximum *a posteriori* (MAP) principle. For computational convenience, we use the logarithms of probabilities to represent *a priori* and *a posteriori* information. In describing the BCJR algorithm for two-user decoding, the following notations are used: $P_l^I(u,v)$ and $P_l^O(u,v)$ denote the logarithms of *a priori* and *a posteriori* probabilities of the pair (u,v), respectively; e denotes a transition between two states; $(u,v) = f(e)$ denotes a mapping from a transition to the pair of bits causing this transition, which is a one-to-one mapping; $\mathcal{E}_l(u,v)$ denotes the set of all possible transitions from the stage l to stage $l+1$ in the trellis caused by the pair (u,v); $S^S(e)$ and $S^E(e)$ denote the start and ending states of transition e, respectively. The output of the BCJR decoder can be presented by a sequence of L vectors, each has 4 elements. In each vector, the first, second, third, and fourth elements represent the logarithms of *a posteriori* probabilities of (u,v) being (0,0), (0,1), (1,0), and (1,1), respectively. Based on the full-state trellis, the BCJR decoder compute the element for (u,v) in the lth vector as follows:

$$P_l^O(u,v) = \log \sum_{e:e\in\mathcal{E}_l(u,v)} \exp\left(\alpha_{l-1}(S^S(e)) + \beta_l(S^E(e))\right.$$
$$\left. + P_l^I(u,v) + M_l(S^S(e), S^E(e))\right), \qquad (5.13)$$

where

$$\alpha_l(S) = \log \sum_{e:S^E(e)=S} \exp\left(\alpha_{l-1}(S^S(e)) + P_{l-1}^I(f(e)) + M_{l-1}(S^S(e), S)\right) \qquad (5.14)$$

and

$$\beta_l(S) = \log \sum_{e:S^S(e)=S} \exp\left(\beta_{l+1}(S^E(e)) + P_{l+1}^I(f(e)) + M_{l+1}(S, S^E(e))\right). \qquad (5.15)$$

If two channel codes at two source nodes are convolutional codes, the Virterbi algorithm can be used to provide an approximate ML performance. For the case of turbo codes, the BCJR algorithm can be used in each constituent decoders the

two turbo codes employs two interleavers with identical structure. In general, a turbo decoder might not provide the ML performance. However, the iterative principle in a turbo decoder should provide very good performance.

5.3.2 Hamming distance analysis for full-state trellis

In this subsection, we focus on examining the diversity order achieved by using the Viterbi algorithm based on the full-state trellis for the case of convolutional codes. Let P_{mac} and P_{bc} denote the message error probabilities (or frame error probabilities (FERs)) for MAC and BC phases, respectively. If an XORed message sequence is incorrectly decoded in either MAC or BC phases and is correctly decoded in the other phase, the overall decision must be incorrect. In addition, an XORed message sequence is incorrectly decoded in both MAC and BC phases, the probability of correct decision in overall end-to-end transmission is only $1/(2^L - 1)$. Therefore, the end-to-end FER is given by

$$
\begin{aligned}
P_{\mathrm{EtoE}} &= P_{\mathrm{mac}}\left(1 - P_{\mathrm{bc}}\right) + P_{\mathrm{bc}}\left(1 - P_{\mathrm{mac}}\right) + \frac{2^L - 2}{2^L - 1} P_{\mathrm{mac}} P_{\mathrm{bc}} \\
&= P_{\mathrm{mac}} + P_{\mathrm{bc}} - \frac{2^L}{2^L - 1} P_{\mathrm{mac}} P_{\mathrm{bc}} \\
&\approx P_{\mathrm{mac}} + P_{\mathrm{bc}} - P_{\mathrm{mac}} P_{\mathrm{bc}},
\end{aligned}
\tag{5.16}
$$

where the approximation in the last line of (5.16) can be used for sufficiently large L. From (5.16), it can be seen that P_{EtoE} is lower- and upper-bounded by $\max\{P_{\mathrm{mac}}, P_{\mathrm{bc}}\}$ and $(P_{\mathrm{mac}} + P_{\mathrm{bc}})$, respectively. Therefore, the diversity of end-to-end transmission is decided by the minimum diversity of MAC and BC. The diversity order of BC is given by the free distance of $\mathcal{C}_{\mathfrak{R}}$. The remaining is that the diversity order of MAC needs to be examined.

If only considering the MAC phase, since the mapping from a pair of binary message sequences to its XORed message sequence is a many-to-one mapping, it is possible that the XORed message sequence can be correctly decoded for incorrectly decoded individual message sequences. However, the error probability of XORed message decoding for given a set of channel realizations is still upper-bounded by a sum of probabilities, each of them is the probability of that

89

an incorrect pair of message sequences is decoded. Such kind of probabilities is referred to as the pair-wise error probability (PEP). Note that each PEP is the probability that an incorrect path is decoded and each path is labeled by a distinct joint output sequence. Therefore, the diversity order of MAC phase is the minimum two-user Hamming distance among all the pairs of joint output sequences. Let us define the two-user Hamming distance between two joint output sequences as follows:

Definition 1 Let $\mathbf{a} = \{a_{l,i}\}$ and $\mathbf{a}' = \{a'_{l,i}\}$ be two different joint output sequences of length LN, where their elements are the pairs of coded bits, i.e., $a_{l,i} = (b_{l,i}, c_{l,i})$, $a'_{l,i} = (b'_{l,i}, c'_{l,i})$. The two-user Hamming distance between $\mathbf{a}$ and $\mathbf{a}'$ is the number of the places where the two corresponding elements of $\mathbf{a}$ and $\mathbf{a}'$ are different from each other.

The following lemma helps us to find the minimum two-user Hamming distance among all the pairs of joint output sequences.

Lemma 1 Let $d_{\text{free},k}$ be the free distance of $\mathcal{C}_k$. Let $d_{\min}$ be the minimum two-user Hamming distance among all the pairs of joint output sequences from $\mathcal{C}_1$ and $\mathcal{C}_2$. We have

$$d_{\min} = \min \{d_{\text{free},1}, d_{\text{free},2}\}. \tag{5.17}$$

Proof: Consider

$$\mathbf{a} = \{(b_{1,1}, c_{1,1}), \ldots, (b_{1,N}, c_{1,N}), \ldots, (b_{L,1}, c_{L,1}), \ldots, (b_{L,N}, c_{L,N})\}$$
$$\text{and } \mathbf{a}' = \{(b'_{1,1}, c'_{1,1}), \ldots, (b'_{1,N}, c'_{1,N}), \ldots, (b'_{L,1}, c'_{L,1}), \ldots, (b'_{L,N}, c'_{L,N})\},$$

which are two different joint output sequences from $\mathcal{C}_1$ and $\mathcal{C}_2$, where $\mathbf{b}, \mathbf{b}' \in \mathcal{C}_1$ and $\mathbf{c}, \mathbf{c}' \in \mathcal{C}_2$. Denote by d_{H} the Hamming distance between two such sequences. If $\mathbf{b} \neq \mathbf{b}'$, the Hamming distance between $\mathbf{b}$ and $\mathbf{b}'$ is not less than $d_{\text{free},1}$. Therefore, $d_{\text{H}} \geq d_{\text{free},1}$. Similarly, if $\mathbf{c} \neq \mathbf{c}'$, $d_{\text{H}} \geq d_{\text{free},2}$. Since at least one of two cases must occur, we have $d_{\min} \geq \min \{d_{\text{free},1}, d_{\text{free},2}\}$. Assume that $d_{free,2} \leq d_{free,1}$, the equality holds since we can choose $\mathbf{b} = \mathbf{b}'$, and $\mathbf{c}$ and $\mathbf{c}'$ are two different sequences with $d_{free,2}$ Hamming distance. From this, we have (5.17) and completes the proof. $\qquad\square$

Although FER is considered so far, the same diversity can also be observed
by bit error rate (BER).
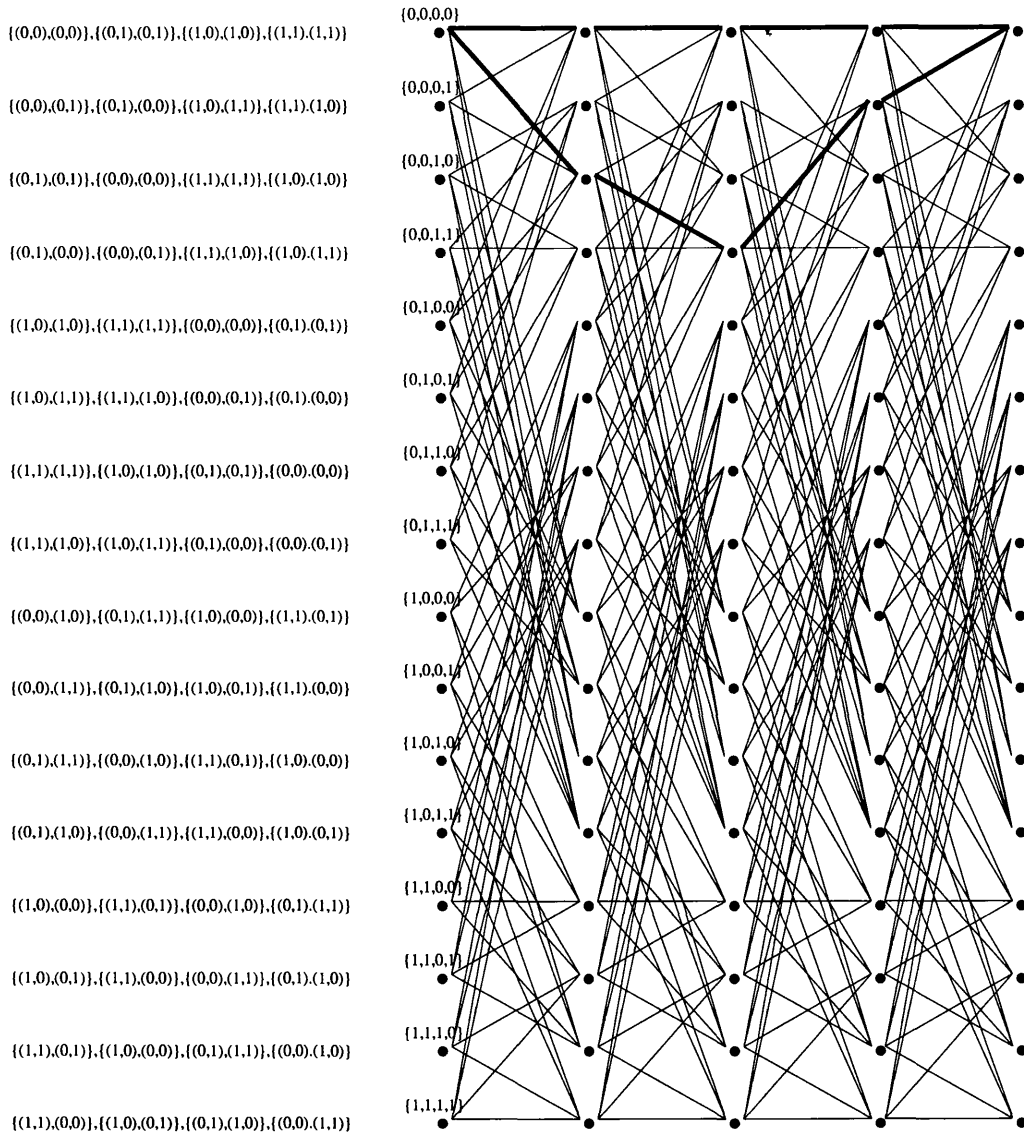
Figure 5.2: Full-state trellis for the pair of (5,7) and (6,7) convolutional codes.

Figure 5.2 illustrates a trellis diagram for a joint encoder with C_1 and C_2 of
generators (5,7) and (6,7), respectively, both are of memory length 2. On the
left of each state is the list of joint output sequences resulting from transitions

91

triggered by the pairs of message bits, $(0,0),(0,1),(1,0)$, and $(1,1)$, respectively. The two paths that are merged after 4 stages shown by thicker lines represent the two joint output sequences corresponding to the sequence of pairs of zeros and $\{(0,1),(0,1),(0,0),(0,0),(0,1),(0,0),(0,0),(0,1),\ldots\}$. The resulting Hamming distance is 4, which is the free distance of the (6,7) convolutional code.

On the selection for a pair of convolutional codes, which are constrained on the memory lengths of codes, the optimal choice for convolutional codes at source nodes can be easily found from Lemma 1. That is, the two source nodes should choose the same convolutional code, which has the largest free distance over all the convolutional codes for a given memory length constraint. For example, if $\nu_1, \nu_2 \leq 2$, the convolutional code of $(5,7)$ is optimal for two source nodes.

Note that for turbo codes, the diversity gain is not very important but the distribution of the weights for Hamming distances. Although a performance analysis for turbo codes could be difficult to derive, we deem that the two turbo codes used at two source nodes also need to be identical since it can maximize the decoding performance at each constituent decoder.

5.4 Reduced-state decoding

Based on the full-state trellis structure, the complexity of a decoding algorithm is $\mathcal{O}(2^{\nu_1+\nu_2})$, where $\nu_k, k = 1, 2$, is the memory length of the convolutional encoder at S_k. That is, the decoding complexity exponentially increases with the sum of memory length. Compared to a receiver in a system of direct link, the complexity at the relay node is approximately squared. Therefore, it could be desirable to find a lower decoding method at the relay node. Since the relay node only needs to decode the XORed message sequence rather than two original message sequences, say $\mathbf{u}$ and $\mathbf{v}$, there might be efficient decoding schemes that only decode the XORed message sequence. In this section, we study such a decoding scheme by exploiting a reduced-state trellis.

Our proposed reduced-state trellis is constructed by merging every disjoint group of states in the full-state trellis into a single merged state. For convenience,

we assume that two constituent convolutional encoders have the same memory length, i.e., $\nu_1 = \nu_2 = \nu$. (If their memory lengths are different, the shorter memory can be extended and the extension does not affect the outputs of encoder.) Let $\tilde{S}$ denote the state alphabet for $\mathcal{C}_k$ (due to the same memory length, $\tilde{S}$ is identical for both codes). The full-state state alphabet for joint two-user decoding is $\mathcal{S} = \tilde{S} \times \tilde{S}$. Any group of full-state states $S_l = \{u_{l-1}, \ldots, u_{l-\nu}, v_{l-1}, \ldots, v_{l-\nu}\}$ that have the same $\{u_{l-1} \oplus v_{l-1}, \ldots, u_{l-\nu} \oplus v_{l-\nu}\}$ is merged into a single merged state defined by $\tilde{S}_l = \{u_{l-1} \oplus v_{l-1}, \ldots, u_{l-\nu} \oplus v_{l-\nu}\} \in \mathcal{R}$, where $\mathcal{R}$ denotes the state alphabet of the reduced-state trellis. Clearly, $\mathcal{R} = \tilde{S}$. From now on, we refer the states in the full-state and reduced-state trellis to as type-A and type-B states, respectively. In addition, multiple parallel transitions from a group to another of type-A states, where the elements in each group are merged into a type-B state, are also merged into a single transition in the reduced-state trellis. While there is a one-to-one correspondence between transitions and their labels (a label is the joint output sequence triggered by a transition) in the full-state trellis, each transition in the reduced-state trellis is associated with multiple labels.

It is clear that any path in the reduced-state trellis uniquely corresponds to an XORed message sequence. Therefore, if a type-B state sequence, denoted by $\{\tilde{S}_l\}$, is recovered from the reduced-state trellis, the corresponding XORed message is immediately decoded, which is what we want at R with a PNC protocol. Based on the reduced-state trellis, the branch metric is modified to be

$$\tilde{M}_l\left(\tilde{S}_l, S_{l+1}\right) = \max_{\substack{S_l, S_{l+1}: \\ S_l \in \mathcal{P}(\tilde{S}_l) \\ S_{l+1} \in \mathcal{P}(\tilde{S}_{l+1})}} M_l\left(S_l, S_{l+1}\right), \tag{5.18}$$

where $\mathcal{P}(\tilde{S}_l) = \{S_l \mid \tilde{S}_l = \{u_{l-1} \oplus v_{l-1}, \ldots, u_{l-\nu} \oplus v_{l-\nu}\}\}$. The Viterbi and BCJR algorithms described above are applied for decoding with some modification: (u_l, v_l) is replaced by its XORed version given by $m_l = u_l \oplus v_l$; and (5.12) is replaced by (5.18).

Although we need additional multiple binary comparators and the number of comparators is decided by the number of distinct labels on each reduced-state transition (for the case of $\mathcal{C}_1 = \mathcal{C}_2$ the number of binary comparators is $2^N - 1$), it is only required to track 2^ν survival paths in each stage. Thus, the complexity

of reduced-state decoding is approximately equal to a square root of that of the full-state decoding.

Let us define the free distance of the reduced-state trellis as:

Definition 2 The free distance of a reduced-state trellis is the minimum two-user Hamming distance over all the pairs of paths in this trellis.

The following lemma shows that the diversity order of reduced-state decoding is same as that of the full-state decoding provided that the two identical codes are used at the source nodes.

Lemma 2 *If $\mathcal{C}_1 = \mathcal{C}_2 = \mathcal{C}$ and denote by d_{free} the free distance of these codes, the free distance of the reduced-state trellis is equal to the free distance of $\mathcal{C}$, i.e., d_{free}.*

Proof: Consider the following joint output sequence:

$$\mathbf{a} = \left\{ (b_{1,1}, c_{1,1}), \ldots, (b_{L,N}, c_{L,N}) \right\},$$

which is associated with a state sequence $\tilde{\mathbf{S}}$ from the reduced-state trellis, where $\mathbf{b}, \mathbf{c} \in \mathcal{C}$. Let $\tilde{\mathbf{a}} = \mathbf{b} \oplus \mathbf{c}$, which is called the XORed-coded version of $\mathbf{a}$. Let $\mathbf{u} = \mathcal{C}^{-1}(\mathbf{b})$ and $\mathbf{v} = \mathcal{C}^{-1}(\mathbf{c})$. Due to the linear property of convolutional codes, $\tilde{\mathbf{a}} = \mathcal{C}(\mathbf{u} \oplus \mathbf{v})$. This shows that the XORed-coded versions of all joint output sequences associated with $\tilde{\mathbf{S}}$ are identical to $\tilde{\mathbf{a}}$.

Now, we regard the XORed-coded sequence associated with each path in the reduced-state trellis as the secondary label, which is unique. The minimum Hamming distance between two secondary labels associated with two different paths is equal to d_{free}. Since $(\mathbf{b}, \mathbf{c}) \neq (\mathbf{b}', \mathbf{c}')$ if $\mathbf{b} \oplus \mathbf{c} \neq \mathbf{b}' \oplus \mathbf{c}'$, we can conclude that the free distance of the reduced-state trellis is equal to d_{free}. $\qquad \square$

The result in Lemma 2 shows that the diversity gain of decoding based on a reduced-trellis is identical to that based on a full-trellis over fading channels. Thus, the use of a reduced-trellis in decoding can efficiently reduce the complexity

{{(0,0),(0,0)},{(0,0),(1,1)},{(1,1),(0,0)},{(1,1),(1,1)}}
{{(0,1),(0,1)},{(0,1),(1,0)},{(1,0),(0,1)},{(1,0),(1,0)}}

{{(0,1),(0,1)},{(0,1),(1,0)},{(1,0),(0,1)},{(1,0),(1,0)}}
{{(0,0),(0,0)},{(0,0),(1,1)},{(1,1),(0,0)},{(1,1),(1,1)}}

{{(0,0),(0,1)},{(0,0),(1,0)},{(1,1),(0,1)},{(1,1),(1,0)}}
{{(0,1),(0,0)},{(0,1),(1,1)},{(1,0),(0,0)},{(1,0),(1,1)}}

{{(0,1),(0,0)},{(0,1),(1,1)},{(1,0),(0,0)},{(1,0),(1,1)}}
{{(0,0),(0,1)},{(0,0),(1,0)},{(1,1),(0,1)},{(1,1),(1,0)}}
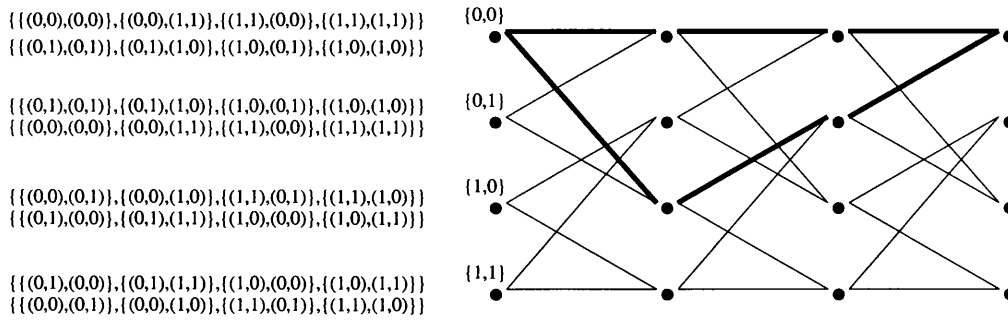
Figure 5.3: Reduced-state trellis for the pair of two (5,7) convolutional codes.

without a significant performance loss. Note that the number of binary comparisons is $2^N - 1$ in computing each branch metric if $\mathcal{C}_1 = \mathcal{C}_2$ as implied by the proof of Lemma 2.

We illustrate the reduced-state trellis from two identical (5,7) convolutional codes in Figure 5.3. At the right of each state, the list of labels on the transitions caused by $u_l \oplus v_l = 0$ and $u_l \oplus v_l = 1$ are given in the first and second rows, respectively. For instance, the transition from the (0,0) to (1,0) type-B state is constructed by merging a set of type-A transitions, each is from an element of state group $\{(0,0,0,0),(0,1,0,1),(1,0,1,0),(1,1,1,1)\}$ to an element of the group $\{(0,0,1,0),(0,1,1,1),(1,0,0,0),(1,1,0,1)\}$. The distinct labels for such transition are $\{(0,1),(0,1)\}$, $\{(0,1),(1,0)\}$, $\{(1,0),(0,1)\}$, and $\{(1,0),(1,0)\}$. In the depicted reduced-state trellis, the free distance is 5, the same as that of the (5,7) convolutional code.

Although the diversity order of reduced-state decoding are kept unchanged, the modification of branch metric leads to that the path associated with maximum modified path metric might not be aligned with the optimal path. Therefore, the decoding based on reduced-state trellis is considered as sub-optimal in terms of ML. The loss of performance as a cost for reduced complexity will be seen through simulations.

5.5 Simulation results

In this section, we use two simulation setups to: i) confirm that the same diversity order can be achieved over fading channels for the full-state and reduced-state decoding if two identical convolutional codes are used at two source nodes; ii) see the gap between the performance of full-state and reduced-state decoding when the channels are non-fading. In both the simulation setups, BPSK is used for modulation. Furthermore, we assume that identical transmission powers are used at the all nodes and and they are also affected by the same noise power. Although the performance is significantly affected by weakest link in the case of imperfect power control, the diversity analyses still hold. Therefore, we consider only the case of perfectly equal power control to confirm the diversity analyses.

In the first simulation setup, we assume that $\{h_t^{(k)}\}$ and $\{g_t^{(k)}\}$, $k = 1, 2$, are independent. Furthermore, each element in these sequences of channel gains is a CSCG random variable with zero mean and unit variance (Rayleigh fading channels). All channel codes have the same code rate such that $r = r' = 1/2$. For a given memory length, we choose the convolutional code with maximum Hamming distance in the BC phase for all simulations, i.e., if memory length is 2, the (5,7) convolutional code is chosen, while (23,35) convolutional code is used for the memory length 4 constraint. The performance index is the average end-to-end BER over two communication flows.

As shown in Figure 5.4, when the two source nodes use the same (5,7) convolutional code and the relay node uses the full-state decoding, the BER slope is 2 dB/decade. For a comparison purpose, we consider another case, where two different channel codes, (5,7) and (6,7) non-recursive convolutional codes, are used. This case provides the 2.5 dB/decade BER slope, which confirms that the diversity order of the system is equal to the free distance of the worst code. This two supporting results also confirm the principle of choosing codes for a given memory length constraint.

As mentioned, the diversity order is retained with reduced-state trellis decoding provided that the same code is used at both the source nodes. It is verified in Figure 5.4 for two cases of a) the same (5,7) non-recursive convolutional code and
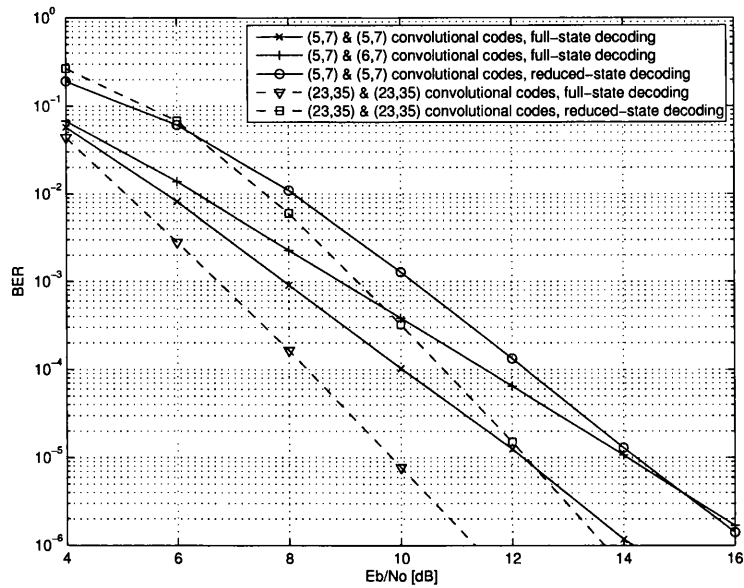
Figure 5.4: Simulation results for full-state decoding using the same and different convolutional codes and reduced-state decoding using the same convolutional codes, Rayleigh fading channels.

b) the same (23,35) non-recursive convolutional code. However, there are about 2 dB performance degradation in both the cases. The performance loss can be seen as the cost resulting from the reduced decoding complexity.

In the second simulation setup, we assume that all channels are AWGN. Furthermore, we consider two cases of using channel codes: convolutional codes and turbo codes. In both the cases, identical channel codes, either convolutional codes or turbo codes, are employed at the two source nodes and relay node. In the first case, the (5,7) non-recursive convolutional codes are used. In the second case, all the nodes use the same turbo codes, each are constructed from two identical constituent recursive convolutional codes whose transfer functions are 1 and $(1 + D^2)/(1 + D + D^2)$.

Figure 5.5 exhibits small performance gaps over AWGN channels. For the case of convolutional codes, the performance gap is only 0.3 dB SNR, while the gap is wider to be 0.5 dB SNR for the case of turbo codes. From the simulation
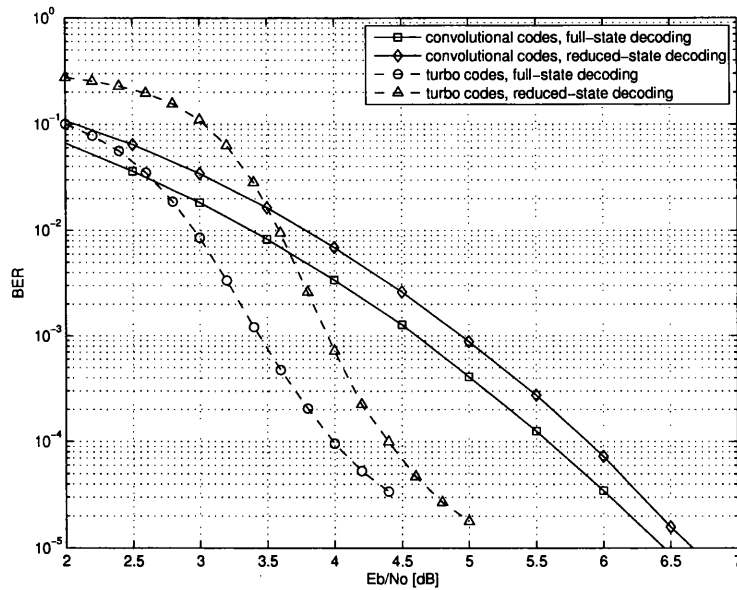
Figure 5.5: Simulation results for AWGN channels.

results for two types of channels, fading and non-fading, reduced-state decoding is shown to be a good proposal since it can provide a performance that is not far from that of full-state decoding while the decoding complexity is significantly reduced.

5.6 Summary

In this chapter, we studied the use of convolutional codes for TWRNs with PNC protocol. It was shown that a nearly-optimal decoding for element-wise XORed messages can be achieved at the relay node using a Viterbi algorithm based decoder over a two-user trellis where the number of states is the product of numbers of states for individual codes. This decoding scheme provided the same diversity order as the free distance of the worst code for fading channels. Consequently, it was shown that the optimal selection for two source nodes' convolutional codes is the pair of the same code that has the largest free distance for a given memory length constraint. In addition, due to the nature of PNC protocols, where only

XORed messages need to be decoded rather than individual messages at the relay node, we proposed the use of a reduced-state trellis for decoding to reduce decoding complexity. It was shown that the complexity of the reduced-state decoding is an approximately square root of that of the full-state decoding, while there is no loss of diversity gain for fading channels. Simulation results showed that, however, there is a performance gap of approximately 2 dB SNR paying for the complexity reduction. In addition, the BCJR algorithm can work on a reduced-state trellis. Therefore, a low complexity decoding can be performed for the case of turbo codes. Simulation results also showed that small performance gaps between reduced-state and full-state decoding over AWGN channels were achieved, which are about 0.3 and 0.5 dB SNRs for convolutional and turbo codes, respectively.

6

PNC in TWRNs: Antenna diversity in networks of single antenna relays

6.1 Introduction

In Chapter 5, we investigated a low complexity decoding method for physical-layer network coding (PNC) in conjunction with channel codes in two-way relay networks (TWRN). It was shown that if two identical convolutional codes are used at two source nodes, low complexity decoding can be employed at the relay node and a diversity gain equal to the free distance of convolutional codes can be achieved. This diversity is a time diversity, which comes from the fact that consecutive coded signals are transmitted with independent fading gains.

Another form of diversity is antenna diversity [12]. To exploit it, a transmitter and/or receiver need to be equipped with multiple antennas. In this chapter, we consider a two-way relay system, in which there are multiple antennas at both the source nodes. In addition, the performance is examined in finding closed-form expressions of upper and lower bounds on symbol error probability (SEP).

In the literature, there is a number of research works that investigate the performances of TWRNs. In [89], the authors derived upper and lower bounds

on SEP for the system with a single antenna at each node. In [90], the performance for a system with multiple cooperative relays was investigated. However, to the best of our knowledge, there has been no research work considering the performance when the source nodes are equipped with multiple antennas yet.

The system to be considered in this chapter has multiple antennas at both source nodes. For simplicity, we assume that each source node is equipped with two antennas while there is only one antenna at the relay node. The reason of equipping the relay node with a single antenna is that one would like to keep a low implementation cost at the relay node. To exploit the transmit diversity, the Alamouti code [18], which can achieve the full transmit diversity [12], is employed at both the source nodes. Upper and lower bounds on SEP are derived for Binary Phase Shift Keying (BPSK) modulation scheme. From the derived bounds, it is shown that a diversity order of two can be achieved even though the relay node has only a single antenna. Simulation results are provided to confirm the analysis for the SEP.

The remainder of this chapter is organized as follows. Section 6.2 presents the system model. In Section 6.3, we derive upper and lower bound on SEP of the system. Simulation results are provided in Section 6.4. Section 6.5 summarizes this chapter.
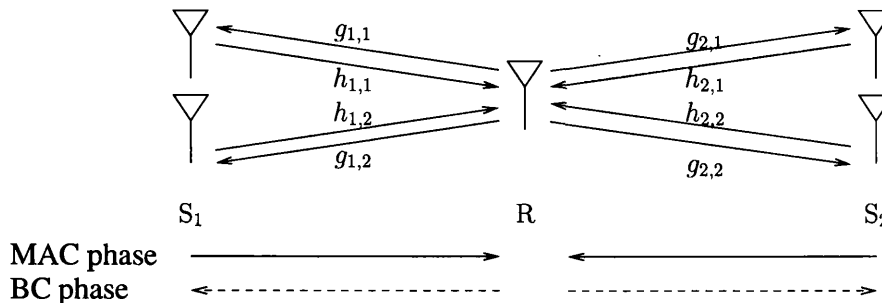
6.2 System model

Figure 6.1: System model.

Even though we focus on the SEP with binary phase shift keying (BPSK), we consider the system model for arbitrary modulation scheme including BPSK in this section. The system model of a two-way relay system consisting of two source node S_1 and S_2 and a relay node R is illustrated in Figure 6.1. S_1 and S_2 exchange their information messages with the help of a relay R. We assume that the channel state does not change during two consecutive time slots in each phase for all links. Let k, i, and j denote the indices of source nodes, antennas, and time slots, respectively. Assume that the same signal constellation $\mathcal{M}$ of size M is used at all nodes. (We believe that the same constellation size is necessary to construct a network coding at the relay node.) In the MAC phase, S_1 and S_2 send $\mathbf{U} = \begin{bmatrix} u_1 & -u_2^* \\ u_2 & u_1^* \end{bmatrix}$ and $\mathbf{V} = \begin{bmatrix} v_1 & -v_2^* \\ v_2 & v_1^* \end{bmatrix}$, $u_1, u_2, v_1, v_2 \in \mathcal{M}$, simultaneously, respectively. Note that the jth columns of both $\mathbf{U}$ and $\mathbf{V}$ are transmitted in time slot j. The received signal vector at R is

$$\mathbf{r}^T = \sqrt{\frac{E_1}{2}} \mathbf{h}_1^T \mathbf{U} + \sqrt{\frac{E_2}{2}} \mathbf{h}_2^T \mathbf{V} + \mathbf{w}^T, \qquad (6.1)$$

where $\mathbf{h}_k = [h_{k,1} \; h_{k,2}]^T$, $k = 1, 2$, is the channel vector of the kth link, E_k is the transmit powers at S_k, and $\mathbf{w} \sim \mathcal{CN}(\mathbf{0}_{2,1}, \sigma_R^2 \mathbf{I}_2)$ is the background noise vector at R.

Let the XORed-like version of (u_i, v_i), $i = 1, 2$, be [90]

$$z_i = f(u_i, v_i) = \ell^{-1}\left((\ell(u_i) + \ell(v_i)) \pmod{M}\right), \qquad (6.2)$$

where $\ell(x) \in \{0, 1, \ldots, M-1\}$ is the label index of x in $\mathcal{M}$. Assuming that the channel state information (CSI) is perfectly known at R, z_i, $i = 1, 2$, is detected as

$$\hat{z}_i = \arg\max_{z \in \mathcal{M}} \sum_{(\mathbf{U}, \mathbf{V}): f(u_i, v_i) = z} \exp(-T(\mathbf{U}, \mathbf{V})), \qquad (6.3)$$

where

$$T(\mathbf{U}, \mathbf{V}) = \left\| \frac{\mathbf{r}^T}{\sigma_R} - \sqrt{\frac{\bar{\gamma}_1}{2}} \mathbf{h}_1^T \mathbf{U} - \sqrt{\frac{\bar{\gamma}_2}{2}} \mathbf{h}_2^T \mathbf{V} \right\|^2 \qquad (6.4)$$

and $\bar{\gamma}_k = E_k / \sigma_R^2$ is the signal-to-noise ratio (SNR) at the relay node for the signal from S_k to R. The solution in (6.3) is uniquely decided unless the two channel vectors have certain relations. For example, if BPSK is employed and

$h_{1,1} = h_{2,2}$ and $h_{1,2} = -h_{2,1}$, the solution might not be unique. However, the probability of that $\mathbf{h}_1$ and $\mathbf{h}_2$ have such relations is zero if they are independent fading channels.

In BC phase, $\hat{z}_1$ and $\hat{z}_2$ are broadcasted by R. In time slot j of the BC phase, S_k receives:

$$\mathbf{y}_{k,j} = \sqrt{E_R}\mathbf{g}_k\hat{z}_j + \mathbf{n}_{k,j}, \ j = 1, 2, \tag{6.5}$$

where E_R is the transmit power at R, $\mathbf{g}_k = [g_{k,1} \ g_{k,2}]^T$ is the channel vector of the link from R to S_k, $\mathbf{n}_{k,j} \sim \mathcal{CN}(\mathbf{0}_{2,1}, \sigma_k^2 \mathbf{I}_2)$ is the background noise vector. S_k detects $\hat{z}_j$ as

$$\tilde{z}_{k,j} = \arg\min_{z \in \mathcal{M}} \left\| \frac{\mathbf{y}_{k,j}}{\sigma_k} - \sqrt{\bar{\gamma}_{k+2}}\mathbf{g}_k z \right\|^2, \tag{6.6}$$

where $\bar{\gamma}_{k+2} = E_R/\sigma_k^2$ is the SNR at the sink k. Finally, each sink detects the symbols sent by the other source as

$$\hat{v}_i = \ell^{-1}\left((\ell(\tilde{z}_{1,j}) - \ell(u_i)) \pmod{M}\right);$$
$$\text{and } \hat{u}_i = \ell^{-1}\left((\ell(\tilde{z}_{2,j}) - \ell(v_i)) \pmod{M}\right), \tag{6.7}$$

where $i = j \in \{1, 2\}$. For fixed v, the mapping from u to $f(u, v)$ is a one-to-one mapping. Hence, the combination of (6.6) and (6.7) is actually the maximum likelihood (ML) detection for u_i and v_i.

6.3 Error probability analysis

In the system model, $\mathbf{g}_k$ could be modeled to be identical to or independent of $\mathbf{h}_k$ depending on whether the links between S_k and R are reciprocal or not. In this section, we focus on the case of $\mathbf{g}_k = \mathbf{h}_k$, $k = 1, 2$. In addition, for analysis, we assume that $h_{k,i}$'s, $k = 1, 2$, $i = 1, 2$, are independent and $h_{k,i} \sim \mathcal{CN}(0, 1)$, i.e., Rayleigh fading channels. Note that the upper and lower bounds resulting from the analysis for this case still hold for the case of independent $\mathbf{g}_k$ and $\mathbf{h}_k$.

6.3.1 Symbol error probability

Let P_{mac} denote the SEP in the MAC phase for given $\mathbf{h}_1$ and $\mathbf{h}_2$, which is defined as

$$P_{mac} \triangleq \frac{\Pr\{\hat{z}_1 \neq f(u_1, v_1)|\mathbf{h}_1, \mathbf{h}_2\} + \Pr\{\hat{z}_2 \neq f(u_2, v_2)|\mathbf{h}_1, \mathbf{h}_2\}}{2}. \tag{6.8}$$

Let $P_{bc,k}$ denote the SEP in the BC phase at S_k for given $\mathbf{h}_k$:

$$P_{bc,k} \triangleq \frac{[\Pr\{\tilde{z}_{k,1} \neq \hat{z}_1|\mathbf{h}_k\} + \Pr\{\tilde{z}_{k,2} \neq \hat{z}_2|\mathbf{h}_k\}]}{2}. \tag{6.9}$$

In a one-way transmission, e.g., only the flow from S_1 to S_2 is considered, if there is only an error at one of the two phases, a symbol cannot be correctly detected by the receiver node. Furthermore, if both the phases have errors, the probability of correct detection is only $1/(M-1)$. Therefore, the end-to-end SEP, denoted by P_{EtoE}, which is averaged over the transmissions of two ways, is given by

$$\begin{aligned} P_{EtoE} &= P_{mac}\left(1 - \frac{P_{bc,1} + P_{bc,2}}{2}\right) + (1 - P_{mac})\frac{P_{bc,1} + P_{bc,2}}{2} \\ &\quad + \frac{M-2}{M-1}P_{mac}\frac{P_{bc,1} + P_{bc,2}}{2} \\ &= P_{mac} + \frac{P_{bc,1} + P_{bc,2}}{2} - \frac{M}{M-1}P_{mac}\frac{P_{bc,1} + P_{bc,2}}{2}. \end{aligned} \tag{6.10}$$

The average end-to-end SEP is then $\overline{P}_{EtoE} = \mathbb{E}[P_{EtoE}]$, where the expectation is taken w.r.t. the distribution of $(\mathbf{h}_1, \mathbf{h}_2)$. As we consider BPSK, we have $\mathcal{M} = \{-1, 1\}$ and $f(u, v) = uv$ in (6.2).

6.3.2 Lower and upper bounds

Now, we derive lower and upper bounds. For BPSK, $P_{bc,k}$ can be exactly obtained by

$$P_{bc,k} = Q\left(\sqrt{2\bar{\gamma}_{k+2}\left\|\mathbf{h}_k\right\|^2}\right), \tag{6.11}$$

where $Q(\cdot)$ is the Gaussian Q-function [22, Equation 2-1-97].

In the MAC phase, as the Alamouti codeword alphabets at S_1 and S_2 are

$$\mathcal{U} = \{\mathbf{U}_1, \mathbf{U}_2, \mathbf{U}_3, \mathbf{U}_4\}$$

and

$$\mathcal{V} = \{\mathbf{V}_1, \mathbf{V}_2, \mathbf{V}_3, \mathbf{V}_4\},$$

respectively, where

$$\mathbf{U}_1 = \mathbf{V}_1 = \begin{bmatrix} 1 & -1 \\ 1 & 1 \end{bmatrix}, \; \mathbf{U}_2 = \mathbf{V}_2 = \begin{bmatrix} 1 & 1 \\ -1 & 1 \end{bmatrix},$$

$$\mathbf{U}_3 = \mathbf{V}_3 = \begin{bmatrix} -1 & 1 \\ -1 & -1 \end{bmatrix}, \; \mathbf{U}_4 = \mathbf{V}_4 = \begin{bmatrix} -1 & -1 \\ 1 & -1 \end{bmatrix},$$

the detection regions cannot be easily specified. Therefore, we will derive upper and lower bounds on P_{mac}. Furthermore, it is extremely hard to analyze the SEP for the ML detection rule in (6.3) since the metric is a sum of exponential functions. We will analyze its modification based on max-log approximation. The modified detection rule at R is given by

$$\hat{z}_i = \arg \min_{z \in \{-1,1\}} \; \min_{(\mathbf{U}, \mathbf{V}): u_i v_i = z} T(\mathbf{U}, \mathbf{V}). \tag{6.12}$$

Based on the rule given in (6.12), the following lemma shows the upper and lower bounds on P_{mac} for given $\mathbf{h}_1$ and $\mathbf{h}_2$.

Lemma 3 *For given channel realizations $\mathbf{h}_1$ and $\mathbf{h}_2$, P_{mac} is upper- and lower-bounded by P_{mac}^U and P_{mac}^L, respectively. Here,*

$$P_{mac}^U \triangleq \sum_{(m,n) \neq (1,1)} P_{PEP,m,n}, \tag{6.13}$$

where $P_{PEP,m,n} \triangleq Q\left(q_{m,n}\right)$ with $q_{m,n} \triangleq \left\| \sqrt{\frac{\bar{\gamma}_1}{4}} \mathbf{h}_1^T (\mathbf{U}_1 - \mathbf{U}_m) + \sqrt{\frac{\bar{\gamma}_2}{4}} \mathbf{h}_2^T (\mathbf{V}_1 - \mathbf{V}_n) \right\|$, $1 \leq m, n \leq 4$. Note that m and n are the indices for codewords. Furthermore,

$$P_{mac}^L \triangleq Q\left(\sqrt{\min\left(\bar{\gamma}_1 \|\mathbf{h}_1\|^2, \bar{\gamma}_2 \|\mathbf{h}_2\|^2 \right)} \right). \tag{6.14}$$

Proof: Without loss of generality, we assume that $(\mathbf{U}_1, \mathbf{V}_1)$ is sent. Therefore, the actual XORed-like symbols are $z_1 = z_2 = 1$. Let

$$T_1 = \min_{\substack{(\mathbf{U},\mathbf{V}):\, u_1v_1=1 \\ (\mathbf{U},\mathbf{V})\neq(\mathbf{U}_1,\mathbf{V}_1)}} T(\mathbf{U},\mathbf{V});$$

$$T_2 = \min_{(\mathbf{U},\mathbf{V}):\, u_1v_1=-1} T(\mathbf{U},\mathbf{V}).$$

Considering the error detection probability for z_1, we have

$$\Pr\{\hat{z}_1 = -1 | (\mathbf{U}_1, \mathbf{V}_1), \mathbf{h}_1, \mathbf{h}_2\}$$
$$= \Pr\{\min(T(\mathbf{U}_1, \mathbf{V}_1), T_1) > T_2 | (\mathbf{U}_1, \mathbf{V}_1), \mathbf{h}_1, \mathbf{h}_2\}$$
$$= \Pr\{(T_1 \geq T(\mathbf{U}_1, \mathbf{V}_1)) \& (T(\mathbf{U}_1, \mathbf{V}_1) > T_2) | (\mathbf{U}_1, \mathbf{V}_1), \mathbf{h}_1, \mathbf{h}_2\}$$
$$+ \quad \Pr\{(T(\mathbf{U}_1, \mathbf{V}_1) > T_1) \& (T_1 > T_2) | (\mathbf{U}_1, \mathbf{V}_1), \mathbf{h}_1, \mathbf{h}_2\}$$
$$\leq \Pr\{T(\mathbf{U}_1, \mathbf{V}_1) > T_2 | (\mathbf{U}_1, \mathbf{V}_1), \mathbf{h}_1, \mathbf{h}_2\}$$
$$+ \quad \Pr\{T(\mathbf{U}_1, \mathbf{V}_1) > T_1 | (\mathbf{U}_1, \mathbf{V}_1), \mathbf{h}_1, \mathbf{h}_2\}$$
$$\leq \sum_{(m,n)\neq(1,1)} \Pr\{T(\mathbf{U}_1, \mathbf{V}_1) > T(\mathbf{U}_m, \mathbf{V}_n) | (\mathbf{U}_1, \mathbf{V}_1), \mathbf{h}_1, \mathbf{h}_2\}$$
$$= \sum_{(m,n)\neq(1,1)} P_{PEP,m,n}.$$

Note that the last line of this equation is the union bound of error probability for the detection of $(\mathbf{U}, \mathbf{V})$, which is the summation of the pair-wise error probabilities (PEPs). In combining with the same derivation of the error detection probability for z_2, the upper bound on P_{mac} can be obtained.

To derive the lower bound, we assume that there is a genie who informs the detector at the relay node about $\mathbf{U}$ if $\bar{\gamma}_1 \|\mathbf{h}_1\|^2 \geq \bar{\gamma}_2 \|\mathbf{h}_2\|^2$, or $\mathbf{V}$ otherwise. With the aid of genie, the performance must be better than the original system model described in Section 6.2. If $\mathbf{U}$ is known, $P_{mac} \geq Q\left(\sqrt{\bar{\gamma}_2 \|\mathbf{h}_2\|^2}\right)$. If $\mathbf{V}$ is known, $P_{mac} \geq Q\left(\sqrt{\bar{\gamma}_1 \|\mathbf{h}_1\|^2}\right)$. Thus, we have (6.14) and it completes the proof. $\square$

From the bounds on P_{mac}, the following theorem shows the upper and lower bounds on $\overline{P}_{EtoE}$.

Theorem 1 *For BPSK, the average end-to-end SEP is upper- and lower-bounded by $\overline{P}^U_{EtoE}$ and $\overline{P}^L_{EtoE}$, respectively. Here,*

$$\overline{P}^U_{EtoE} \triangleq \frac{1}{2}\phi(2,\bar{\gamma}_3) + \frac{1}{2}\phi(2,\bar{\gamma}_4) + \sum_{\substack{1 \le m,n \le 4 \\ (m,n) \ne (1,1)}} \phi(2, \frac{\bar{\alpha}_{m,n}}{2}), \qquad (6.15)$$

where $\phi(L,x) \triangleq \left[\frac{1-\mu(x)}{2}\right]^L \sum_{l=0}^{L-1} \binom{L-1+l}{l} \left[\frac{1+\mu(x)}{2}\right]^l$ with $\mu(x) \triangleq \sqrt{\frac{x}{1+x}}$ [22, Equation 14-4-15] and the $\bar{\alpha}_{m,n}$'s, $1 \le m, n \le 4$, $(m,n) \ne (1,1)$, are given in Table 6.1. Furthermore,

$$\overline{P}^L_{EtoE} \triangleq \max \left\{ c_1 \bar{\gamma}^2 \phi\left(2, \frac{\bar{\gamma}}{2}\right) + c_2 \bar{\gamma}^2 \phi\left(3, \frac{\bar{\gamma}}{2}\right), \right.$$
$$\left. \frac{1}{2}\phi(2,\bar{\gamma}_3) + \frac{1}{2}\phi(2,\bar{\gamma}_4) \right\}, \qquad (6.16)$$

where $c_1 = \frac{1}{\bar{\gamma}_1^2} + \frac{1}{\bar{\gamma}_2^2}$, $c_2 = \frac{2}{\bar{\gamma}_1 \bar{\gamma}_2}$, and $\bar{\gamma} = \frac{\bar{\gamma}_1 \bar{\gamma}_2}{\bar{\gamma}_1 + \bar{\gamma}_2}$.

Table 6.1: Values of $\bar{\alpha}_{m,n}$.

$m \backslash n$	1	2	3	4
1		$\bar{\gamma}_2$	$2\bar{\gamma}_2$	$\bar{\gamma}_2$
2	$\bar{\gamma}_1$	$\bar{\gamma}_1 + \bar{\gamma}_2$	$\bar{\gamma}_1 + 2\bar{\gamma}_2$	$\bar{\gamma}_1 + \bar{\gamma}_2$
3	$2\bar{\gamma}_1$	$2\bar{\gamma}_1 + \bar{\gamma}_2$	$2\bar{\gamma}_1 + 2\bar{\gamma}_2$	$2\bar{\gamma}_1 + \bar{\gamma}_2$
4	$\bar{\gamma}_1$	$\bar{\gamma}_1 + \bar{\gamma}_2$	$\bar{\gamma}_1 + 2\bar{\gamma}_2$	$\bar{\gamma}_1 + \bar{\gamma}_2$

Proof: From (6.10) and Lemma 3, we have

$$\max \left(\mathbb{E}\left[P^L_{mac}\right], \frac{\mathbb{E}\left[P_{bc,1}\right] + \mathbb{E}\left[P_{bc,2}\right]}{2} \right) \le \overline{P}_{EtoE} \le \mathbb{E}\left[P^U_{mac}\right] + \frac{\mathbb{E}\left[P_{bc,1}\right] + \mathbb{E}\left[P_{bc,2}\right]}{2}. \tag{6.17}$$

Since $\|\mathbf{h}_k\|^2$ is chi-square distributed with 4 degrees of freedom, we have

$$\mathbb{E}\left[P_{bc,k}\right] = \mathbb{E}\left[Q\left(\sqrt{2\bar{\gamma}_{k+2}\|\mathbf{h}_k\|^2}\right)\right]$$
$$= \phi(2,\bar{\gamma}_{k+2}).$$

In addition, since $(\mathbf{U}_1 - \mathbf{U}_m)$ and $(\mathbf{V}_1 - \mathbf{V}_n)$ are both orthogonal matrices, we have $\mathbf{q}_{m,n} = \sqrt{\bar{\alpha}_{m,n}} \|\mathbf{a}^T_{m,n}\|$, where $\mathbf{a}_{m,n} = [a_{m,n,1}\ a_{m,n,2}]^T \sim \mathcal{CN}(\mathbf{0}_{2,1}, \mathbf{I}_2)$ and $\bar{\alpha}_{m,n}$

is given in Table 6.1. The average PEP is given by

$$\mathbb{E}\left[P_{PEP,m,n}\right] = \mathbb{E}\left[Q\left(\mathbf{q}_{m,n}\right)\right]$$
$$= \phi\left(2, \frac{\bar{\alpha}_{m,n}}{2}\right).$$

From this, the upper bound on $\overline{P}_{EtoE}$ can be found as in (6.15).

For the lower bound on $\overline{P}_{EtoE}$, we need to find $\mathbb{E}\left[P^L_{mac}\right]$. Let $\gamma_k = \bar{\gamma}_k \left\|\mathbf{h}_k\right\|^2$, $k = 1, 2$, and $\beta = \min\left(\gamma_1, \gamma_2\right)$. Note that γ_1 and γ_2 are assumed to be independent. As the pdf and cumulative distribution function (cdf) of γ_k are given by

$$f_{\gamma_k}(\xi) = \frac{\xi}{\bar{\gamma}_k^2} e^{-\frac{\xi}{\bar{\gamma}_k}} u(\xi)$$

and

$$F_{\gamma_k}(\xi) = \left[1 - e^{-\frac{\xi}{\bar{\gamma}_k}} - \frac{\xi}{\bar{\gamma}_k} e^{-\frac{\xi}{\bar{\gamma}_k}}\right] u(\xi),$$

respectively, where

$$u(\xi) = \begin{cases} 1 & \text{if } \xi \geq 1, \\ 0 & \text{otherwise}, \end{cases}$$

the probability density function (pdf) of β becomes [91, Equation (8.6)]

$$f_\beta(\xi) = f_{\gamma_1}(\xi)\left(1 - F_{\gamma_2}(\xi)\right) + f_{\gamma_2}(\xi)\left(1 - F_{\gamma_1}(\xi)\right)$$
$$= \left(\frac{1}{\bar{\gamma}_1^2} + \frac{1}{\bar{\gamma}_2^2}\right)\xi e^{-\left(\frac{1}{\bar{\gamma}_1} + \frac{1}{\bar{\gamma}_2}\right)\xi} u(\xi) + \frac{1}{\bar{\gamma}_1\bar{\gamma}_2}\left(\frac{1}{\bar{\gamma}_1} + \frac{1}{\bar{\gamma}_2}\right)\xi^2 e^{-\left(\frac{1}{\bar{\gamma}_1} + \frac{1}{\bar{\gamma}_2}\right)\xi} u(\xi)$$
$$= c_1 \xi e^{-\frac{\xi}{\bar{\gamma}}} u(\xi) + \frac{c_2}{2\bar{\gamma}} \xi^2 e^{-\frac{\xi}{\bar{\gamma}}} u(\xi),$$

where the definitions of c_1, c_2, and $\bar{\gamma}$ are defined in the statement of the theorem. Its moment generating function (mgf) is then given by

$$M_\beta(s) = \mathbb{E}\left[e^{s\xi}\right]$$
$$= \frac{c_1 \bar{\gamma}^2}{(1 - \bar{\gamma}s)^2} + \frac{c_2 \bar{\gamma}^2}{(1 - \bar{\gamma}s)^3}.$$

Therefore, by using [92, Equation 5.1], [92, Equation 5.3], and [92, Equation 5.17a], we have

$$\mathbb{E}\left[P^L_{mac}\right] = \mathbb{E}\left[Q\left(\sqrt{\beta}\right)\right]$$
$$= c_1 \bar{\gamma}^2 \phi\left(2, \frac{\bar{\gamma}}{2}\right) + c_2 \bar{\gamma}^2 \phi\left(3, \frac{\bar{\gamma}}{2}\right),$$

In combining with the derivation of $\mathbb{E}[P_{bc,k}]$, the lower bound on $\overline{P}_{EtoE}$ can be found as in (6.16) and it completes the proof. $\qquad\square$

Note that (6.17) holds for the case of independent $\mathbf{h}_k$ and $\mathbf{g}_k$, $k = 1, 2$. Thus, Theorem 1 is also applicable to that case.

Since $\phi(L, x) \approx \binom{2L-1}{L} \left(\frac{1}{4x}\right)^L$ for $x \gg 1$ [22, Equation 14-4-18], we can confirm that the diversity order is two through $\overline{P}^U_{EtoE}$ and $\overline{P}^L_{EtoE}$.

6.4 Simulation results
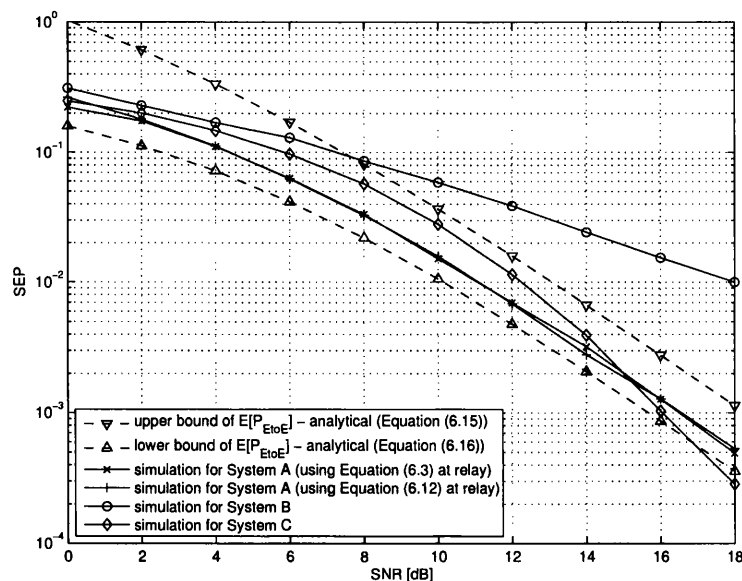
Figure 6.2: Upper and lower bounds and simulation results.

In simulations we compare the following three systems: A) the relay system described in Section 6.2, B) the relay system with single antenna at all nodes, and C) the system of direct-transmission of 2×2 MIMO without relay, which achieves the diversity of order four. For both Systems A) and B) the relay node is assumed to be at equal distance from the two source nodes. For a fair comparison, we assume that the total transmit power of a source node (of two antennas)

in System A is equal to that of a source node (of single antenna) in System B. Furthermore, since System C has no relay, we assume that the distance between the two nodes is a double of that between a source node and the relay in Systems A and B and the path-loss exponent is 3 (thus, the variance of the channel gains in System C is 1/8 of that of System A). All the nodes are affected by the same noise variances. For all the systems, the system SNR is defined as the SNR at the sinks of System A. BPSK is used for modulation in all the systems. Furthermore, perfect synchronization is assumed. Figure 6.2 shows that the SEPs of the original ML detection rule and its modification ((6.3) and (6.12), respectively), which are very close to each other, are within the upper and lower bound curves ((6.15) and (6.16), respectively). The agreement between the analytical bounds and simulated SEPs for System A shows that our derived bounds can predict the performance well. In addition, System A outperforms System B because of a higher diversity gain. System A performs better than System C in the low SNR regime. Although system A needs addition power for relay transmission, this is the cost for the performance improvement. This shows an advantage of relay systems when transmit powers are limited.

6.5 Summary

We derived the upper and lower bounds on SEP for a two-way relay system using Alamouti scheme with PNC protocol. The derived bounds showed that a two-fold diversity order can be achieved even the relay node has only a single antenna. The simulation results confirmed the analytically derived results.

7

Conclusions

In this thesis, we proposed a number of techniques for coded systems in wireless communications. Two problems were addressed for systems without relay and two others are discussed in systems with relays. The contributions of the thesis are summarized as follows:

First, we considered a wireless systems when a relay and a feedback link are not available. At the receiver, iterative decoding is employed. We proposed the flatness criterion for symbol mapping design in conjunction with a specific channel code. The proposed criterion is suitable for two practical scenarios: i) a fast fading channel with a limited number of decoding iterations and ii) a slow fading channel with an unlimited number of decoding iterations. In addition, the parametric approach was proposed for design purposes. The design problem was shown to become a least squares problem. The simulation results confirmed that the mapping rule obtained by the proposed criterion can provide two desirable properties: i) a fast convergence rate for fast fading channels and ii) a low outage probability for slow fading channels, when a (64-state) convolutional code is employed.

Second, we considered a multiband OFDM system in which a feedback link is available. In practice, the amount of feedback information could be limited. In order to increase the system throughput and at the same time avoid an excessive feedback, we proposed a power control method in which transmission power levels

111

and modulation and coding schemes are adaptively controlled for each the whole OFDM symbol. To facilitate the proposed method, two optimization algorithms based on greedy and dynamic programming principles are discussed and a trade-off between the performance and complexity is provided. Simulation results show that the proposed power allocation method allows a signal to noise ratio (SNR) gain of 2.5 dB at a goodput of 2.5 bps/Hz over the multiband OFDM systems with equal power allocation.

Third, we considered a coded two-way communication system with a single relay. For a better spectral efficiency, in exchanging information between two source nodes, we can use the physical-layer network coding method, by which a relay decodes network coded signals in the first phase and broadcasts them to two source nodes in the second phase. Since each source node knows its own information, it can decode the information sent by the other from the network coded signals. We showed that the Viterbi algorithm can be used by approximating the maximum likelihood decoding for XORed messages as two-user decoding. For a given memory length constraint, the two source nodes can choose the same convolutional code that has the largest free distance in order to maximize the performance. Motivated by the fact that the relay node only needs to decode XORed messages, a low complexity decoding scheme was proposed using a reduced-state trellis. We showed that the reduced-state decoding can achieve the same diversity gain as the full-state decoding for fading channels. As a turbo code is a parallel concatenation of two convolutional codes, we showed the reduced-state decoding method is applicable when two identical turbo codes are used at two source nodes.

Finally, we derived upper and lower bounds for a two-way relay system in which the source nodes have two antennas and the relay node has a single antenna. The derived bounds showed that a diversity order of two can be achieved even though the relay node has only a single antenna.

From the results presented in this work, several extensions are sought:

- The parametric approach based on an EXIT chart seems to be interesting. For future works, this approach can be considered for other systems, such

as MIMO systems and systems with relays, in which iterative decoding is employed.

- We can see the impact of the fading degrees of freedom on the system performance. However, based on the EXIT chart, for a very small value of the fading degrees of freedom, i.e., the channel state varies very slowly, a robust statistical model for the EXIT function of the demapper has not been suggested yet. In this case, the symbol mapping design for such situation needs to be further investigated.

- For the power allocation problem at coded OFDM symbol level, more practical scenarios shall be considered. In addition, we assumed that channel state information for the next OFDM symbols are perfectly predicted. In further works, methods of channel prediction need to be studied. One possible way is to approximate the channel as a Markov process and predict channel states by an adaptive method. If it was the case, the performance analysis for imperfect channel state information would be desirable.

- The reduced-state decoding in two-way relay networks was shown to be advantageous due to its low complexity. The main idea of this method is to merge some states in the full-state trellis into a state in the reduced-state trellis such that the states in the reduced-state trellis can have sufficient information about the XORed message constructed by two message transmitted by two source nodes. Now, if we change the model for this setup as follows: i) the channels become intersymbol interference, ii) no channel coding is employed, and iii) the modulation/mapping could be higher order than BPSK, XORed symbols can be detected by a method of the maximum likelihood sequence detection. As this method is based on a trellis, our proposed low-complexity decoding is applicable. In this case, however, a strategy for merging states in the full-state trellis into a single state in the reduced-state trellis is yet to be suggested and should be investigated. In addition, symbol mapping can affect the performance. Symbol mapping and state grouping/merging hence might be considered jointly.

113

- Other space-time codes could be used in two-way relay systems with multiples antennas. It could be interesting to investigate a trade off between multiplexing gain and diversity gain in a two-way relay system.

- For a two-way relay setup with multiple relays, where each is equipped with a single antenna, we consider a problem of relay selection, in which, depending on the channel condition, a subset (but not all) of relays is selected for a transmission in order to provide the best performance. The relay selection is required in the scenario that we want to effectively allocate system resources (bandwidth, power) to relays. The solution to this problem will have some practical impact.

Bibliography

[1] T. Rappaport, *Wireless Communications: Principles and Practice.* Prentice Hall, second ed., 2001. 1, 8

[2] 3GPP, TS 36.201, *Evolved Universal Terrestrial Radio Access (E-UTRA); LTE Physical Layer; General Description (Release 10)*, 2010. 1

[3] 3GPP TS 36.211, *Evolved Universal Terrestrial Radio Access (E-UTRA); Physical Channels and Modulations (Release 10)*, 2010. 1, 39

[4] D. Tse and P. Viswanath, *Fundamentals of Wireless Communication.* Cambridge University Press, 2005. 2

[5] G. Caire, G. Taricco, and E. Biglieri, "Bit-interleaved coded modulation," *IEEE Trans. Inform. Theory*, vol. 44, pp. 927–946, May 1998. 2, 4, 30, 31, 33, 46, 47, 48, 55, 61

[6] A. Guillén i Fàbregas, A. Martinez, and G. Caire, "Bit-interleaved coded modulation," in *Foundations and Trends on Communications and Information Theory*, vol. 5, pp. 1–153, Now Publishers, 2008. 2, 30, 31, 46

[7] C. Berrou, G. Glavieux, and P. Thitimajshima, "Near Shannon limit error correction coding and decoding: turbo codes," in *Proc. IEEE Int. Symp. Inform. Theory*, (Geneva, Switzerland), pp. 1064–1070, May 1993. 2, 15

[8] X. Li and J. A. Ritcey, "Bit-interleaved coded modulation with iterative decoding," *IEEE Commun. Lett.*, vol. 1, pp. 169–171, Nov. 1997. 2, 31, 46, 50

[9] A. Chindapol and J. A. Ritcey, "Design, analysis, and performance evaluation for BICM-ID with square QAM constellations in Rayleigh fading channels," *IEEE J. Sel. Areas Commun.*, vol. 19, pp. 944–957, May 2001. 2, 4, 33, 46, 61

[10] R. W. Chang and R. A. Gibbey, "Theoretical study of performance of an orthogonal multiplexing data transmission scheme," *IEEE Trans. Commun. Technol.*, vol. 16, pp. 529–540, Aug. 1968. 3, 34

[11] S. Zhang, S. C. Liew, and P. Lam, "Hot topic: Physical-layer network coding," in *Proc. ACM MobiCom '06*, pp. 358–365, Sept. 2006. 3, 43, 79

[12] V. Tarokh, H. Seshadri, and A. R. Calderbank, "Space-time codes for high data rate wireless communication: performance criterion and code construction," *IEEE Trans. Inform. Theory*, vol. 44, pp. 744–765, Mar. 1998. 3, 28, 39, 100, 101

[13] F. Schreckenbach, N. Görtz, J. Hagenauer, and G. Bauch, "Optimization of symbol mappings for bit-interleaved coded modulation with iterative decoding," *IEEE Commun. Lett.*, vol. 7, pp. 593–595, Dec. 2003. 4, 33, 46, 48, 60

[14] J. Tan and G. L. Stüber, "Analysis and design of interleaver mappings for iteratively decoded BICM," *IEEE Trans. Wireless Commun.*, vol. 4, pp. 662–672, Mar. 2005. 4, 33, 46

[15] S. ten Brink, "Convergence behavior of iteratively decoded parallel concatenated codes," *IEEE Trans. Commun.*, vol. 49, pp. 1727–1737, Oct. 2001. 4, 46

[16] A. Viterbi, "Error bounds for convolutional codes and an asymptotically optimum decoding algorithm," *IEEE Trans. Inform. Theory*, vol. 13, pp. 260–269, Apr. 1967. 5, 15, 19, 80

[17] L. Bahl, J. Cocke, F. Jelinek, and J. Raviv, "Optimal decoding of linear codes for minimizing symbol error rate," *IEEE Trans. Inform. Theory*, vol. 20, pp. 284–287, Mar. 1974. 5, 19, 80

[18] S. M. Alamouti, "A simple transmit diversity technique for wireless communications," *IEEE J. Sel. Areas Commun.*, vol. 16, pp. 1451–1458, Oct. 1998. 5, 39, 40, 101

[19] A. Goldsmith, *Wireless Communications*. Cambridge University Press, 2005. 8, 10, 11

[20] P. Bello, "Characterization of randomly time-variant linear channels," *IEEE Trans. Commun. Syst.*, vol. 11, pp. 360–393, Dec. 1963. 10

[21] E. Biglieri, J. G. Proakis, and S. Shamai, "Fading channels: information-theoretic and communication aspects," *IEEE Trans. Inform. Theory*, vol. 44, pp. 2619–2692, Oct. 1998. 10

[22] J. Proakis, *Digital Communications*. McGraw-Hill, fourth ed., 2000. 11, 76, 104, 107, 109

[23] P. Elias, "Coding for noisy channels," *IRE Conv. Rec.*, vol. 4, pp. 37–46, 1955. 15

[24] A. J. Viterbi and J. K. Omura, *Principles of Digital Communication and Coding*. McGraw-Hill, 1979. 15

[25] C. E. Shannon, "A mathematical theory of communication," *Bell Syst. Tech. J.*, vol. 27, pp. 379–423, July 1948. 15

[26] IEEE Standard for Information technology – Telecommunication and information exchange between systems – Local and metropolitan area networks – Specific requirements, *Part 11: Wireless LAN Medium Access Control (MAC) Physical Layer (PHY) Specifications*, June 2007. 15, 39, 65

[27] IEEE Standard for Local and metropolitan area networks, *Part 16: Air Interface for Broadband Wireless Access Systems*, May 2009. 15, 39, 65

[28] J. Cain, G. Clark, and J. Geist, "Punctured convolutional codes of rate $(n-1)/n$ and simplified maximum likelihood decoding," *IEEE Trans. Inform. Theory*, vol. 25, pp. 97–100, Jan. 1979. 16

[29] J. Hagenauer, "Rate-compatible punctured convolutional codes (RCPC codes) and their applications," *IEEE Trans. Commun.*, vol. 36, pp. 389–400, Apr. 1988. 16

[30] G. D. Forney, Jr., "Convolutional codes I: Algebraic structure," *IEEE Trans. Inform. Theory*, vol. 16, pp. 720 – 738, Nov. 1970. 17

[31] S. Lin and D. J. Costello, Jr, *Error Control Coding: Fundamentals and Applications*. Englewood Cliffs, N.J.: Prentice Hall, 1983. 17

[32] G. D. Forney, Jr., "The Viterbi algorithm," *Proc. IEEE*, vol. 61, pp. 268–278, Mar. 1973. 20

[33] G. D. Forney, Jr., *Concatenated Codes*. Cambridge, Massachusetts: MIT Press, 1967. 23

[34] L. C. Perez, J. Seghers, and D. J. Costello, Jr, "A distance spectrum interpretation of turbo codes," *IEEE Trans. Inform. Theory*, vol. 42, no. 6, pp. 1698–1709, 1996. 27

[35] G. Ungerboeck, "Channel coding with multilevel/phase signals," *IEEE Trans. Inform. Theory*, vol. 28, pp. 56–67, Jan. 1982. 27

[36] A. R. Calderbank and N. J. A. Sloane, "New trellis codes based on lattices and cosets," *IEEE Trans. Inform. Theory*, vol. 33, pp. 177–195, Mar. 1987. 28

[37] E. Zehavi, "8-PSK trellis codes for a Rayleigh channel," *IEEE Trans. Commun.*, vol. 40, pp. 873–884, May 1992. 30, 46

[38] X. Li and J. A. Ritcey, "Trellis coded modulation with bit interleaving and iterative decoding," *IEEE J. Sel. Areas Commun.*, vol. 17, pp. 715–724, Apr. 1999. 31

[39] S. Benedetto, D. Divsalar, G. Montorsi, and F. Pollara, "A soft-input soft-output maximum a posteriori (MAP) module to decode parallel and serial concatenated codes," tech. rep., TDA Progress Rep. 42-126, 1996. 32

[40] S. Benedetto, D. Divsalar, G. Montorsi, and F. Pollara, "A soft-input soft-output APP module for iterative decoding of concatenated codes," *IEEE Commun. Lett.*, vol. 1, pp. 22–24, Jan. 1997. 32

[41] J. Choi, *Adaptive and Iterative Signal Processing in Communications*. Cambridge University Press, 2006. 34

[42] G. J. Foschini, "Layered space-time architecture for wireless communications in a fading environment when using multi-element antennas," *Bell Labs Syst. Tech. J.*, vol. 1, no. 2, pp. 41–59, 1996. 39

[43] G. J. Foschini and M. J. Gans, "On limits of wireless communications in a fading environment when using multiple antennas," *Wireless Personal Commun.*, vol. 6, pp. 311–335, Jan. 1998. 39

[44] E. Telatar, "Capacity of multi-antenna gaussian channels," *European Trans. Telecommun.*, vol. 10, no. 26, pp. 585–595, 1999. 39

[45] G. Golden, C. Foschini, R. Valenzuela, and P. Wolniansky, "Detection algorithm and initial laboratory results using v-blast space-time communication architecture," *Electron. Lett*, vol. 35, pp. 14–16, Jan. 1999. 39

[46] D. Gesbert, M. Shafi, D. shan Shiu, P. J. Smith, and A. Naguib, "From theory to practice: an overview of MIMO space-time coded wireless systems," *IEEE J. Sel. Areas Commun.*, vol. 21, pp. 281–302, Apr. 2003. 39

[47] V. Tarokh, H. Jafarkhani, and A. R. Calderbank, "Spacetime block codes from orthogonal designs," *IEEE Trans. Inform. Theory*, vol. 45, pp. 1456–1467, July 1999. 39, 40

[48] L. Zheng and D. N. C. Tse, "Diversity and multiplexing: A fundamental tradeoff in multiple-antenna channels," *IEEE Trans. Inform. Theory*, vol. 49, pp. 1073–1096, May 2003. 39

[49] T. M. Cover and J. A. Thomas, *Elements of Information Theory*. NJ: John Wiley, second ed., 2006. 42, 66

[50] R. Ahlswede, N. Cai, S.-Y. R. Li, and R. W. Yeung, "Network information flow," *IEEE Trans. Inform. Theory*, vol. 46, pp. 1204–1216, July 2000. 43, 79

[51] S.-Y. R. Li, R. W. Yeung, and N. Cai, "Linear network coding," *IEEE Trans. Inform. Theory*, vol. 49, pp. 371–381, Feb. 2003. 43

[52] R. Koetter and M. Medard, "An algebraic approach to network coding," *IEEE/AMC Trans. Netw.*, vol. 11, pp. 782–795, Oct. 2003. 43

[53] R. Dougherty, C. Freiling, and K. Zeger, "Insufficiency of linear coding in network information flow," *IEEE Trans. Inform. Theory*, vol. 51, pp. 2745–2759, Aug. 2005. 43

[54] S. Zhang, S. C. Liew, and L. Lu, "Physical-layer network coding schemes over finite and infinite fields," in *Proc. IEEE GLOBECOM '08*, Nov. 2008. 43, 79

[55] R. Rankov and A. Wittneben, "Spectral efficient protocols for half-duplex fading relay channels," *IEEE J. Sel. Areas Commun.*, vol. 25, pp. 379–389, Feb. 2007. 43, 79

[56] S. ten Brink, "Designing iterative decoding schemes with the extrinsic information transfer chart," *AEÜ Int. J. Electron. Commun.*, vol. 54, pp. 389–398, Nov. 2000. 46

[57] A. Ashikhmin, G. Kramer, and S. ten Brink, "Extrinsic information transfer functions: model and erasure channel properties," *IEEE Trans. Inform. Theory*, vol. 50, pp. 2657–2673, Nov. 2004. 46, 51, 53, 55, 59

[58] S. ten Brink and G. Kramer, "Design of repeat-accumulate codes for iterative detection and decoding," *IEEE Trans. Signal Process.*, vol. 51, pp. 2764–2772, Nov. 2003. 47, 55

[59] S. ten Brink, G. Kramer, and A. Ashikhmin, "Design of low-density parity-check codes for modulation and detection," *IEEE Trans. Commun.*, vol. 52, pp. 670–678, Apr. 2004. 47, 55

[60] G. Yue and X. Wang, "Optimization of irregular repeat accumulate codes for mimo systems with iterative receivers," *IEEE Trans. Wireless Commun.*, vol. 4, pp. 2843–2855, Nov. 2005. 47

[61] X. Qi, S. Zhou, M. Zhao, and J. Wang, "Design of constellation labeling maps for iteratively demapped modulation schemes based on the assumption of hard-decision virtual channels," *Proc. IEE Commun.*, vol. 152, pp. 1139–1148, Dec. 2005. 47

[62] F. Schreckenbach and G. Bauch, "Bit-interleaved coded irregular modulation," *European Trans. Telecommun.*, vol. 17, no. 2, pp. 269–282, 2006. 47

[63] T.-W. Yu, C.-Y. Wang, C.-H. Wang, and W.-H. Shen, "EXIT-chart based labeling design for bit-interleaved coded modulation with iterative decoding," in *Proc. IEEE Int. Symp. Inform. Theory*, (Nice, France), pp. 56–60, June 2007. 47

[64] Y.-L. Ueng, C.-J. Yeh, M.-C. Lin, and C.-L. Wang, "Turbo coded multiple-antenna systems for near-capacity performance," *IEEE J. Sel. Areas Commun.*, vol. 27, pp. 954–964, Aug. 2009. 47

[65] C. D. Meyer, *Matrix Analysis and Applied Linear Algebra*. SIAM, 2000. 48

[66] L. H. Ozarow, S. Shamai, and A. D. Wyner, "Information theoretic considerations for cellular mobile radio," *IEEE Trans. Veh. Tech.*, vol. 43, pp. 954–964, May 1994. 49

[67] A. Guillén i Fàbregas and G. Caire, "Coded modulation in the block-fading channel: coding theorems and code construction," *IEEE Trans. Inform. Theory*, vol. 52, pp. 91–114, Jan. 2006. 49

[68] F. Schreckenbach and G. Bauch, "EXIT chart for iteratively decoded multilevel modulation," in *12th European Signal Proccess. Conf. (EUSIPCO)*, (Viena, Austria), Sept. 2004. 54, 55

[69] F. Brännström and L. K. Rasmussen, "Classification of unique mappings for 8PSK based on bit-wise distance spectra," *IEEE Trans. Inform. Theory*, vol. 55, pp. 1131–1145, Mar. 2009. 54

[70] E. Sharon, A. Ashikhmin, and S. Litsyn, "EXIT functions for binary input memoryless symmetric channels," *IEEE Trans. Commun.*, vol. 54, pp. 1207–1214, July 2006. 55

[71] J. J. Boutros, A. Guillén i Fàbregas, and E. C. Strinati, "Analysis of coding on non-ergodic block-fading channels," in *43rd Allerton Conf. Commun. Control Comput.*, (Monticello, IL, USA), Sept. 2005. 57

[72] R. G. Gallager, *Information Theory and Reliable Communication.* John Wiley, 1968. 66

[73] K.-B. Song, A. Ekbal, S. T. Chung, and J. M. Cioffi, "Adaptive modulation and coding (AMC) for bit-interleaved coded OFDM (BIC-OFDM)," in *Proc. IEEE GLOBECOM '04*, vol. 6, pp. 3197–3201, 2004. 66

[74] H. Moon and D. C. Cox, "Efficient power allocation for coded OFDM systems," *IEEE Trans. Commun.*, vol. 57, pp. 943–947, Apr. 2009. 66

[75] C. Bockelmann, D. Wubben, and K.-D. Kammeyer, "Efficient coded bit and power loading for BICM-OFDM," in *Proc. IEEE Vehicular Technology Conference 2009 – Spring (VTC '09 – Spring)*, (Barcelona, Spain), Apr. 2009. 66

[76] A. Kenarsari-Anhari and L. Lampe, "Power allocation for coded OFDM via linear programming," *IEEE Commun. Lett.*, vol. 13, pp. 887–889, Dec. 2009. 66

[77] C. K. Sung, S.-Y. Chung, J. Heo, and I. Lee, "Adaptive bit-interleaved coded OFDM with reduced feedback information," *IEEE Trans. Commun.*, vol. 55, pp. 1649–1655, Sept. 2007. 66, 67, 76

[78] S. Nagaraj, "Symbol-level adaptive modulation for coded OFDM on block fading channels," *IEEE Trans. Commun.*, vol. 57, pp. 2872–2875, Oct. 2009. 66, 67

[79] IEEE Standard for Information technology – Telecommunications and information exchange between systems – Local and metropolitan area networks – Specific requirements, *Part 15.3: Wireless Medium Access Control (MAC) and Physical Layer (PHY) Specifications for High Rate Wireless Personal Area Networks (WPANs)*, June 2003. 66

[80] J. Campello, "Optimal discrete bit loading for multicarrier modulation systems," in *Proc. IEEE Int. Symp. Inform. Theory (ISIT '98)*, (Cambridge, Mass., USA), p. 193, Aug. 1998. 73

[81] N. Papandreou and T. Antonakopoulos, "Bit and power allocation in constrained multicarrier systems: the single-user case," *EURASIP J. Advances Signal Process.*, vol. 2008, Jan. 2008. 73

[82] A. Federgruen and H. Groenevelt, "The greedy procedure for resource allocation problems: Necessary and sufficient conditions for optimality," *Oper. Res.*, vol. 34, pp. 909–918, Nov.–Dec. 1986. 73

[83] P. Frenger, P. Orten, T. Ottosson, and A. Svensson, "Multi-rate convolutional codes," tech. rep., Chalmers University of Technology, 1998. 76

[84] J. Liu, M. Tao, Y. Xu, and X. Wang, "Superimposed XOR: a new physical layer network coding scheme for two-way relay channels," in *Proc. IEEE GLOBECOM '09*, Nov.Dec. 2009. 80

[85] T. Koike-Akino, P. P. Popovski, and V. Tarokh, "Optimized constellations for two-way wireless relaying with physical network coding," *IEEE J. Sel. Areas Commun.*, vol. 27, pp. 773–787, June 2009. 80

[86] S. Zhang and S.-C. Liew, "Channel coding and decoding in a relay system operated with physical-layer network coding," *IEEE J. Sel. Areas Commun.*, vol. 27, pp. 788–796, June 2009. 80, 83

[87] R. Peterson and D. J. Costello, Jr, "Binary convolutional codes for a multiple-access channel," *IEEE Trans. Inform. Theory*, vol. 25, pp. 101–105, Jan. 1979. 80

[88] M. V. Eyuboğlu and S. U. H. Qureshi, "Reduced-state sequence estimation with set partitioning and decision feedback," *IEEE Trans. Commun.*, vol. 36, pp. 13–20, Jan. 1988. 80

[89] M.-C. Ju and I.-M. Kim, "Error performance analysis of BPSK modulation in physical layer network-coded bidirectional relay networks," *IEEE Trans. Commun.*, vol. 58, pp. 2770 –2775, Oct. 2010. 100

[90] T. Cui, F. Gao, T. Ho, and A. Nallanathan, "Distributed space-time coding for two-way wireless relay networks," *IEEE Trans. Signal Process.*, vol. 57, pp. 658–671, Feb. 2009. 101, 102

[91] M. K. Simon, *Probability Distributions Involving Gaussian Random Variables: A Handbook for Engineers and Scientists*. Springer, 2002. 108

[92] M. K. Simon and M. Alouini, *Digital Communication over Fading Channels: A Unified Approach to Performance Analysis*. John Willey, 2000. 108